# Liquid dosing on the micro-scale

## A quest for increased resolution

Maarten Benjamin Blankespoor

Reportnumber : 2022.009
Committee: : dr. M.K. Ghatkesar
dr. ir T. Manzaneque Garcia
dr. M. Mastrangeli
Specialization: : Micro and Nano Engineering
Type of report: : Masters Thesis
Date: : April 14th, 2022

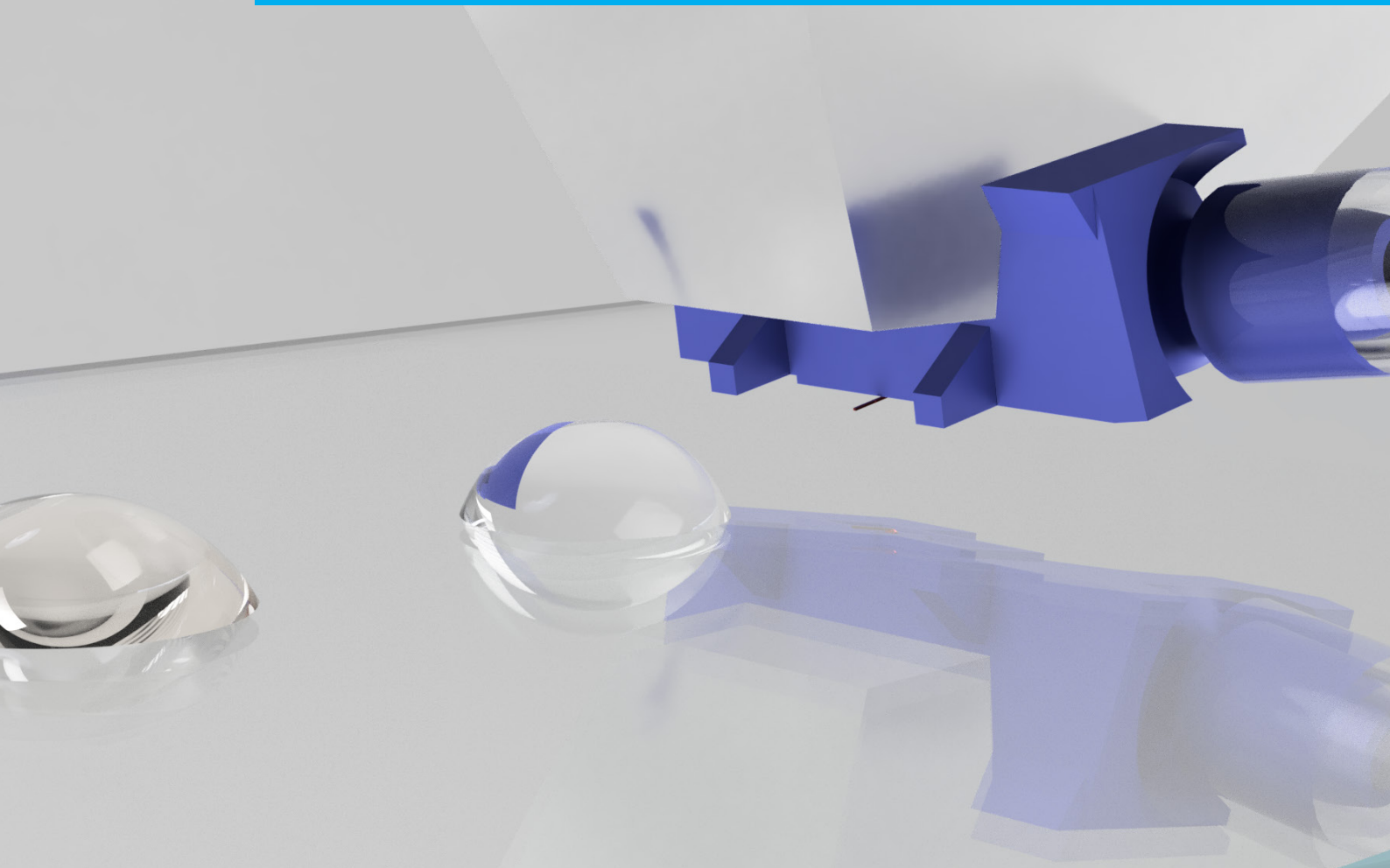

TU Delft Delft University of Technology

Department of Precision and Microsystems Engineering, 3mE

# Liquid dosing on the micro-scale

## A quest for increased resolution

by

Maarten Benjamin Blankespoor

to obtain the degree of Master of Science
at the Delft University of Technology,
to be defended publicly on Thursday April 14, 2022 at 9:30 CEST.


| | | |
|---|---|---|
| Student number: | 4344448 | |
| Project duration: | February 1, 2021 – April 14, 2022 | |
| Thesis supervisors: | dr. M.K. Ghatkesar, | TU Delft, Chair |
| | dr. ir. T. Manzaneque Garcia, | TU Delft, Daily supervisor |
| | dr. M. Mastrangeli | TU Delft, External member |




TU Delft

# Preface

*The understanding of the basic building blocks of life is of capital importance for biology and medicine. However, as things get smaller, they tend to be more difficult to study. As modern technology is progressing towards a better knowledge of the smallest scale, different disciplines such as biology, chemistry and physics start to blend and complement each other. The field of micro engineering is exactly such a blend of disciplines. The ever advancing innovation in this field holds the promise of improved tools to study and influence life on its smallest scale. Today, we know a lot about the workings of our basic building blocks, but still huge mysteries and challenges remain. I hope that this work may be a small contribution to innovation, to science and to the understanding of life's mysteries.*

Dear reader, before you lays a manuscript that is the culmination of all the knowledge that I gained during my studies here in Delft, leading up to this graduation project. Throughout the last year, I have given this project my all, and I am very content with where it has brought me. Through the pages of this thesis, I will share an insight in the journey I have made and the lessons I have learned.

I could not have travelled so far on my own, therefore I would like to express my gratitude to some people who have played an important role throughout this project. Murali, thank you for your wisdom and your incredibly useful hands-on tips to go about collecting literature, structuring information, and in general: research. I especially enjoyed our 'philosophical' meetings, where we brainstormed in-depth about all the possible applications and implications of this project. Tomás, thank you for all the practical knowledge you gave me that I could instantly apply in the lab. I wouldn't have been able to work my way past the many instruments I needed without your experience with so many of them. You repeatedly offered new insights by asking the right questions and pointing my attention to the right details. I am also much indebted to Pieter. His work has cleared a path for me that otherwise would have hidden huge obstacles which I am not sure I would have been able to tackle. Special thanks to Jikke, with whom I could exchange tips and tricks in the lab, and to all the others working in the labs: Henrie, Qais, Gürhan, Thijs, Katerina, Ahmed, Ebrahim, Michał, Saleh, Niels and Yujiang. And last but definitely not least, I am very grateful for the help I received from the lab technicians, Gideon, Patrick, Spiridon and Rob. They pointed me to invaluable solutions and learned me how to operate the tools needed to bring this project to a good end.

*Maarten Benjamin Blankespoor*
*Delft, March 2022*

# Abstract

The processes that take place within cells are complex. Single-cell analysis is a method that is employed to gain further understanding of the working mechanisms on a single-cellular level. The controlled transport of substances through the cell membrane is important for studying the behaviour and responses of single living cells. Femtopipettes are used as a means to accurately target and sample cells with high viability rates. Different actuation principles exist for femtopipettes, but pressure actuation is identified as the most versatile and straightforward method. However, the volume dosing resolution of pressure driven femtopipettes lags behind other actuation methods. Throughout literature, the minimum reported dose is identified as 100 femtolitre (1 fL= $10^{-15}$L), achieved by applying a pressure pulse to a femtopipette. In this work, two new concepts are proposed and researched with the goal of increasing the volume dosing resolution of pressure driven femtopipettes. A multi-scale 3D printing strategy was employed where functional femtopipettes were successfully printed using two-photon-polymerization (2PP). The first concept incorporates a physical barrier in the form of a flexible membrane into the femtopipette. It was expected that the volume actuated by the deformation of the membrane could be controlled and calibrated. The deformation of 2PP printed membranes was characterized and the achieved volume displacement was well in the desired range of 100 fL. However, tests with liquid dosing did not succeed in achieving this same range, and difficulties were experienced with reproducibility. The second concept exploited the phenomenon of capillarity by incorporating axisymmetrical phaseguides as a means to control the position of the liquid-air meniscus. Consecutive geometrical steps were created that allowed for discrete and robust control over the liquid portion within the femtopipette. Step sizes of 10 picolitre (1 pL= $10^{-12}$L), 200 fL and 60 fL were fabricated and successfully tested, breaching beyond the current state of the art. This concept thus demonstrates both the level of customization and the unprecedented volume dosing resolution that was achieved.

# Contents

# Introduction

The cell is the basic building block of all known lifeforms. First observed and described by Robert Hooke and Antonie van Leeuwenhoek in the 17th century [1], the discovery of the cell has had a major impact on biology and the way we understand life [2]. Life has evolved from single-cellular organisms to organisms that contain many trillions of cells. The human body, for example, is estimated to contain approximately 40 trillion ($4 \cdot 10^{13}$) cells [3]. Each type of cell with its own function, properties and behaviour. In the decades and centuries after its first discovery, the study of the cell has become an entire field on its own. We now know that the properties of each cell are diverse, even among cells of the same type [4]. This so called 'heterogeneity' makes it important to analyse cells at the individual level, in contrast to ensemble measurements, where the average properties of a collection of cells are measured. Cell properties even change over time due to the ever changing expression of proteins, the functional molecules within the cell. The entire set of proteins within a cell is called the 'proteome' and its study has become a new field of science since the late 1990s, called 'proteomics' [5]. The study of the proteome leads to a better understanding of the activity of cells, the communication within and between cells and its reaction to stimuli, ultimately leading to a better knowledge of diseases and possible treatments.

Cell-to-cell variations can only be captured by the analysis of single cells. Recently this topic has received increased attention and new methods are being developed for single-cell analysis (SCA) [6]. Particularly, SCA provides useful insight on the level of proteomics but also the genomics, transcriptomics and metabolomics benefit from the single-cell approach [7].

Most techniques for SCA apply a separation and/or sorting technique to isolate cells. The next step is usually to 'open up' the cells to access their inner organelles and molecules by lysis (dissolving of the cell membrane) or dissection (cutting thin slices for microscopic analysis) as reviewed by Lindström and Heath [6], [8]. However, in most of these methods, cells are analysed away from their natural environment, and most methods kill cells in the process (postmortem analysis). The obvious disadvantages are that the cells may behave differently than in their natural state, and that cells can only be analysed once. New and innovative methods have been proposed more recently, that study the contents of cells while they stay alive [9]. This means that cultured cells can be accessed and small extracts of the cell can be taken for further research without affecting the viability of the cell. The research possibilities are huge, because this way, different samples can be taken over time, providing a dynamic representation of the processes within the cell. The terms 'cell biopsy' or even 'cell surgery' are being coined in literature, indicating the access to cellular content that can otherwise not cross the cell membrane such as DNA, proteins and even whole organelles. It becomes obvious that the tools for sampling cells at this scale need to be extremely small and precise, and only a few methods exist that meet such requirements [10]. Among the methods described, the concept of the so-called *femtopipette* is the most versatile, as it can be moved to a desired target location. Moreover, the femtopipette can be used not only to extract but also to inject material into cells.

In general, two types of femtopipette exist that can operate in a liquid environment. The first and oldest femtopipettes were produced by heating small glass tubes, and then pulling them apart, resulting in two separate hollow femtopipettes. Apertures as small as several tens of nanometers could be successfully produced. Production is relatively easy, and can be done without the need for cleanrooms [11]. The second technique is based on the principle of the Atomic Force Microscope (AFM), where a small channel is made within the AFM cantilever, in order to be connected to an external pressure controller. Such a setup has been been pioneered and successfully applied to the analysis of single cells by the research group of Meister et al. [12]. The main advantage of the AFM setup is that apart from the pipetting functionality, also a force-distance curve is obtained. This information can be used to determine the force exerted on a cell, which can serve as a means of contact detection but also as a way to mechanically characterize cells.

The dosing of liquids at this small scale is inherently difficult. Generally, the pipetted dosage can be controlled by either 1) electrowetting, 2)thermal actuation, or 3) pressure control [10]. Electrowetting is a physical effect where the surface tension of a liquid-liquid interface is modified by applying an

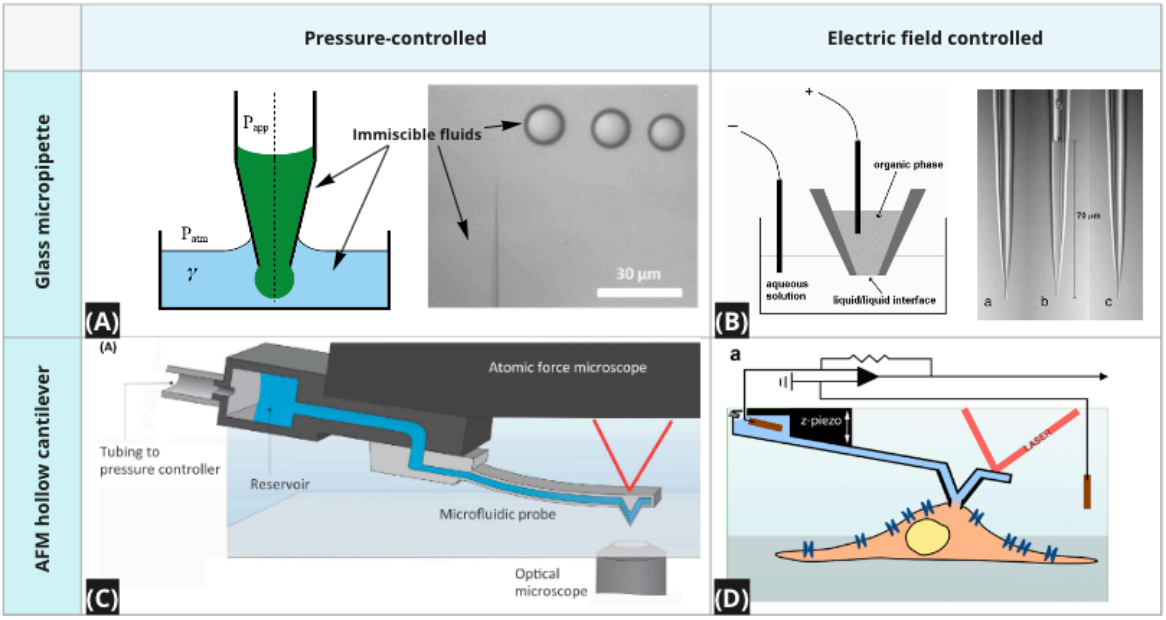


Figure 1: *Generalisation of examples for different fluid-based single-cell probing methods. Either with a glass femtopipette or a microfluidic AFM cantilever, and either by electrowetting or pressure based. (A) Pressure based volume control of liquid dispensed with a glass femtopipette. Different sized droplets are shown next to a glass femtopipette on the left. Resolution of* $\sim 100$ *femtolitres (fL). Adapted from [13]; (B) Glass femtopipette with actuation based on electrowetting. Resolution down to* $\sim 10$ *attolitres (aL). Adapted from [14]; (C) Hollow AFM cantilever, actuated by pressurized reservoir. Resolution of* $\sim 100$ *fL. Adapted from [15]; (D) Hollow AFM cantilever equipped with electrode. Successful application of a patch-clamp. No injection based on electrowetting has been reported here. Adapted from [16].*

electrical potential, enabling the liquid interface to be drawn into the pipette. This allows for precise control but requires both liquids to be conducting [14]. Thermal actuation is achieved by adding metalic nanoparticles to the liquid, which undergo thermal expansion when heated [17]. Pressure control simply means the pipette channel is connected to an external pressure controller. The dosed volume is then controlled by varying the time and magnitude of applied pressure. Successful extraction and injection into cells have been demonstrated using electrowetting and pressure actuation [15], [18], [19].

The highest precision in dosing is achieved by electrowetting and thermal actuation, where volumes could be successfully controlled in the range from picolitres ($10^{-12}$ L) down to attolitres ($10^{-18}$ L) [14], [17]. Current pressure control methods can at best deliver a resolution in the range of 100 fL ($100 \cdot 10^{-15}$ L) [19]. The latter article describes that precision of the dosed volume depends greatly on the duration of applied pressure pulse, and can be affected by non-uniform sample conditions such as variations in viscosity or intracellular pressure from cell to cell. It is important to note that both mentioned methods rely on optical evaluation for determining the aspirated/injected volume. This puts limits on the certainty of measured volumes.

Pressure actuated liquid dosing methods are lagging behind in terms of volume dosing resolution. However, pressure actuation comes with significant advantages over both other methods in terms of choice in working liquid and straightforward usage. In this thesis, it is researched whether it is possible to increase the volume dosing resolution of pressure actuated femtopipettes.

In the first part, relevant literature is surveyed on the topics of single-cell analysis and liquid manipulation on the small scale. The knowledge gained from this literature is then used to form a research question and to set a goal for this thesis. There, two different concepts are proposed that might improve upon the volume dosing resolution of pressure actuated femtopipettes. These concepts are treated in depth and tested in the second part. The appendices provide extra information on the design steps and the production and experimental methods.

# I

# Literature Survey

# 1

# Single-Cell Analysis

Although a cell is an utterly small object that is generally not even visible to the naked eye, the working processes of life on its smallest scale are incredibly complex. Increasing our knowledge of the functioning of a cell has become an important part of science. The study of single cells is of major importance, as argued in the introduction. Classically, cell biology slowly gains terrain by zooming in on one process and then trying to carefully isolate substances or reactions in a controlled environment. In consequence, it becomes clear that the introduction or extraction of controlled amounts of substance is key to setting up the boundaries of cell experiments.

Each cell separates itself from the environment by its *plasma membrane*—the outer shell of the cell. This membrane is made of a thin ($\sim 5$ nm) bilayer of phospholipids, but many other functional molecules and proteins are embedded in the bilayer. Some small molecules such as gases and solvents may passively pass through the membrane whereas certain peptides and proteins rely on active transportation, but in general the membrane is a hard-to-pass barrier for most molecules [20]. This means that clever tricks need to be invented in order to introduce or extract targeted substances. Many such methods exist, and in an extensive review by Stewart et al. [21] all methods are broken down in either 1) *carrier-mediated transport* or 2) *membrane disruption based transport*.

Carrier mediated transport methods mainly focus on the transfection of genetic materials, by means of nanoparticles that are actively transported into the cell, or by means of using deliberate viral infection with desired genetic material. More recent techniques also succeed in transporting certain proteins with specifically designed carriers or vesicles through the membrane [22], [23]. In this review, the emphasis lays on the physical means for membrane disruption based transport. A plethora of different techniques are known to physically facilitate transportation, but for the interest of the subject of this review, we will focus on techniques where micro-engineering is an enabling factor. Although sometimes micro-engineering is also used to implement carrier-based methods, for example through preparation of nanoparticles by a microfluidic system [24], carrier mediated transport is mainly part of the biochemical domain, and therefore out of scope of this review.

Membrane disruptive transport includes all techniques that (temporarily) open up the membrane to introduce or extract molecules of interest. Again, many methods exist and can generally be divided into two main categories: 1) **Permeabilization** and 2) **Direct penetration** of the cell membrane. Combinations of both methods also exist [25]. A graphical representation of all general membrane transportation mechanisms is provided in figure 1.1.

## 1.1. Permeabilization

The deliberate creation of pores in the cell membrane is called *permeabilization*. In general, permeabilization uses a provocative method that disrupts the normal membrane function, to open a proverbial ‘gate’ through which substances may be transported which could otherwise not pass the cell membrane by themselves. Permeabilization relies on the physical perturbation of a cell by means of a) electrical, b) mechanical, c) optical, d) thermal or e) biochemical stimulus [21]. The stimuli need to be applied in just the right intensity and time; created pores should be big enough and opened long enough for the desired substance to pass through, but should not be too big or opened too long

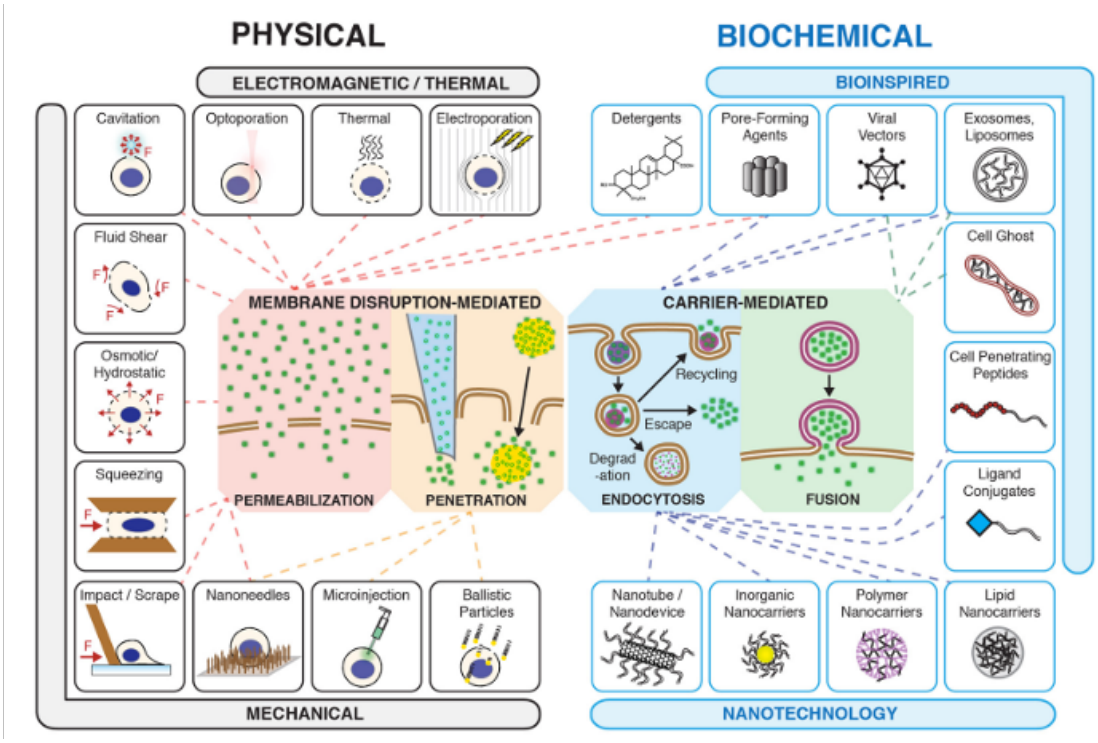


Figure 1.1: *Overview schematic of possible ways for transportation through the cell membrane, as adapted from [21].*

for the cell to be unable to recover from its disturbance [26].

One of the first, and still major permeabilization techniques is called *electroporation* and was pioneered in the 1980's by Neuman et al. [27]. In short, with electroporation an electric potential is applied to the cell. Small pores that are already present in the cell membrane create a conducting connection between the liquid inside and outside the cell membrane. At first the electrical resistance is very high due to the small natural pore size ($< 0.5$ nm), but due to the build up of charge, it becomes energetically favourable to increase the pore size, thereby relaxing the electrical expanding pressure [28]. This principle has been widely studied, and is used in a lot of micro-engineered biological applications [29]. When applied to the bulk of cell containing buffer, all exposed cells are addressed more or less uniformly. Higher specificity can be obtained by applying geometrical adaptations like a porous substrate [30] or arrays of micro-pillars [31]. Single cells can be targeted with microchannels [32] or even single probes [33], [34].

Mechanical perturbation is a broad approach to permeabilization that involves the application of physical strain to cells. In the context of micro-engineering, many implementations exist in the domain of microfluidics [35]. A common approach is to use microfluidic channels with a constriction 30-80% smaller than the cells in study [36]. The flow in these channels is such that cells in suspension are forced ('squeezed') through the constriction, resulting in membrane disruptions, see figure 1.2A. Many adaptations exist, including experiments with different constriction shapes for optimized transportation efficiency [37]. Another such approach is using a technique called *hydroporation*, where shear stress in the cell is achieved by exposing the cells to a cross-directional fluid flow [38]. Due to the 'soft' interaction with the fluid, the last mentioned method is claimed to provide the highest cell viability [29]. Transportation efficiency can be tuned through the Reynolds number of the fluid flow. Using microfluidic systems, single cells can be targeted, sorted and isolated in high throughput [6]. Other ways that mechanically perturb many cells at once have also been reported, but since the focus of this report is the analysis of single cells, they are left out of this review.

Yet another technique to permeate the cell membrane that uses high intensity light is called *optoporation*. The application of focussed, pulsed lasers generally allows for a high level of precision. Optoporation of cells was first introduced by Tsukakoshi et al. in 1984 [39] by using a nanosecond pulsed laser to practically 'burn' a hole of several microns wide in the cell membrane. With the introduction of femtosecond lasers, the procedure became more refined due to the higher specificity of the power dose, resulting in a much higher cell viability [40]. Not only can the focal point of the fem-

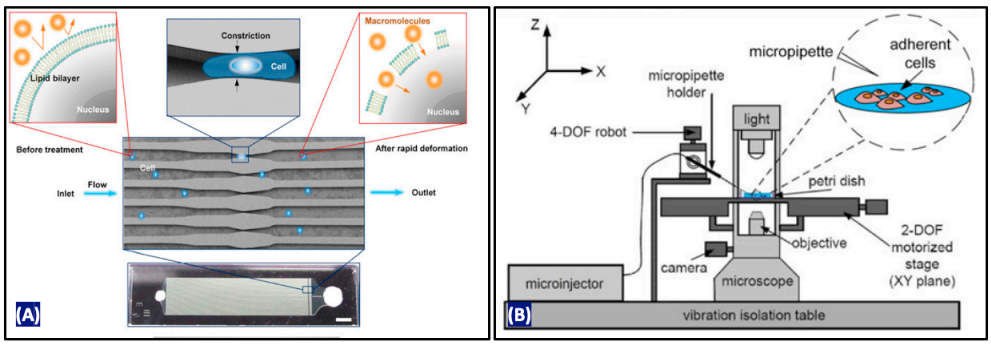


Figure 1.2: *Example of typical cell analysis tools. (A) Microfluidic cell permeabilization system that applies a constriction to perturb the cell. (B) Typical setup of a cell injection system using a glass capillary as femtopipette. Figures adapted from [36] and [44] respectively.*

tosecond laser be used to directly perturb the cell membrane, it can also be used to target particles close to the membrane, which in turn can cause bubbles (cavitation) that can apply shear stress on the cell membrane [41]. A disadvantage coming with the high specificity of optoporation is that it is difficult to obtain high throughput.

Closely related to the optoporation method is *thermoporation*, which uses temperature changes to disrupt the cell membrane [42]. Temperature changes can be applied globally to the entire sample, but local influence can also be achieved with the aforementioned optical techniques.

The last category of permeabilization is biochemical, meaning that biochemical agents are used to permeate the membrane [43]. Thermoporation and biochemical permeabilization are mainly part of the biological domain, without the explicit use of micro engineering techniques. Furthermore, most temperature and biochemical methods are not specific to single cells. Therefore, the last mentioned two methods are out of the scope of this review.

## 1.2. Direct penetration

We speak of direct penetration when the cell membrane is physically penetrated to provide direct access to the cellular contents. Among the many variant approaches to penetrate cell membranes that have emerged, one can distinguish three trends in general. First and foremost is the classical concept of injection, where a hollow tube is inserted into a cell, after which fluid can be either injected or extracted. Because of its relevance for this report, the concept of micro injection will be treated in more depth in section 2.2.

Secondly, a technique developed in the late 1980's penetrates the cell membrane with tiny ballistic projectiles, often referred to as *biolistics*. The projectiles, usually heavy metal particles to achieve high momentum, are coated or functionalized with the substance of interest, and subsequently fired with high velocity at the cells on the substrate. The article that first reported this technique used actual gunpowder filled blank ammunition to propel a nylon projectile that was coated with nanoparticles towards a stopping plate with a small 1 mm aperture. Upon hitting the stopping plate, the nanoparticles conserved their momentum and continued travelling through the aperture with reported speeds of $430\,\mathrm{m\,s^{-1}}$ [45]. Miraculously, most cells survived this shootout, and initially this technique yielded even higher cell viability than some of the micro injection methods. With the improvement of this method, a wider variety of cells could be targeted, even down to small yeast cells that are difficult to inject by classical methods even today [46]. However, the number of substances that can be introduced with this technique remains limited, and it is clear that this method can only be used for one-way transportation.

A third method utilizes more modern nanotechnology production techniques to fabricate thin nanorods, usually up to several 100 nanometres. These rods are often referred to as *nanoneedles*, *nanowires* or *nanostraws* in literature. Arrangements can consist of single probes up to entire arrays on a substrate for higher throughput. The first nanorods were produced in 2003, where Chemical Vapour Deposition (CVD) was used to make an array of 'spikes'. These spikes could then be functionalized with DNA that was passively transported into cells which were forced onto the spikes [47]. Although nanorods have been fabricated from many different materials, a popular candidate emerged from the development of carbon nanotubes (CNT) [48] due to their favourable small size,

high aspect ratio and flexibility. Particles that adhered to the CNT were passively absorbed by the cell after penetration [49]. A more versatile method using CNT was reported by Singhal et al., when they found a method for interfacing a CNT to the end of a glass capillary [50]. This way, they were able to fill the glass capillary from the backside, so that particles were successfully injected into cells by diffusing through the CNT. They also experimented with filling the CNT with magnetic particles from a ferrofluid, so that the movement of the flexible CNT could be controlled externally with a magnetic field.

Producing and aligning the CNT remains challenging, and other ways to produce high aspect ratio rods, like Focussed Ion Beam (FIB) milling, have also been proposed [51]. The latter article demonstrates the benefits of a nanorod probe, by which high detail, resolution and specificity are obtained when combined with the functionality of an atomic force microscope (AFM). The strategy of using an AFM was also applied for the first extraction of mRNA from single living cells, where the mRNA was passively absorbed to the AFM tip when held penetrated into the cell for 45s [52].

Above treated methods give an overview of the many reported ways that enable successful transportation substances through the cell membrane, with a focus on methods that could be applied to single cell analysis. Most methods are limited to specific types of cargo to be transported. The classic concept of single cell injection is the oldest technique known for accessing cellular content and holds the promise of allowing for a wide variety of cargo to be both injected an extracted. To get a deeper understanding of the notion of micro injection, the next section will start broad by looking into the many concepts that exist for manipulating fluid at the small scale, finally progressing towards an overview of techniques that can be applied to single cells.

# 2

# Fluid manipulation on the small scale

In order to come up with solutions for the handling of liquids at the small scale, one can start broad by looking into the many applications where small amounts of liquid are required. Perhaps the most common device for the manipulation of liquid at the small scale is the inkjet printer that is widely used in offices and households everyday. Inkjet printers make use of a small reservoir of liquid ('ink') that gets dispersed through a nozzle by either piezo-electric, thermal or electrostatic actuation. Droplet volumes can be achieved in the order of femtolitres [53]. A big advantage of the inkjet technique is that many different kinds of fluid can be handled, and new applications like specialised 3D printing are continuing to emerge [54]. It must be noted, however, that the droplets are 'fired' at the substrate, and deposition cannot be done within a liquid. Moreover, it becomes clear that such deposition methods can only dispense, and not aspirate fluid.

A common application in labs to circumvent these problems, is the so called *syringe-pump*, which is conceptually very simple. A regular syringe can be inserted in the machine, where the piston of the syringe is then connected to a linear actuator. The precision of the actuator thus directly influences the precision of the deposited or aspirated volumes. Many commercial systems are available, the smallest volume resolution reaching down to the sub-nanolitre range.

For the use in single-cell analysis, we are ultimately looking for even higher resolution volume control. This search leads past some of the most precise fluid manipulation techniques that exist today.

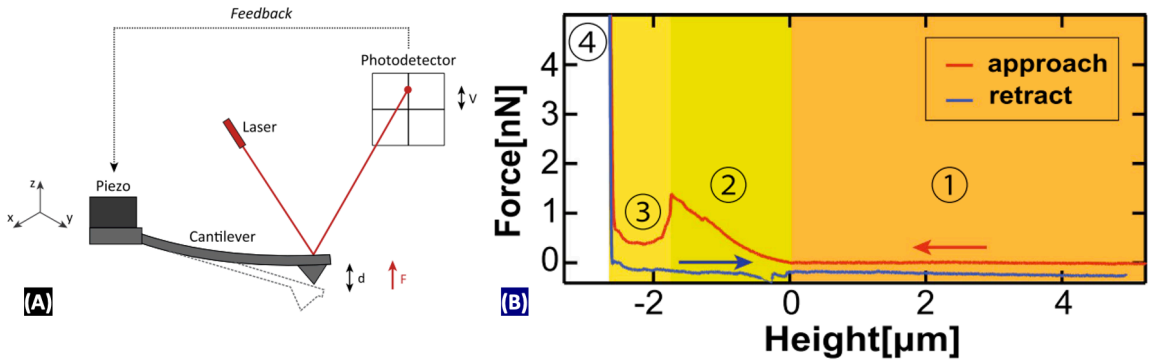


Figure 2.1: *The force sensing principle of the Atomic Force Microscope (AFM). (A) A schematic representation of the AFM cantilever with a sharp tip. The piezo-stage controls the vertical position of the cantilever. A laser is being reflected from the cantilever surface onto a photodetector, to measure the deflection. With the stiffness of the cantilever and its deflection, the exerted force can be determined. Adapted from [15]. (B) A typical force-distance curve for the penetration of a cell. In region (1), the force is constant, indicating the approach. Then, in region (2), the force increases after contact with the cell until it punctures the membrane and region (3) is entered. The blue line represents the retraction of the cantilever. Adapted from [55].*

## 2.1. AFM-based deposition

After their groundbreaking success of the first ever realization of imaging at the atomic scale by use of the scanning tunneling microscope (STM) in 1982 [56], many scanning-probe based concepts have emerged. Most notably, the same authors invented the atomic force microscope (AFM) a few years later [57], just before being awarded the nobel prize for their work on the STM. In principle, the AFM comprises a flexible cantilever with a very sharp tip at its end. The surface of interest is then approached by the tip. Due to the interaction of atomic forces between the tip and the sample, the cantilever deflects. This deflection is then measured by reflecting a laser from the surface of the cantilever, see figure 2.1A. By scanning the cantilever across the surface, a map can be made of the forces at each location. This in turn can represent the surface topograpy, and as such, high resolution images can be obtained at the atomic level.

Many different kinds of AFM and operation modes have evolved since, and researchers are coming up with ever more clever ways to use the AFM in characterization and manipulation at the small scale [58]. Not long after its invention, it was discovered that the AFM could also be successfully used to make images of surfaces while submerged in liquid [59]. And later, even liquid droplets themselves were imaged using an AFM [60]. Another breakthrough was achieved in 1999 when researchers managed to actually deposit particles on a substrate by dipping the AFM tip in an 'ink' of particles, and then 'writing' the tip across a surface [61]. The appropriate name "Dip-pen Nanolithography" was assigned to this technique. A first improvement to this technique came in 2003, when a small reservoir was included on the cantilever [62]. It was dubbed Nano-Dispenser, or NADIS for short. This passive pipetting enabled the deposition of tiny liquid droplets on a surface, their volume reaching the attolitre ($10^{-18}$ L) range, depending on contact time, relative humidity and surface characteristics [63]. Variants of this design were later able to deposit droplet volumes as small as zeptolitres ($10^{-21}$ L), by using conductive ink, and applying an electric field between the tip and the substrate [64].

Another advance in the design of a fluid-depositing AFM cantilever was made when the research group of Espinosa et al. managed for the first time to make small hollow channels inside an AFM cantilever [65]. The channels where connected from a small on-chip reservoir to the tip of the cantilever that was shaped like a fountain pen. Following the original naming tradition, it was titled "nano-fountain probe", or NFP for short. The advantage of this method was that liquid could be deposited in a continuous manner, just like the writing of a pen. Written line resolutions could be achieved below 100nm [66]. Schematic representations of the aforementioned devices are shown in figure 2.2. When the fabrication method for the NFP design was improved a few years later [67], different kinds of applications emerged from other research groups. It has been used, for instance, in the deposition of nanoparticles [68], where sub-femtolitre droplet volumes where achieved. Another variant of this design was using a joule-heated wire, sealed in the reservoir, to control the deposition of droplets of several femtolitres [69]. The on-chip reservoir makes it difficult to control the pressure in the fluid, limiting the possibilities for pumping the fluid, but this problem was creatively circumvented by Garza et al. by making use of evaporation [70]. A u-shaped channel was used, where liquid was supplied from one side, and evaporation took place on the other. This created a pumping effect due to the capillarity of the channel, by which liquid could be successfully aspirated through the tip aperture until the process came to a natural stop by the depletion of the evaporation reservoir.

All of the above mentioned methods deposit droplets on a surface outside of a liquid environment [71]. This has a major influence on the physical effects determining the deposited volume. Properties like relative humidity, surface energies, viscosity and temperature play an important role in the shape of the liquid meniscus [72]. An important remark here, however, is that when an application on live cellular matter is envisioned, the operation will always take place within a liquid. This can be the intracellular liquid, or the buffer liquid outside the cells that is part of the cell environment.

When liquid is being expelled through a tiny aperture into an air environment, a high pressure is needed to overcome the Laplace pressure that is caused by the surface tension of the liquid-air interface [73]. When this aperture is submerged in liquid however, there is no air-liquid interface and hence the applied pressure needed to expel the liquid is only dependent on the hydrodynamic resistance of the aperture and fluid channels. This requires different approaches than the ones described above. An overview of different methods used to inject single cells within a liquid environment is

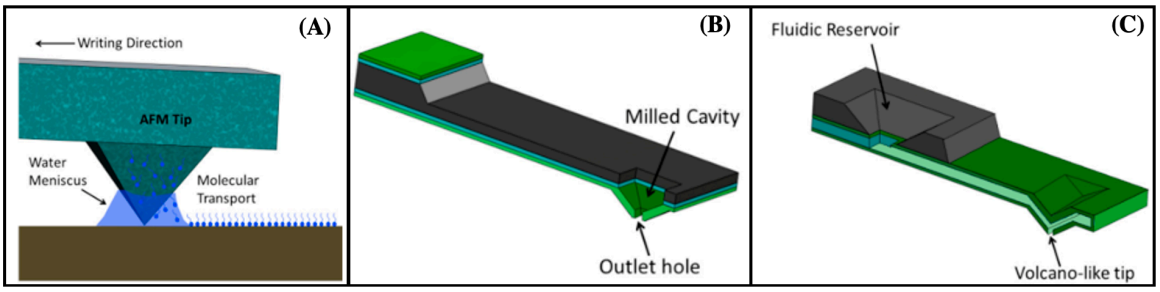


Figure 2.2: *Schematic representation of the working function of (A) Dip-pen Nanolithography, (B) Nano dispenser (NADIS) and (C) Nanofountain probe (NFP). Figures adapted from [71].*

given in the following section.

## 2.2. Cell injection

The concept of microinjection has been the oldest among the many ways to access cellular contents treated in chapter 1. The first recorded deliberate penetration of the cell membrane dates back to more than a century ago, where a method for creating glass capillaries by hand was conceived in 1911 to deliver a bacterium into a plant cell [74]. Many variants and improvements have emerged since then.

Glass micro capillaries are relatively easy to fabricate by heating a small glass tube and then pulling it apart to form two very sharp hollow apertures. This technique does not require cleanroom production facilities and still is accurate enough to be used for the injection of single cells. This explains the popularity of the glass micro capillaries, which can be found in many applications to cell biology, still today. Since its early use and manual production, the fabrication process of the capillaries has been optimized and automated [11]. Whereas the early micro capillaries had micrometer sized apertures [74], recent techniques are able to produce apertures ranging from 300 nm down to even 50 nm [18]. Apart from advances in the production process, the concept has remained largely unchanged.

A first big improvement in terms of operation came with the emergence of computer technology more than half a century after the first introduction of micro injection: in 1988, Pepperkok et al. connected a glass microneedle on a motorized XYZ stage to a digital microscope system [75]. The operator could select desired locations on a screen, and the microneedle would automatically inject cells at the chosen positions. While manual operation is only suited for small batches and single cells, this setup opened up the possibility of relatively high throughput cell injection, with a reported automatic injection rate of up to 1500 cells per hour. Recently, more modern variants of this idea have also been described, where automatic cell detection, computer vision and optimized injection paths have been advertised [44], [76], [77]. Usually these methods rely on visual inspection where image processing algorithms are used to identify cells, however difficulty remains due samples that are often transparent, cell clustering and varying shapes of cells [78], [79]. A schematic representation of a typical modern microinjection setup is shown in figure 1.2B. In yet another attempt to increase the throughput of cell injection, arrays of stationary micro needles were fabricated where cells in suspension were captured and moved onto the needles with microfluidic systems [80].

Other advancements of the micro injection technique have been proposed in relation to the volume resolution that could be achieved. The vast majority of microinjection platforms use transient pressure control for the injected dosage, meaning that the dose is quantified by controlling the injection pressure and/or time [13], [81]. Usually, cell injected volume resolutions down to $\sim 100$ fL are achieved with this technique. An interesting approach to improve this resolution was proposed in 1999, when Knoblauch et al. used a femtopipette filled with liquid metal alloy particles that expanded due to controlled changes in temperature [17]. With a tip aperture of 100nm they were able to achieve resolution down to the attolitre level. Successful injection in cells was also reported.

Another interesting progression was made possible by the invention of Scanning Ion-Conductance Microscopy (SICM) in 1989 [82]. SICM is a scanning-probe technique operating inside a liquid, that uses a glass microcapillary filled with a conducting, electrolyte solution. The liquid around the probe is also conducting, and the current is measured between the reservoir and the

inside of the capillary. When the probe approaches a surface, the flow of ions through the aperture is restricted, decreasing the conductance. A feedback loop is then applied to keep the conductance constant by changing the height of the probe above the sample. When the probe is scanned across the sample, a high-detail surface topography can be obtained without ever coming into contact with the sample.

The SICM opened doors in the world of cell biology, as cells could be imaged in high resolution with this technique, without physically perturbing them [83]. The realization that the SICM technique could also be used to dose liquid in and out of the capillary came as a breakthrough in 2007 when Laforge et al. described the principle of electrochemical control over a liquid inside the capillary [14]. The electrochemical liquid actuation makes use of the surface tension in a liquid-liquid interface, that can be altered by setting an electrical potential over the two liquids. The change in surface tension causes the liquid-liquid meniscus to move either up or down the conical walls of the capillary. A small illustration of this technique can be seen in figure 1B. By using this electrochemical principle instead of pressure-based actuation, deposition resolution was improved down to attolitres.

The high resolution of this technique has proven useful for single-cell analysis. The group of Actis et al. coined the term 'Nanobiopsy' because of he ability to extract very small amounts from a cell: in one of their articles they succeed in extracting volumes as small as 50 fL, which corresponded to $< 1\%$ of the total cell volume [18]. The small amount of extraction, together with the small aperture size of 50 nm invade the cell in a minimal way. Using this technique, multiple extractions from the same living cell are possible, enabling the study of genome expression over time. Moreover, multiple extractions at different locations within the same cell enabled mapping of the mRNA species to specific compartments [84].

A downside to the use of a glass femtopipette is that there is no force feedback from the tip interacting with the sample. In application to cells, this means that it is difficult to detect the cell surface for penetration. Classically, this is done by visual inspection, but when the aforementioned SICM technique is applied, the ion conductance through the femtopipette can be a measure for the distance from the tip to the sample. Similarly, one interesting technique was proposed that uses a double-barrelled glass capillary. Ion conductance from one barrel to the other was measured during the cell approach, so that when the tip comes close to an object, this flow is obstructed, indicating arrival at the cell membrane [85]. Subsequently, the cell could be injected by either of the two barrels, or a mixture thereof, enabling multi substance injection only limited by the number of barrels. The technique of using a double barrelled glass pipette had previously already shown exceptional volume dosing within liquid, where single attolitre control was reported by Rodolfa et al. [86]. In their experiment, de-ionized water was deposited on a glass coverslip submerged in organic liquid by positioning the pipette tip $\sim 100$nm above the surface, and applying a voltage pulse before quickly retracting the tip. Fluorescence microscopy was needed to determine the droplet size, as the droplets were too small to observe with a regular optical microscope. Double barrelled glass pipettes can also be used to collect a sequence of multiple samples within the same femtopipette [87].

## 2.3. FluidFM

The use of glass microcapillaries has proven invaluable for the research of cells and the fine control over depositions inside a liquid environment. However, as stated before, an important disadvantage is the lack of force sensing at the tip interface. As presented in section 2.2, some clever tricks have been invented that use electrochemical properties of the working and surrounding liquid to gain sensory information of the interface. In practice, this limits the experimental setup to the use of conducting liquids, and thereby narrows the variety of liquids that can be worked with. The AFM based concepts, described in section 2.1, inherently provide information about the forces acting between the tip and the sample. An example of the typical force response of a cell puncture is shown in figure 2.1B. This functionality is especially useful for the application to cells, where 'gentle' handling provides benefits. Moreover, the ability to sense the surface of the cell is an enabling factor for the automation of the injection process, which could significantly improve the throughput of cell injection methods [88]. In this section, the AFM based deposition methods will be taken further towards the application to single-cell analysis.

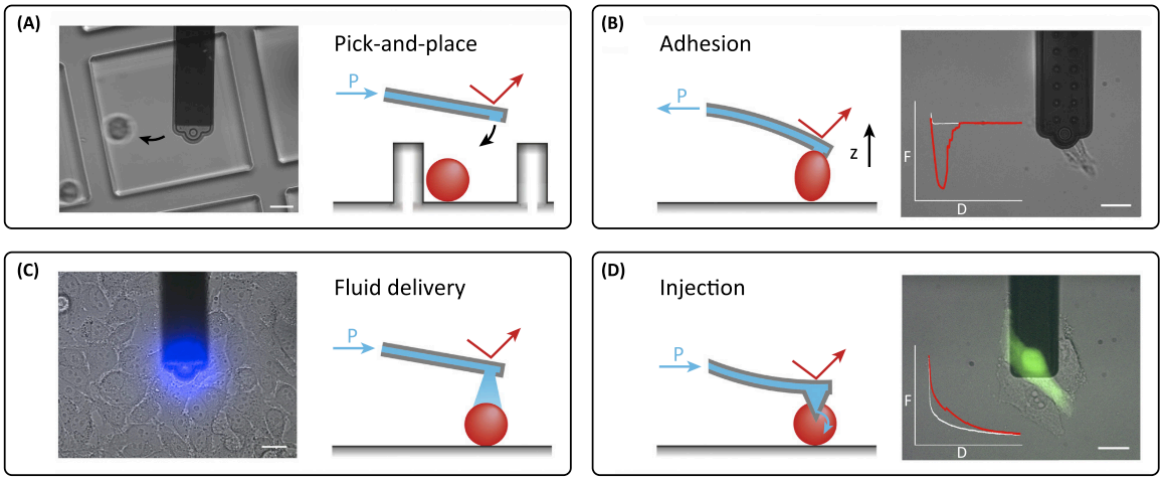


Figure 2.3: *Multiple functionalities of the FluidFM system. (A) Spatial control over cells by applying suction to temporarily adhere cells to the cantilever. (B) Adhesion force measurements of single cells. (C) Fluid delivery to single-cells. (D) Injection of single-cells. Figure adapted from [15]*

We left off in section 2.1 with the introduction of channels inside an AFM cantilever, enabling a fluidic connection between the tip and an on-chip reservoir. The stage was set for the connection of the cantilever channels to the 'outside world'. This step was first taken by the group of Meister et al. in 2009 [12], when they drilled a hole in the AFM probeholder in order to connect the hollow AFM cantilever to an off-chip pressure controller. They dubbed the system *Fluidic Force Microscopy* (FluidFM), representative of the functionalities that were now added with respect to fluid handling and operation within another fluid. Successful cell injection was reported, where they applied a pressure pulse to eject fluid from the hollow cantilever into the cell. The amount of injected fluid was estimated based on the flowrate that was determined from a numerical simulation, and was claimed to be in the order of 10 fL. Furthermore, thanks to the functionality of the AFM, a force-distance curve was obtained where penetration of the cell membrane was clearly visible.

The breakthrough of the FluidFM method also facilitated other ways to analyse single cells. The same research group continued developing the FluidFM and changed the tip of the hollow cantilever to a wider aperture so that it could now be used to 'suck' entire cells to the cantilever [89]. This proved useful to move a wide variety of single-cells from one location to another, using the force feedback so as not to damage the cells. Later, also single-cells from an adherent culture could be detached by first depositing trypsin locally, after which they could be transported by applying suction to the cantilever [90]. Subsequent studies of this group demonstrated the potential for the use in viral studies by delivering viruses to a single cell [91] and the ability to determine adhesion forces from multiple types of single living cells [92] and even bacteria [93]. The group also succeeded in injecting single-cell nuclei, but reported that the injected volume could not be reliably controlled by the pressure pulse, so that the volume could only be detected post-injection by optical inspection [94]. The lack in delivery precision was suspected to be due to varying intracellular fluid properties. An overview of several functions of the FluidFM system is represented in figure 2.3. The wide variety of uses for the FluidFM platform eventually lead several members of the group to found of a company called *Cytosurge*, that now has developed appropriate software and commercially sells the FluidFM systems [95].

In the meantime, several other research groups produced their own versions of the FluidFM system, where the main differences were mainly the microchip production processes and the way it was interfaced with the external fluid controllers [96]–[99]. In 2014, Ghatkesar et al. were the first to demonstrate pressure-controlled aspiration through the hollow cantilever using their version of the setup [98]. This principle was later used for the extraction of cellular content from single living cells in 2016 [19]. The cantilever was pre-filled with mineral oil, so that the tiny amounts of extract would not be diluted inside the cantilever channel. Cells were stained with fluorescent dye beforehand. This way, extracted amounts could be determined from the intensity of fluorescence within the transparent cantilever, as compared to a reference value. Extracted amounts ranged from 0.1 pL to 7 pL, which was reported to be the upper limit for cell viability. An aperture size of 400 nm was used, which inter-

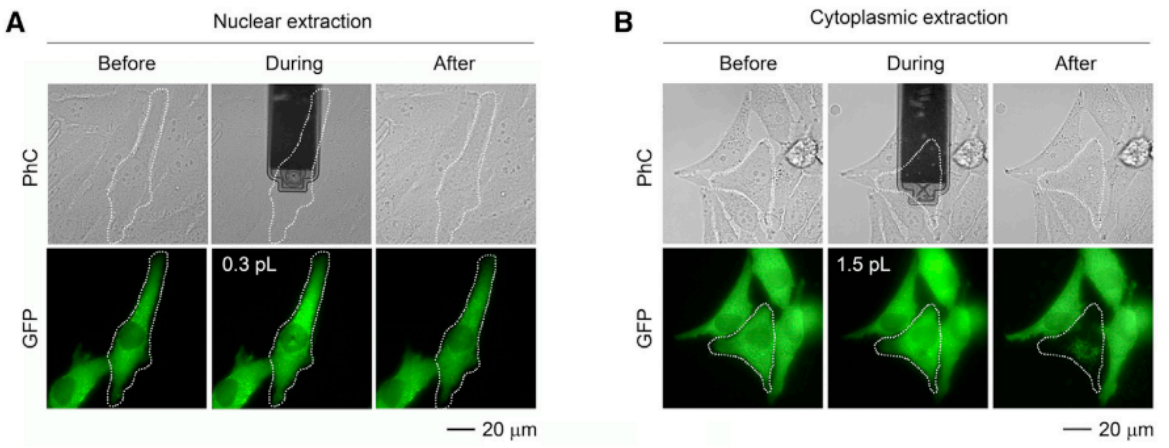


Figure 2.4: *Cells imaged before, during and after extraction of cellular content. Both optical and fluorescent images are displayed.(A) Extraction of content from the cell nucleus. (B) Extraction from the cell cytoplasma. Figure adapted from [19].*

estingly was observed to act as a filter since no particles larger than 400 nm were observed in the analysis of the extract. The surface of the cantilever was treated to prevent the adsorption of cellular content. Figure 2.4 shows successful extraction from both the cell nucleus and the cytoplasm.

Interesting additions to the functionality of the FluidFM came when an electrode was added to the fluidic interface of the cantilever. Now, the system combined the functionalities of the AFM and the SICM, bringing interesting imaging possibilities [100]. Furthermore, this system was successfully used for a so called *patch-clamp* of a cell. The added benefit was that the patch clamp could now also sense the force between the patch and the cell, allowing for a more 'gentle' patching, and control over the patch position such that it could resist vibrations, contractions and volume changes of the cell without damaging it [16].

All of the above mentioned systems are made of silicon based materials, rendering them generally hard and stiff. A few examples exist of fluidic cantilevers that are made out of polymer to enhance the flexibility and force sensitivity. Most are made of SU-8, a photoresistive polymer, because of its wide application in photolithography. The use of SU-8 AFM cantilevers has been known since 1999 [101], when it was developed mainly for its mechanical properties, but also the ease of production. Different types of hollow SU-8 cantilevers with microfluidic functionality were made later [102], [103], showing the ability to perform cell adhesion measurements [104] and spatial cell manipulation [105]. Reported advantages include higher force sensitivity and more flexibility in terms of complex design and surface modifications.

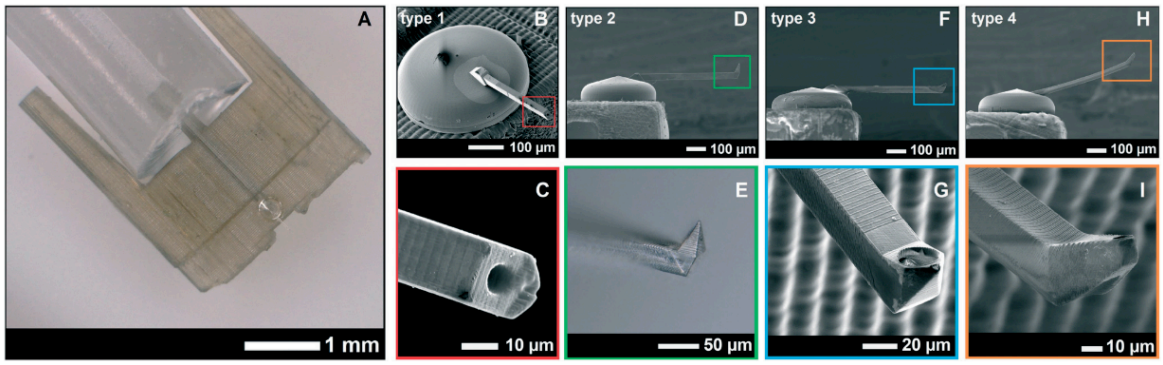


Figure 2.5: *Example of a microfluidic AFM cantilever system produced by multiscale 3D printing. (A) Overview of the whole system, including connection tube to pressure controller. (B-I) Scanning Electron Microscope (SEM) images of different cantilevers with varying tip geometries. Figure adapted from [106].*

Lastly, one method for the production of a microfluidic AFM cantilever stands out: the recent approach developed by Kramer et al. that makes use of Two-Photon-Polymerization (2PP) for 3D printing a custom, polymeric hollow cantilever on the micro scale [106]. Successful cell puncturing,

cell aspiration and AFM functionality were demonstrated. The produced device and its interface are shown in figure 2.5. This article is the only one that reported a production technique different than the classical cleanroom, photolithographic processes. It deserves special attention because this way of fabrication could greatly reduce the time and cost of the production, while offering more flexibility in terms of complex 3D design.

# 3

# Conclusion

In this part, an overview is provided of methods to transport material through the cell membrane, focussing on techniques that can target single cells. Membrane disruptive techniques were divided into permeabilization and direct penetration and each was treated in more depth. Microinjection is identified as a multifunctional tool for single-cell analysis with a wide range of applications. To deepen the understanding of the manipulation of liquid at the small scale, different mechanisms were reviewed, leading towards an overview of the different methods that have been reported for cell injection. In this context, the recent development of the FluidFM system is reviewed.

The relevant literature on cell injection is summarized in table 3.1. We can conclude that the highest resolution volume control in cell injection currently can be achieved with a glass femtopipette using the phenomena of electrowetting or thermal actuation, enabling attolitre resolution [14], [17]. However, electrowetting and thermal actuation are both limiting the choice in working liquids. Pressure based systems can handle a wider variety of fluids, but the highest resolution that can be achieved with pressure-driven cell injection is in the range of 100 fL, for both glass femtopipettes [13] and FluidFM systems [94]. Precision is predicted to be limited mainly by varying fluid properties within the cell. Evaluation of injected and extracted amounts is done optically, setting bounds on the measurement precision. Attempts have also been made to increase the throughput of single-cell injection. Automated systems have shown to be able to reach injection rates of 1500 cells per hour [75]. Automatic cell detection systems are often based on digital image processing techniques, sometimes suffering from sample transparency, cell cluttering and cell shape variations [78], [79]. Force sensing capability is recognized as a potential enabling technique that could significantly aid in the automatic injection process [88].

This survey has shown the wide variety of single-cell injection methods and the promising new developments in this field. The benefits of pressure-driven injection are discussed, but also its limits in terms of resolution are exposed. This highlights the room for possible improvement to be made in pressure-driven volume dosing. A graphical summary is provided in figure 3.1.

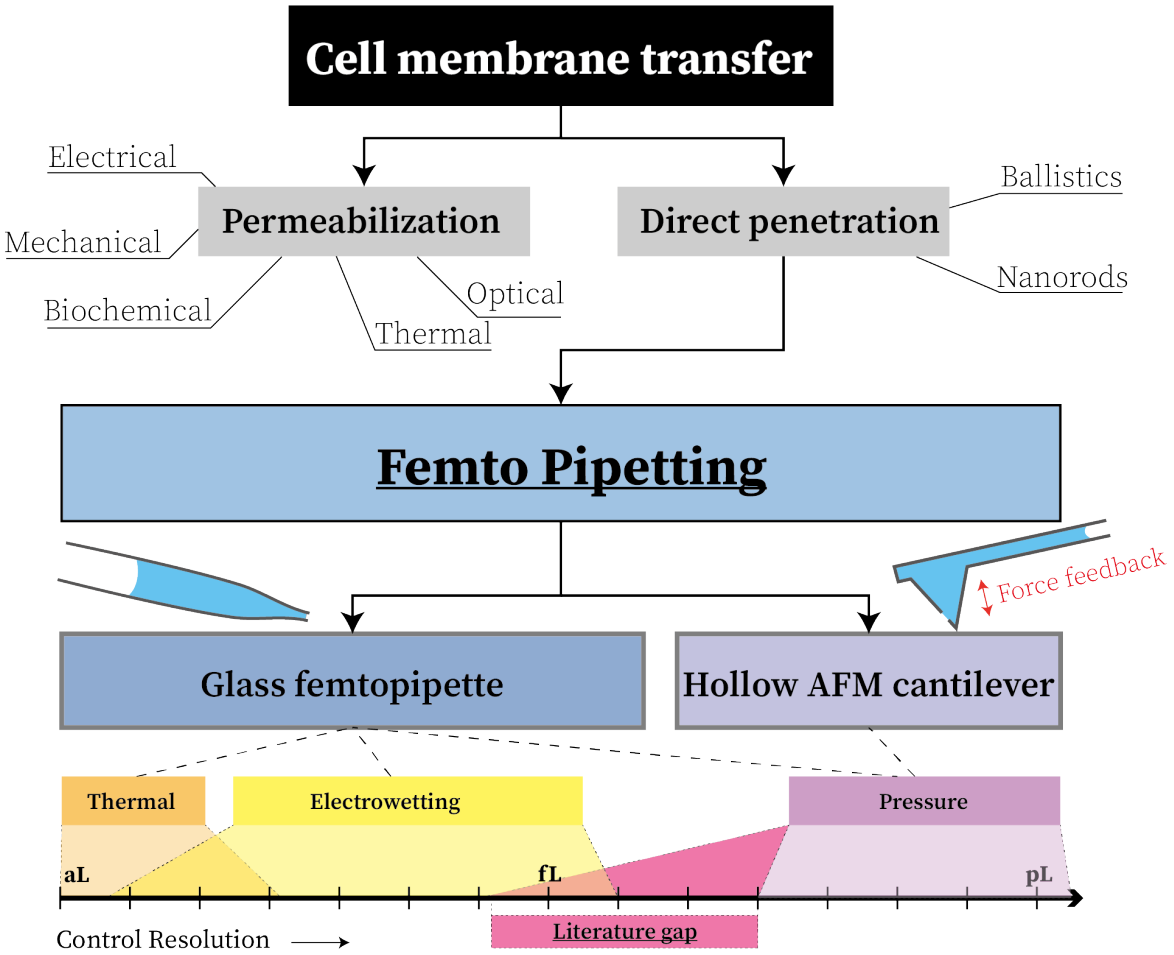


Figure 3.1: *Graphical summary of the performed literature survey. Different techniques to transport substances through the cell membrane are mentioned. The focus is laid upon femtopipetting as a precise and accurate technique. Within femtopipetting, three actuation methods were reported, and compared based on their relative volume dosing resolution.*

| Type | Aperture size | Actuation | Resolution | Material | Sensing | Cell analysis potential | Reference |
|---|---|---|---|---|---|---|---|
| Femtopipette with expanding metal particles | 100 nm | Therm. expansion | aL - fL[1] | Glass | No | Successful injection | [17] |
| Femtopipette with electrode | 50 nm | Electrowetting | 50 fL | Glass | Possible SICM | Successful extraction of cell compartments | [18] |
| Femtopipette with electrode | 100 nm | Electrowetting | 50 fL | Quartz | Possible SICM | Multiple samples from same cell | [84] |
| Femtopipette with electrode | 150 nm | Electrowetting | 25 fL | Glass | Possible SICM | Successful injection | [14] |
| Double barrelled pipette | 100 nm | Electrowetting | 5 aL - 300 fL | Glass | Possible SICM | Extreme resolution, no cell injection reported | [86] |
| Double barrelled pipette | 100 nm | Electrowetting | - | Glass | Cell surface detection | Multi component cell injection | [85] |
| Double barrelled pipette | 800 nm | Pressure | 200 pL | Glass | No | Multiple separate samples within same pipette | [87] |
| Femtopipette | 500 nm | Pressure | 100 fL | Glass | No | Successful injection | [13] |
| Microfluidic AFM cantilever | 250 nm | Pressure | 10 fL[2] | $SiO_2$ + $Si_3N_4$ | Force | Force controlled cell penetration, injection | [12] |
| Microfluidic AFM cantilever | 300 nm | Pressure | 100 fL[3] | $SiO_2$ + $Si_3N_4$ | Force | Force controlled cell penetration, successful injection | [94] |
| Microfluidic AFM cantilever | 400 nm | Pressure | 100 fL | $SiO_2$ + $Si_3N_4$ | Force | Force controlled cell penetration, succesfull extraction | [19] |
| Microfluidic AFM cantilever | 600 nm | Electro-osmosis | 100 fL | $SiO_2$ + $Si_3N_4$ | Force, possible SICM | AFM + SICM imaging, force controlled injection | [97] |
| Microfluidic AFM cantilever | 1000 nm | Pressure | - | Polymer | Force | Force controlled cell penetration, successful cell aspiration | [106] |

Table 3.1: *Overview of the state of the art in successful cell micro injection. The highest resolution in volume control is generally achieved with glass femtopipettes using either electrowetting or thermal expansion. For pressure-based systems, 100 fL seems to be the lower limit of volume resolution.*

# 4

# Research question

## 4.1. Research goal

In this survey, relevant literature is reviewed to gain an overview of the state-of-the art of existing femtopipetting techniques. The main problem found is the lack of precise control over pressure dosed volume in liquid. To the best of the authors knowledge, the best volume dosing resolution by means of pressure-actuation found in literature has a lower limit of 100 fL. This raises the question whether it could be possible to improve upon this resolution. Therefore, the ressearch question is posed as follows:

> **"How can a pressure-actuated femtopipette reach a volume dosing resolution beyond 100fL?"**

This question will be the overarching theme of this research. In the process, some other useful sub-questions are posed.

1. How can two-photon-polymerization (2PP) be applied to produce a functional femtopipette?
2. Which manufacturing method is suitable for the creation of the fluidic interface?
3. How can the functionality of a 2PP printed membrane be characterized?
4. Can the integration of phaseguides allow for discrete volume dosing control?
5. How can the wettability of a 2PP printed femtopipette be characterized?
6. What is the range of volumes that can be successfully aspirated or deposited?

## 4.2. Proposed concepts

In the previous chapters, the state of the art is reviewed, and it is concluded that there are opportunities for improvement in pressure-driven volume dosing. Therefore, in this part, two new solutions are proposed that might greatly improve the dosing resolution of a pressure-driven femtopipette.

Two versions of the proposed concept are presented in figure 4.1. In principle, the concept of a regular femtopipette is extended. In the first concept (fig. 4.1A), a membrane will be positioned between the microfluidic channel—connected to the 'outside world' pressure controller—and the nozzle. Therefore, there will be no direct fluidic connection from the 'outside world' to the sample. In this version, the membrane will fully close of the nozzle chamber. Control over the volume in the nozzle chamber is thus directly related to the deformation of this membrane. The second concept makes use of the principle of 'phaseguides' [107]. These are sudden geometrical changes, causing the liquid-air meniscus to pin at specified locations. When the liquid meniscus pins due to capillarity, an external pressure is needed to overcome this barrier. By implementing multiple phaseguides in successive steps, discrete amounts of volume could be controlled.

Both concepts will be briefly explained below, but more in-depth information can be found in the following part.

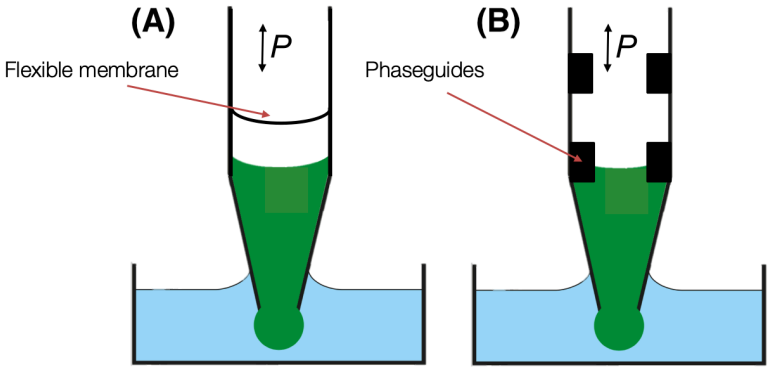


Figure 4.1: *Schematic overview of the proposed concepts to improve the resolution of pressure-based volume dosing. Two versions of this concept are proposed: (A) A closed membrane that will fully disconnect the microfluidic channel from the nozzle. Volume control will be performed by deforming the closed membrane. (B) This version incorporates so called 'Phaseguides' into the walls of the femtopipette. At specified locations, the liquid-air meniscus will pin, providing a way to control the liquid dose.*

### 4.2.1. Deflecting membrane

The nozzle will form a small chamber, bounded by the membrane and nozzle walls. In order to enable control over the aspiration or expulsion of fluid from the aperture, pressure is applied from the side of the microfluidic channel. Applied under or over pressure will deform the membrane in upward or downward direction respectively. The deformation of the membrane changes the volume of the nozzle chamber, see figure 4.2. Just like a regular syringe, where the volume inside the chamber is changed by moving the piston, fluid can be aspirated or dispensed from this chamber.

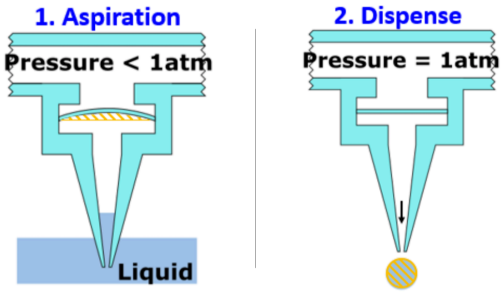


Figure 4.2: *Schematic representation of the working principle of the deflecting membrane. In this example, sample liquid is first aspirated by applying negative pressure to the microfluidic channel, which deforms the membrane upward. When the pressure is released, the membrane will elastically return to its initial position, dispensing the liquid again.*

### 4.2.2. Phaseguides

The concept of so called 'phaseguides' is an out-of-the-box idea that could serve as a back-up in the case the membrane concepts are prone to setbacks. Phaseguides are applied in microfluidic systems and their working principle relies on the phenomenon of capillarity [107]. Capillary action may be stopped by sudden geometrical changes. This was shown to be the case if the angle of the capillary $\beta$ together with the wetting angle $\theta$ is larger than 90°, in the case of figure 4.3: $\theta + \beta > 90°$. This creates the possibility to deliberately influence the behaviour of the fluid inside the channel. Vulto et al. were the first to coin the term 'phaseguides' [108], and they have been used in lab-on-a-chip applications [109] and even passive microvalves [110].

In the case of axisymmetrical phaseguides, the pressure required to overcome the barrier as shown in figure 4.3, is given by Chen et al. [111] as

$$\Delta P = \frac{2\gamma \sin(\alpha)}{R}. \tag{4.1}$$

Here, the surface tension of the liquid-air meniscus is indicated as $\gamma$ and $\alpha$ is defined as $\alpha =$

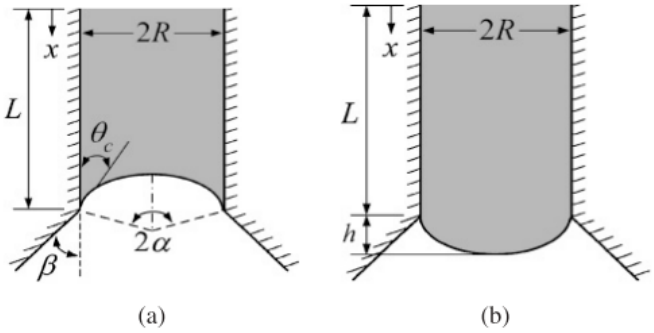


Figure 4.3: *Schematic representation of an axisymmetrical phaseguide inside a microfluidic channel. The meniscus changes from concave ($\alpha > 0$) to convex ($\alpha < 0$). Several important parameters are indicated in the figure. Adapted from [111].*

$90^\circ - \theta - \beta$, with $\theta$ the contact angle between the liquid and the solid walls, and $\beta$ the angle of the expanding walls. This expression was tested experimentally and it was shown that, indeed, the fluid is always retained at the front edge of the phaseguide before enough pressure is applied to advance the fluid meniscus.

The notion of phaseguides could also be applied inside the nozzle of the femtopipette, as shown in figure 4.4. This way, the fluid will be confined up till the next phaseguide, which may then be surpassed by varying the applied pressure. The volume that is confined is thus clearly defined by the geometry, holding the promise for very precise and controllable volume dosing.

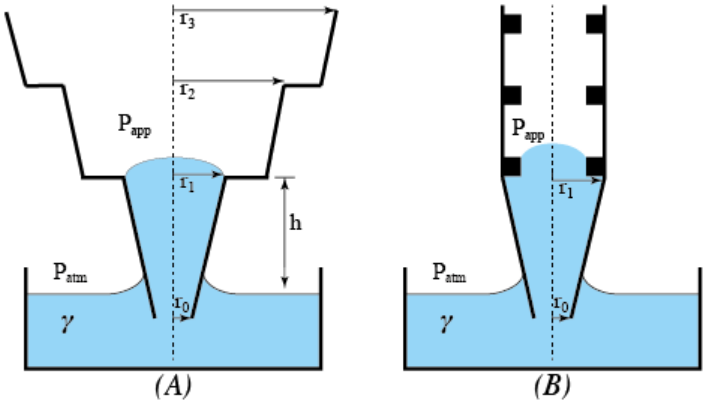


Figure 4.4: *Two conceptual versions of phaseguides applied to a femtopipette.*

The addition of a membrane or phaseguides to the principle of a femtopipette has never been performed in literature. It might offer substantial benefits, especially in application to single-cell analysis. To summarize, both concepts could have the following key benefits over the existing femtopipette concepts:

- **Decoupling of transient behaviour.** The dosing of a regular femtopipette is dependent on the magnitude and duration of the applied pressure. With these concepts, however, the displaced volume is only dependent on the deflection of the membrane or the spacing of the phaseguides. This deflection of the membrane or the bursting of a phaseguide is only dependent on the applied pressure, irrespective of the duration. This practically removes the time component from the control, removing one source of uncertainty.

- **Controlled volume displacement.** The total capacity of the fluid chamber can be chosen by design, giving an upper limit for the displaced volume.

- **No dilution of the sample.** In case of the membrane: due to the enclosed volume in the chamber, the sample fluid will not be exposed to the microfluidic channel. Therefore, the sample will not be diluted, which can greatly benefit the analysis of the sample.

- **Wide variety of fluids.** Both concepts are pressure based, and do not rely on phenomena such as electrowetting or thermal expansion. This means that the selection of fluids is not limited to the conductivity or thermal properties of the substance.

# Literature Survey References


[1] H. Gest, “The discovery of microorganisms by robert hooke and antoni van leeuwenhoek, fellows of the royal society”, *Notes and records of the Royal Society of London*, vol. 58, no. 2, pp. 187–201, 2004.

[2] A. Maton, D. Lahart, J. Hopkins, M. Q. Warner, S. Johnson, and J. D. Wright, *Cells: Building blocks of life*. Pearson Prentice Hall, 1997.

[3] E. Bianconi, A. Piovesan, F. Facchin, A. Beraudi, R. Casadei, F. Frabetti, L. Vitale, M. C. Pelleri, S. Tassani, F. Piva, *et al.*, “An estimation of the number of cells in the human body”, *Annals of human biology*, vol. 40, no. 6, pp. 463–471, 2013.

[4] S. J. Altschuler and L. F. Wu, “Cellular Heterogeneity: Do Differences Make a Difference?”, *Cell*, vol. 141, no. 4, pp. 559–563, 2010.

[5] W. P. Blackstock and M. P. Weir, “Proteomics: Quantitative and physical mapping of cellular proteins”, *Trends in Biotechnology*, vol. 17, no. 3, pp. 121–127, 1999.

[6] S. Lindström and H. Andersson-Svahn, “Overview of single-cell analyses: Microdevices and applications”, *Lab on a Chip*, vol. 10, no. 24, pp. 3363–3372, 2010.

[7] D. Wang and S. Bodovitz, “Single cell analysis: The new frontier in ’omics’”, *Trends in Biotechnology*, vol. 28, no. 6, pp. 281–290, 2010.

[8] J. R. Heath, A. Ribas, and P. S. Mischel, “Single-cell analysis tools for drug discovery and development”, *Nature Reviews Drug Discovery*, vol. 15, no. 3, pp. 204–216, 2016.

[9] G. Bulbul, G. Chaves, J. Olivier, R. Ozel, and N. Pourmand, “Nanopipettes as Monitoring Probes for the Single Living Cell: State of the Art and Future Directions in Molecular Biology”, *Cells*, vol. 7, no. 6, p. 55, 2018.

[10] P. Actis, “Sampling from Single Cells”, *Small Methods*, vol. 2, no. 3, p. 1 700 300, Mar. 2018.

[11] T. K. Chowdhury, “Fabrication of extremely fine glass micropipette electrodes”, *Journal of Physics E: Scientific Instruments*, vol. 2, no. 12, pp. 1087–1090, 1969.

[12] A. Meister, M. Gabi, P. Behr, P. Studer, J. Vörös, P. Niedermann, J. Bitterli, J. Polesel-Maris, M. Liley, H. Heinzelmann, and T. Zambelli, “FluidFM: Combining atomic force microscopy and nanofluidics in a universal liquid delivery system for single cell applications and beyond”, *Nano Letters*, vol. 9, no. 6, pp. 2501–2507, 2009.

[13] Y. T. Chow, S. Chen, R. Wang, C. Liu, C. W. Kong, R. A. Li, S. H. Cheng, and D. Sun, “Single cell transfection through precise microinjection with quantitatively controlled injection volumes”, *Scientific Reports*, vol. 6, no. April, pp. 1–9, 2016.

[14] F. O. Laforge, J. Carpino, S. A. Rotenberg, and M. V. Mirkin, “Electrochemical attosyringe”, *Proceedings of the National Academy of Sciences of the United States of America*, vol. 104, no. 29, pp. 11 895–11 900, 2007.

[15] O. Guillaume-Gentil, E. Potthoff, D. Ossola, C. M. Franz, T. Zambelli, and J. A. Vorholt, “Force-controlled manipulation of single cells: From AFM to FluidFM”, *Trends in Biotechnology*, vol. 32, no. 7, pp. 381–388, 2014.

[16] D. Ossola, M. Y. Amarouch, P. Behr, J. Vörös, H. Abriel, and T. Zambelli, “Force-controlled patch clamp of beating cardiac cells”, *Nano Letters*, vol. 15, no. 3, pp. 1743–1750, 2015.

[17] M. Knoblauch, J. M. Hibberd, J. C. Gray, and A. J. Van Bel, “A galinstan expansion femtosyringe for microinjection of eukaryotic organelles and prokaryotes”, *Nature Biotechnology*, vol. 17, no. 9, pp. 906–909, 1999.

[18] P. Actis, M. M. Maalouf, H. J. Kim, A. Lohith, B. Vilozny, R. A. Seger, and N. Pourmand, “Compartmental genomics in living cells revealed by single-cell nanobiopsy”, *ACS Nano*, vol. 8, no. 1, pp. 546–553, 2014.

[19] O. Guillaume-Gentil, R. V. V. Grindberg, R. Kooger, L. Dorwling-Carter, V. Martinez, D. Ossola, M. Pilhofer, T. Zambelli, and J. A. A. Vorholt, “Tunable Single-Cell Extraction for Molecular Analyses”, *Cell*, vol. 166, no. 2, pp. 506–516, 2016.

[20] N. J. Yang and M. J. Hinner, “Getting across the cell membrane: An overview for small molecules, peptides, and proteins”, *Site-specific protein labeling*, pp. 29–53, 2015.

[21] M. P. Stewart, R. Langer, and K. F. Jensen, “Intracellular delivery by membrane disruption: Mechanisms, strategies, and concepts”, *Chemical Reviews*, vol. 118, no. 16, pp. 7409–7531, 2018.

[22] S. Mitragotri, P. A. Burke, and R. Langer, “Overcoming the challenges in administering biopharmaceuticals: Formulation and delivery strategies”, *Nature reviews Drug discovery*, vol. 13, no. 9, pp. 655–672, 2014.

[23] M. J. Lawrence and G. D. Rees, “Microemulsion-based media as novel drug delivery systems”, *Advanced drug delivery reviews*, vol. 64, pp. 175–193, 2012.

[24] Z. Toprakcioglu, P. K. Challa, D. B. Morse, and T. Knowles, “Attoliter protein nanogels from droplet nanofluidics for intracellular delivery”, *Science Advances*, vol. 6, no. 6, pp. 1–9, 2020.

[25] G. He, N. Hu, A. M. Xu, X. Li, Y. Zhao, and X. Xie, “Nanoneedle Platforms: The Many Ways to Pierce the Cell Membrane”, *Advanced Functional Materials*, vol. 30, no. 21, pp. 1–30, 2020.

[26] A. J. Jimenez and F. Perez, “Plasma membrane repair: The adaptable cell life-insurance”, *Current opinion in cell biology*, vol. 47, pp. 99–107, 2017.

[27] E. Neumann, M. Schaefer-Ridder, Y. Wang, and P. H. Hofschneider, “Gene transfer into mouse lyoma cells by electroporation in high electric fields.”, *The EMBO journal*, vol. 1, no. 7, pp. 841–845, 1982.

[28] J. C. Weaver, “Electroporation theory”, *Plant cell electroporation and electrofusion protocols*, pp. 3–28, 1995.

[29] J. Brooks, G. Minnick, P. Mukherjee, A. Jaberi, L. Chang, H. D. Espinosa, and R. Yang, “High Throughput and Highly Controllable Methods for In Vitro Intracellular Delivery”, *Small*, vol. 16, no. 51, pp. 1–20, 2020.

[30] Y. Cao, E. Ma, S. Cestellos-Blanco, B. Zhang, R. Qiu, Y. Su, J. A. Doudna, and P. Yang, “Nontoxic nanopore electroporation for effective intracellular delivery of biological macromolecules”, *Proceedings of the National Academy of Sciences*, vol. 116, no. 16, pp. 7899–7904, 2019.

[31] E. Lestrell, F. Patolsky, N. H. Voelcker, and R. Elnathan, “Engineered nano-bio interfaces for intracellular delivery and sampling: Applications, agency and artefacts”, *Materials Today*, vol. 33, pp. 87–104, 2020.

[32] M. Fox, D. Esveld, A. Valero, R. Luttge, H. Mastwijk, P. Bartels, A. van den Berg, and R. Boom, “Electroporation of cells in microfluidic devices: A review”, *Analytical and bioanalytical chemistry*, vol. 385, no. 3, pp. 474–485, 2006.

[33] B. Babakinejad, P. Jönsson, A. López Córdoba, P. Actis, P. Novak, Y. Takahashi, A. Shevchuk, U. Anand, P. Anand, A. Drews, A. Ferrer-Montiel, D. Klenerman, and Y. E. Korchev, “Local delivery of molecules from a nanopipette for quantitative receptor mapping on live cells”, *Analytical Chemistry*, vol. 85, no. 19, pp. 9333–9342, 2013.

[34] S. S. P. Nathamgari, N. Pathak, V. Lemaitre, P. Mukherjee, J. J. Muldoon, C. Y. Peng, T. McGuire, J. N. Leonard, J. A. Kessler, and H. D. Espinosa, “Nanofountain Probe Electroporation Enables Versatile Single-Cell Intracellular Delivery and Investigation of Postpulse Electropore Dynamics”, *Small*, vol. 16, no. 43, pp. 1–12, 2020.

[35] R. N. Zare and S. Kim, “Microfluidic platforms for single-cell analysis”, *Annual Review of Biomedical Engineering*, vol. 12, pp. 187–201, 2010.

[36] A. Sharei, J. Zoldan, A. Adamo, W. Y. Sim, N. Cho, E. Jackson, S. Mao, S. Schneider, M. J. Han, A. Lytton-Jean, P. A. Basto, S. Jhunjhunwala, J. Lee, D. A. Heller, J. W. Kang, G. C. Hartoularos, K. S. Kim, D. G. Anderson, R. Langer, and K. F. Jensen, “A vector-free microfluidic platform for intracellular delivery”, *Proceedings of the National Academy of Sciences of the United States of America*, vol. 110, no. 6, pp. 2082–2087, 2013.

[37] Z. Liu, X. Han, Q. Zhou, R. Chen, S. Fruge, M. C. Jo, Y. Ma, Z. Li, K. Yokoi, and L. Qin, "Integrated Microfluidic System for Gene Silencing and Cell Migration", *Advanced Biosystems*, vol. 1, no. 6, pp. 1–7, 2017.

[38] M. E. Kizer, Y. Deng, G. Kang, P. E. Mikael, X. Wang, and A. J. Chung, "Hydroporator: A hydrodynamic cell membrane perforator for high-throughput vector-free nanomaterial intracellular delivery and dna origami biostability evaluation", *Lab on a Chip*, vol. 19, no. 10, pp. 1747–1754, 2019.

[39] M. Tsukakoshi, S. Kurata, Y. Nomiya, Y. Ikawa, and T. Kasuya, "A novel method of DNA transfection by laser microbeam cell surgery", *Applied Physics B Photophysics and Laser Chemistry*, vol. 35, no. 3, pp. 135–140, 1984.

[40] U. K. Tirlapur and K. König, "Targeted transfection by femtosecond laser", *Nature*, vol. 418, no. 6895, pp. 290–291, Jul. 2002.

[41] A. Vogel, N. Linz, S. Freidank, and G. Paltauf, "Femtosecond-laser-induced nanocavitation in water: implications for optical breakdown threshold and cell surgery", *Phys Rev Lett*, vol. 100, no. 3, p. 038 102, Jan. 2008.

[42] K. Jacobson and D. Papahadjopoulos, "Phase transitions and phase separations in phospholipid membranes induced by changes in temperature, ph, and concentration of bivalent cations", *Biochemistry*, vol. 14, no. 1, pp. 152–161, 1975, PMID: 234017.

[43] P. Karande, A. Jain, K. Ergun, V. Kispersky, and S. Mitragotri, "Design principles of chemical penetration enhancers for transdermal drug delivery", *Proc Natl Acad Sci U S A*, vol. 102, no. 13, pp. 4688–4693, Mar. 2005.

[44] J. Liu, V. Siragam, Z. Gong, J. Chen, M. D. Fridman, C. Leung, Z. Lu, C. Ru, S. Xie, J. Luo, R. M. Hamilton, and Y. Sun, "Robotic adherent cell injection for characterizing cell-cell communication", *IEEE Transactions on Biomedical Engineering*, vol. 62, no. 1, pp. 119–125, 2015.

[45] R. M. Klein, E. D. Wolf, R. Wu, and J. C. Sanford, "High-velocity microprojectiles for delivering nucleic acids into living cells. 1987.", *Biotechnology (Reading, Mass.)*, vol. 24, no. 1984, pp. 384–6, 1987.

[46] J. C. Sanford, F. D. Smith, and J. A. Russell, "Optimizing The Biolistic Process for Different Biological Applications", *Methods in Enzymology*, vol. 217, no. C, pp. 483–509, 1993.

[47] T. E. McKnight, A. V. Melechko, G. D. Griffin, M. A. Guillorn, V. I. Merkulov, F. Serna, D. K. Hensley, M. J. Doktycz, D. H. Lowndes, and M. L. Simpson, "Intracellular integration of synthetic nanostructures with viable cells for controlled biochemical manipulation", *Nanotechnology*, vol. 14, no. 5, p. 551, 2003.

[48] K. Yum, N. Wang, and M. F. Yu, "Nanoneedle: A multifunctional tool for biological studies in living cells", *Nanoscale*, vol. 2, no. 3, pp. 363–372, 2010.

[49] X. Chen, A. Kis, A. Zettl, and C. R. Bertozzi, "A cell nanoinjector based on carbon nanotubes", *Proceedings of the National Academy of Sciences of the United States of America*, vol. 104, no. 20, pp. 8218–8222, 2007.

[50] R. Singhal, Z. Orynbayeva, R. V. K. Sundaram, J. J. Niu, S. Bhattacharyya, E. A. Vitol, M. G. Schrlau, E. S. Papazoglou, G. Friedman, and Y. Gogotsi, "Multifunctional carbon-nanotube cellular endoscopes", *Nature Nanotechnology*, vol. 6, no. 1, pp. 57–64, 2011.

[51] I. Obataya, C. Nakamura, S. W. Han, N. Nakamura, and J. Miyake, "Nanoscale Operation of a Living Cell Using an Atomic Force Microscope with a Nanoneedle", *Nanobiotechnology*, vol. 1, no. 4, pp. 347–352, 2005.

[52] T. Osada, H. Uehara, H. Kim, and A. Ikai, "mRNA analysis of single living cells", *Journal of Nanobiotechnology*, vol. 1, pp. 1–8, 2003.

[53] C. Ru, J. Luo, S. Xie, and Y. Sun, "A review of non-contact micro- and nano-printing technologies", *Journal of Micromechanics and Microengineering*, vol. 24, no. 5, 2014.

[54] Y. Guo, H. S. Patanwala, B. Bognet, and A. W. Ma, "Inkjet and inkjet-based 3D printing: Connecting fluid properties and printing performance", *Rapid Prototyping Journal*, vol. 23, no. 3, pp. 562–576, 2017.

[55] M. Penedo, T. Shirokawa, M. S. Alam, K. Miyazawa, T. Ichikawa, N. Okano, H. Furusho, C. Nakamura, and T. Fukuma, “Cell penetration efficiency analysis of different atomic force microscopy nanoneedles into living cells”, *Scientific Reports*, vol. 11, no. 1, pp. 1–8, 2021.

[56] G. Binnig, H. Rohrer, C. Gerber, and E. Weibel, “Surface Studies by Scanning Tunneling Microscopy”, *Physical Review Letters*, vol. 49, no. 1, pp. 57–61, Jul. 1982.

[57] G. Binnig and C. Quate, “Atomic Force Microscope”, *Physical review letters*, vol. 56, no. 9, p. 930, 1986.

[58] D. J. Müller and Y. F. Dufrene, “Atomic force microscopy as a multifunctional molecular toolbox in nanobiotechnology”, *Nanoscience and technology: A collection of reviews from nature journals*, pp. 269–277, 2010.

[59] B. Drake, C. B. Prater, A. L. Weisenhorn, S. A. Gould, T. R. Albrecht, C. F. Quate, D. S. Cannell, H. G. Hansma, and P. K. Hansma, “Imaging crystals, polymers, and processes in water with the atomic force microscope”, *Science*, vol. 243, no. 4898, pp. 1586–1589, 1989.

[60] S. Herminghaus, A. Fery, and D. Reim, “Imaging of droplets of aqueous solutions by tapping-mode scanning force microscopy”, *Ultramicroscopy*, vol. 69, no. 3, pp. 211–217, 1997.

[61] R. D. Piner, J. Zhu, F. Xu, and S. Hong, ““Dip-Pen” Nanolithography”, *Science*, vol. 283, no. January, pp. 661–663, 1999.

[62] A. Meister, S. Jeney, M. Liley, T. Akiyama, U. Staufer, N. F. De Rooij, and H. Heinzelmann, “Nanoscale dispensing of liquids through cantilevered probes”, *Microelectronic Engineering*, vol. 67-68, no. 2003, pp. 644–650, 2003.

[63] A. Meister, M. Liley, J. Brugger, R. Pugin, and H. Heinzelmann, “Nanodispenser for atto-liter volume deposition using atomic force microscopy probes modified by focused-ion-beam milling”, *Applied Physics Letters*, vol. 85, no. 25, pp. 6260–6262, 2004.

[64] K. Kaisei, N. Satoh, K. Kobayashi, K. Matsushige, and H. Yamada, “Nanoscale liquid droplet deposition using the ultrasmall aperture on a dynamic mode AFM tip”, *Nanotechnology*, vol. 22, no. 17, 2011.

[65] K. H. Kim, N. Moldovan, C. Ke, and H. D. Espinosa, “A novel AFM chip for fountain pen nanolithography - Design and microfabrication”, *Materials Research Society Symposium - Proceedings*, vol. 782, pp. 267–272, 2003.

[66] K. H. Kim, N. Moldovan, and H. D. Espinosa, “A Nanofountain Probe with Sub-100 nm Molecular Writing Resolution”, *Small*, vol. 1, no. 6, pp. 632–635, Jun. 2005.

[67] N. Moldovan, K. H. Kim, and H. D. Espinosa, “Design and fabrication of a novel microfluidic nanoprobe”, *Journal of Microelectromechanical Systems*, vol. 15, no. 1, pp. 204–213, 2006.

[68] H. H. Perez Garza, M. K. Ghatkesar, P. Lothman, A. Manz, and U. Staufer, “Enabling local deposition and controlled synthesis of Au-nanoparticles using a femtopipette”, *9th IEEE International Conference on Nano/Micro Engineered and Molecular Systems, IEEE-NEMS 2014*, pp. 323–328, 2014.

[69] H. H. Perez Garza, M. K. Ghatkesar, and U. Staufer, “Combined AFM—nanopipette cartridge system for actively dispensing femtolitre droplets”, *Journal of Micro-Bio Robotics*, vol. 8, no. 1, pp. 33–40, 2013.

[70] ——, “Aspiration through hollow cantilever□based nanopipette by means of evaporation”, *Micro & Nano Letters*, vol. 8, no. 11, pp. 758–761, Nov. 2013.

[71] M. K. Ghatkesar, H. H. Perez Garza, F. Heuck, and U. Staufer, “Scanning probe microscope-based fluid dispensing”, *Micromachines*, vol. 5, no. 4, pp. 954–1001, 2014.

[72] X. Cao, R. de Gruiter, R. van Oorschot, S. Baldi, H. HosseinNia, and M. K. Ghatkesar, “A model for controlled dosing of femto-litre volume liquids using hollow microcantilever”, *IFAC-PapersOnLine*, vol. 50, no. 1, pp. 15 542–15 547, 2017.

[73] E. J. Verlinden, M. Madadelahi, E. Sarajlic, A. Shamloo, A. H. Engel, U. Staufer, and M. K. Ghatkesar, “Volume and concentration dosing in picolitres using a two-channel microfluidic AFM cantilever”, *Nanoscale*, vol. 12, no. 18, pp. 10 292–10 305, May 2020.

[74] M. A. Barber, “A technic for the inoculation of bacteria and other substances into living cells”, *Journal of Infectious Diseases*, vol. 8, no. 3, pp. 348–360, 1911.

[75] R. Pepperkok, C. Schneider, L. Philipson, and W. Ansorge, “Single cell assay with an automated capillary microinjection system”, *Experimental Cell Research*, vol. 178, no. 2, pp. 369–376, Oct. 1988.

[76] W. Wang, Y. Sun, M. Zhang, R. Anderson, L. Langille, and W. Chan, “A system for high-speed microinjection of adherent cells”, *Review of Scientific Instruments*, vol. 79, no. 10, 2008.

[77] F. Pan, S. Chen, Y. Jiao, Z. Guan, A. Shakoor, and D. Sun, “Automated high-productivity microinjection system for adherent cells”, *IEEE Robotics and Automation Letters*, vol. 5, no. 2, pp. 1167–1174, 2020.

[78] X. Long, W. L. Cleveland, and Y. L. Yao, “A new preprocessing approach for cell recognition”, *IEEE Transactions on Information Technology in Biomedicine*, vol. 9, no. 3, pp. 407–412, 2005.

[79] F. Mualla, S. Schöll, B. Sommerfeldt, A. Maier, and J. Hornegger, “Automatic cell detection in bright-field microscope images using sift, random forests, and hierarchical clustering”, *IEEE transactions on medical imaging*, vol. 32, no. 12, pp. 2274–2286, 2013.

[80] Y. Zhang, C. B. Ballas, and M. P. Rao, “Towards ultrahigh throughput microinjection: MEMS-based massively-parallelized mechanoporation”, *Proceedings of the Annual International Conference of the IEEE Engineering in Medicine and Biology Society, EMBS*, pp. 594–597, 2012.

[81] T. V. Tsulaia, N. L. Prokopishyn, A. Yao, N. D. Carsrud, M. C. Carou, D. B. Brown, B. R. Davis, and J. Yannariello-Browna, “Glass needle-mediated microinjection of macromolecules and transgenes into primary human mesenchymal stem cells”, *Journal of Biomedical Science*, vol. 10, no. 3, pp. 328–336, 2003.

[82] P. K. Hansma, B. Drake, O. Marti, A. C. Gould, and C. B. Prater, “The Scanning Ion-Conductance”, *Source: Science, New Series Eds. (Ant. Museum-Ephe*, vol. 3, no. 1966, pp. 1–3, 1987.

[83] M. J. Lab, A. Bhargava, P. T. Wright, and J. Gorelik, “The scanning ion conductance microscope for cellular physiology”, *American Journal of Physiology-Heart and Circulatory Physiology*, vol. 304, no. 1, H1–H11, 2013.

[84] E. N. Tóth, A. Lohith, M. Mondal, J. Guo, A. Fukamizu, and N. Pourmand, “Single-cell nanobiopsy reveals compartmentalization of mRNAs within neuronal cells”, *Journal of Biological Chemistry*, vol. 293, no. 13, pp. 4940–4951, 2018.

[85] R. A. Seger, P. Actis, C. Penfold, M. Maalouf, B. Vilozny, and N. Pourmand, “Voltage controlled nano-injection system for single-cell surgery”, *Nanoscale*, vol. 4, no. 19, pp. 5843–5846, 2012.

[86] K. T. Rodolfa, A. Bruckbauer, D. Zhou, A. I. Schevchuk, Y. E. Korchev, and D. Klenerman, “Nanoscale pipetting for controlled chemistry in small arrayed water droplets using a double-barrel pipet”, *Nano Letters*, vol. 6, no. 2, pp. 252–257, 2006.

[87] A. Saha-Shah, C. M. Green, D. H. Abraham, and L. A. Baker, “Segmented flow sampling with push-pull theta pipettes”, *Analyst*, vol. 141, no. 6, pp. 1958–1965, 2016.

[88] Z. Chi, Q. Xu, and L. Zhu, “A Review of Recent Advances in Robotic Cell Microinjection”, *IEEE Access*, vol. 8, no. 2, pp. 8520–8532, 2020.

[89] P. Dörig, P. Stiefel, P. Behr, E. Sarajlic, D. Bijl, M. Gabi, J. Vörös, J. A. Vorholt, and T. Zambelli, “Force-controlled spatial manipulation of viable mammalian cells and micro-organisms by means of FluidFM technology”, *Applied Physics Letters*, vol. 97, no. 2, pp. 1–4, 2010.

[90] O. Guillaume-Gentil, T. Zambelli, and J. A. Vorholt, “Isolation of single mammalian cells from adherent cultures by fluidic force microscopy”, *Lab on a Chip*, vol. 14, no. 2, pp. 402–414, 2014.

[91] P. Stiefel, F. I. Schmidt, P. Dörig, P. Behr, T. Zambelli, J. A. Vorholt, and J. Mercer, “Cooperative vaccinia infection demonstrated at the single-cell level using fluiDFM”, *Nano Letters*, vol. 12, no. 8, pp. 4219–4227, 2012.

[92] E. Potthoff, O. Guillaume-Gentil, D. Ossola, J. Polesel-Maris, S. LeibundGut-Landmann, T. Zambelli, and J. A. Vorholt, “Rapid and Serial Quantification of Adhesion Forces of Yeast and Mammalian Cells”, *PLoS ONE*, vol. 7, no. 12, 2012.

[93] E. Potthoff, D. Ossola, T. Zambelli, and J. A. Vorholt, “Bacterial adhesion force quantification by fluidic force microscopy”, *Nanoscale*, vol. 7, no. 9, pp. 4070–4079, 2015.

[94] O. Guillaume-Gentil, E. Potthoff, D. Ossola, P. Dörig, T. Zambelli, and J. A. Vorholt, “Force-controlled fluidic injection into single cell nuclei”, *Small*, vol. 9, no. 11, pp. 1904–1907, 2013.

[95] C. AG, *Cytosurge company website*, `https://www.cytosurge.com`, 2021.

[96] N. Kato, T. Kawashima, T. Shibata, T. Mineta, and E. Makino, “Micromachining of a newly designed AFM probe integrated with hollow microneedle for cellular function analysis”, *Microelectronic Engineering*, vol. 87, no. 5-8, pp. 1185–1189, 2010.

[97] T. Shibata, K. Nakamura, S. Horiike, M. Nagai, T. Kawashima, T. Mineta, and E. Makino, “Fabrication and characterization of bioprobe integrated with a hollow nanoneedle for novel AFM applications in cellular function analysis”, *Microelectronic Engineering*, vol. 111, pp. 325–331, 2013.

[98] M. K. Ghatkesar, H. H. Perez Garza, and U. Staufer, “Hollow AFM cantilever pipette”, *Microelectronic Engineering*, vol. 124, pp. 22–25, 2014.

[99] R. van Oorschot, H. H. Perez Garza, R. J. S. Derks, U. Staufer, and M. K. Ghatkesar, “A microfluidic AFM cantilever based dispensing and aspiration platform”, *EPJ Techniques and Instrumentation*, vol. 2, no. 1, p. 4, Dec. 2015.

[100] D. Ossola, L. Dorwling-Carter, H. Dermutz, P. Behr, J. Vörös, and T. Zambelli, “Simultaneous Scanning Ion Conductance Microscopy and Atomic Force Microscopy with Microchanneled Cantilevers”, *Physical Review Letters*, vol. 115, no. 23, pp. 1–5, 2015.

[101] G. Genolet, J. Brugger, M. Despont, U. Drechsler, P. Vettiger, N. F. De Rooij, and D. Anselmetti, “Soft, entirely photoplastic probes for scanning force microscopy”, *Review of Scientific Instruments*, vol. 70, no. 5, pp. 2398–2401, 1999.

[102] A. Gaitas and R. W. Hower, “SU-8 microcantilever with an aperture, fluidic channel, and sensing mechanisms for biological and other applications”, *Journal of Micro/Nanolithography, MEMS, and MOEMS*, vol. 13, no. 3, p. 030 501, Sep. 2014.

[103] H. Han, V. Martinez, M. J. Aebersold, I. Lüchtefeld, J. Polesel-Maris, J. Vörös, and T. Zambelli, “Force controlled SU-8 micropipettes fabricated with a sideways process”, *Journal of Micromechanics and Microengineering*, vol. 28, no. 9, 2018.

[104] V. Martinez, P. Behr, U. Drechsler, J. Polesel-Maris, E. Potthoff, J. Vörös, and T. Zambelli, “SU-8 hollow cantilevers for AFM cell adhesion studies”, *Journal of Micromechanics and Microengineering*, vol. 26, no. 5, p. 055 006, May 2016.

[105] V. Martinez, C. Forró, S. Weydert, M. J. Aebersold, H. Dermutz, O. Guillaume-Gentil, T. Zambelli, J. Vörös, and L. Demkó, “Controlled single-cell deposition and patterning by highly flexible hollow cantilevers”, *Lab on a Chip*, vol. 16, no. 9, pp. 1663–1674, 2016.

[106] R. C. L. N. Kramer, E. J. Verlinden, L. Angeloni, A. van den Heuvel, L. E. Fratila-Apachitei, S. M. van der Maarel, and M. K. Ghatkesar, “Multiscale 3D-printing of microfluidic AFM cantilevers”, *Lab on a Chip*, vol. 20, no. 2, pp. 311–319, Jan. 2020.

[107] P. Vulto, S. Podszun, P. Meyer, C. Hermann, A. Manz, and G. A. Urban, “Phaseguides: A paradigm shift in microfluidic priming and emptying”, *Lab on a Chip*, vol. 11, no. 9, pp. 1596–1602, 2011.

[108] P. Vulto, G. Medoro, L. Altomare, G. Urban, M. Tartagni, R. Guerrieri, and N. Manaresi, “Selective sample recovery of dep-separated cells and particles by phaseguide-controlled laminar flow”, *Journal of Micromechanics and Microengineering*, vol. 16, no. 9, p. 1847, 2006.

[109] P. Vulto, S. Podszun, P. Meyer, and G. A. Urban, “Phaseguide patterns for advanced liquid handling in lab-on-a-chip systems”, *TRANSDUCERS 2009 - 15th International Conference on Solid-State Sensors, Actuators and Microsystems*, pp. 409–412, 2009.

[110] E. Yildirim, S. J. Trietsch, J. Joore, A. Van Den Berg, T. Hankemeier, and P. Vulto, “Phaseguides as tunable passive microvalves for liquid routing in complex microfluidic networks”, *Lab on a Chip*, vol. 14, no. 17, pp. 3334–3340, 2014.

[111] J. M. Chen, C. Y. Chen, and C. H. Liu, “Pressure barrier in an axisymmetric capillary microchannel with sudden expansion”, *Japanese Journal of Applied Physics*, vol. 47, no. 3 PART 1, pp. 1683–1689, 2008.

# II

# Project

# Introduction

In this part, the two concepts that were proposed in section 4.2 will be treated in more depth. Each concept has the goal of increasing the volume dosing resolution on the microscale by means of pressure actuation, but both exploit a different strategy to accomplish this.

Both concepts deserve their own chapter, which is written in the format of a scientific paper. Each chapter is meant to be readable as a stand-alone paper. Note that due to the similarity in the background of the problem that these concepts try to tackle, largely the same introduction is used in both papers. The production methods also overlap.

# 5

# Membrane controlled dosing

# Liquid dosing on the micro-scale: femtopipette with embedded membrane

**Abstract**

Femtopipettes are tools that are used to aspirate and dispense liquids on the micro scale with high positional accuracy. When combined with Atomic Force Microscopy (AFM), these microfluidic devices form a powerful means to perform research on the single-cellular level. Pressure is the most common way to actuate femtopipettes. The smallest volumes are achieved by applying a short pressure pulse, but the resulting dosing resolution is limited. In this work, a new femtopipette concept is proposed that makes use of a flexible membrane barrier to dose liquid by deformation of the membrane. Using a multiscale 3D printing strategy combining stereolithography and two-photon-polymerization, membranes with thickness down to 440nm are fabricated and characterized. Liquid behaviour was tested with a microchannel with integrated membrane, submerged in DI-water. The liquid meniscus was controllable to some extend, but the deflected volume is significantly bigger than expected. The membranes are suspected to be slightly porous making the liquid dosing results ambiguous.

## 5.1. Introduction

Understanding the functioning of cells is of paramount importance for biology and medicine. The research of individual cells is a topic of increasing scientific efforts. Classical methods usually involve steps to sort and/or isolate the cells of interest, after which the cell is opened by lysis or microdissection to gain access to the cell content [1], [2]. Although a lot of insight can be gained this way, obvious disadvantages in most such methods are that the cells are analysed away from their natural environment and are often killed in the process. New and innovative methods have been proposed more recently, that study the contents of cells while they stay alive [3]. An important factor for this way of analysis is the controlled transport of substances of interest through the cell membrane and many methods have been invented for this purpose [4]. Among these methods, the so called femtopipette is a very promising and versatile technique due to its positional accuracy and the possibility for both extraction and delivery of substances in a single living cell [5].

Classically, femtopipettes are fabricated by heating and pulling a glass tube, and modern methods can achieve apertures of several tens of nanometers. Positioning such femtopipettes often relies on optical feedback, and it is difficult to asses whether the targeted cell is indeed penetrated or not.

An interesting extension to the functionality of the femtopipette was proposed by Meister et al. when they made a hollow cantilever for an atomic force microscope (AFM) [6]. They were the first to connect the cantilever to a pressure source such that liquid could be flown through the tip, yielding the appropriate name ‘FluidFM’. The additional gained force feedback provided by the AFM system proved useful to detect contact with the cell surface and even penetration of the cell membrane. Successful injection as well as aspiration was established on living cells [7], [8]. Moreover, cell adhesion force measurements and pick-and-place functionality have been demonstrated using the FluidFM system [9], [10].

Different experiments often require a specific cantilever and/or tip shape design, but since most AFM cantilevers are fabricated by means of photolithography steps, customization is lengthy and precious. An interesting advancement was provided by Kramer et al. when they made a fully functional microfluidic AFM cantilever by means of additive manufacturing [11]. Using digital light processing (DLP) combined with two-photon-polymerization (2PP) allowed for more design freedom whilst also significantly reducing the production time.

For controlling the amount of liquid that is pipetted within a liquid environment, three different actuation methods have been reported: thermally driven, electrochemically driven and pressure driven. Respectively, the first two have been able to obtain volume resolutions down to the attolitre level (1 aL = $10^{-18}$L) [12], [13], but the disadvantage is that these techniques limit the choice of working liquids. Pressure remains the most straightforward actuation method and allows for the widest range of substances to be handled—a useful aspect, especially concerning cell biology. However, the resolution of pressure driven methods is relatively low, with the best results in literature coming down to approximately 100 femtolitre (1 fL = $10^{-15}$L), albeit, with substantial uncertainty [7], [8], [14].

Being able to easily control the volume dosing with higher resolution could be a major enabling factor for single-cell research. Firstly, smaller

samples being injected or aspirated interfere less with the natural functioning of the cell. Secondly, higher specificity in targeting may result in more detailed cell analysis. Finally, supplying cells with an accurate dose could be important for small scale drug testing.

Other envisaged applications in nanotechnology can also greatly benefit from high resolution liquid dosing. For example, delivery of small amounts of substances to nano-sensors or transmission-electron-microscope (TEM) windows could also benefit from increased resolution [15].

Therefore, the goal of this research is aimed to increase the resolution of pressure driven femtopipetting systems. A new femtopipette concept is proposed based on the design and production methods of Kramer et al. [11]. This way, the femtopipette may also benefit from the AFM functionality that was demonstrated by Kramer et al. and Van Altena et al. [11], [16]. Furthermore, the proposed concept introduces a physical barrier in the form of a flexible membrane into the femtopipette. When pressure is applied, this membrane will deform, causing a certain volume to be displaced by the deforming membrane. It is expected that this deformation can be controlled and calibrated, possibly enabling predictable volume dosing.

In the following section, first the relevant theory behind the working of this concept is treated. In the subsequent sections, the experimental methodology is treated, as well as the results and conclusions.

## 5.2. Theory

### 5.2.1. Membrane mechanics

To calculate the mechanical deformation of the membrane, classical plate theory is applied. The following calculations are based on a circular membrane design. For the calculations, we refer to the classical plate theory developed by Timoshenko [17]. This theoretical model is valid for small deflections, and it is widely used in micro-engineering applications [18], [19]. The deflection of a circular plate[1] that is clamped at its perimeter is given by the following equation [17]:

$$w(r) = \frac{P\ a^4}{64\ D}\left(1 - \left(\frac{r}{a}\right)^2\right)^2, \tag{5.1}$$

where, $w$ is the deflection, as a function of the radius $r$, $P$ is the applied pressure, $a$ is the radius of the plate and $D$ is the so called 'bending rigidity'. The bending rigidity is a measure for the 'resistance to bending' that the plate has, and is given by

$$D = \frac{E\ t^3}{12\ (1 - v^2)}, \tag{5.2}$$

with $E$ the Youngs modulus of the material, $t$ the thickness of the plate and $v$ the Poisson ratio. In the following calculations, typical material properties of cured IP-Dip (Nanoscribe GmbH) are used: $E = 2.0$ GPa, $v = 0.35$ [20].

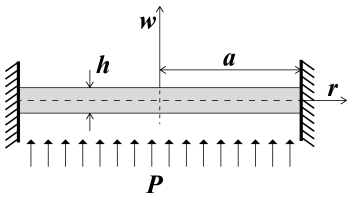


Figure 5.1: *Schematic 2D representation of the membrane as a plate model with clamped boundaries. Illustration of the parameters used in this section.*

The maximum deflection occurs at the center of the membrane, at $r = 0$. From equation (5.1) this yields:

$$w_{\max} = \frac{P\ a^4}{64\ D}. \tag{5.3}$$

For the application to a femtopipette, it is important to know the volume that gets displaced by the deflection of the membrane. This can be determined by 'revolving' the deflection curve around the y-axis. To do this, first, equation (5.1) is rewritten to isolate the radius as a function of deflection[2]:

$$r(w) = -\sqrt{a^2 - \frac{8\sqrt{\mathrm{D}}\sqrt{w}}{\sqrt{P}}}. \tag{5.4}$$

The displaced volume can then be obtained by integrating the circular surface (dependent on $r(w)$) around the y-axis from 0 to $w_{max}$:

$$V = \pi \int_0^{w_{\max}} r^2\,(w)\,\mathrm{d}w. \tag{5.5}$$

Substituting equation (5.4) and solving yields:

$$V = \pi\left(a^2\, w_{\max} - \frac{16\sqrt{\mathrm{D}}\, {w_{\max}}^{3/2}}{3\sqrt{P}}\right). \tag{5.6}$$

Since the envisioned manufacturing technique allows for a lot of freedom in the geometrical design of the membrane, it is useful to get a

[1] Note that the term 'plate' is adopted in this context because the word 'membrane' is used in plate theory to indicate a plate without bending rigidity [17].

[2] Note that there are four roots when solving eq.5.1 for $r$. Since the radius cannot be negative, one of the two symmetric positive outcomes is taken.

better understanding of how the geometrical parameters influence the displaced volume. The influence of the geometrical parameters is portrayed in figure 5.3. As expected, bigger membrane radii increase the displaced volume. Also, thinner membranes tend to deflect more due to their lower bending rigidity (eq. (5.2)) and thus displace more volume.

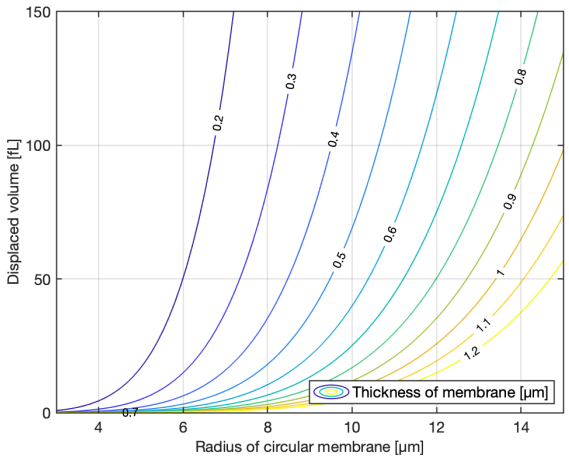


Figure 5.3: *Plot of the displaced volume for changing geometrical parameters. Different values of the membrane radius and thickness are shown while the material properties are held constant, and a pressure of* 1bar *is applied.*

To quickly investigate whether the stresses in the deflecting membrane might be a limiting factor, an analytical expression can be obtained from the classical plate theory. Here we are primarily interested in the maximum stress and its location of occurrence. The radial stress distribution for a set height $z$ within the circular plate with thickness $t$ is given by [17]:

$$\sigma_R = -\frac{3\,P\,z\left(r^2\,(v+3) - a^2\,(v+1)\right)}{4\,t^3}. \tag{5.7}$$

The maximum stress will occur in the radial direction, at the edges on the outer surfaces of the circular plate, $r = a,\ z = t/2$. Filling these in into equation (5.7) yields an expression for the maximum stress:

$$\sigma_{R,max} = -\frac{3\,P\,a^2}{4\,t^2}. \tag{5.8}$$

As an example, for the typical envisioned geometrical values (membrane thickness $t$ = 400 nm, membrane radius $a$ = 10µm, pressure $P = 10^5$ Pa) the maximum stress would become $\pm$ 46.875 MPa. This seems to be well within the range of allowable stress as reported in literature [21].

### 5.2.2. Liquid behaviour

A functional femtopipetting device is envisioned where a 2PP printed cantilever leads to the nozzle-chamber that is closed off by the membrane, see figure 5.7A. This scenario can be simplified by merely looking at the liquid behaviour inside nozzle-chamber. In general, it is expected that some amount of liquid will enter spontaneously due to capillarity. After equilibrium is reached, the membrane can be actuated, thus controlling the position of the liquid position.

Capillary pressure causes liquid to enter small channels (capillaries) that are hydrophilic, meaning, the wetting angle $\theta$ between the material and the liquid is less than $90°$. The wetting of the walls of a capillary cause the liquid to form a spherical meniscus. Due to the spherical form, the Laplace

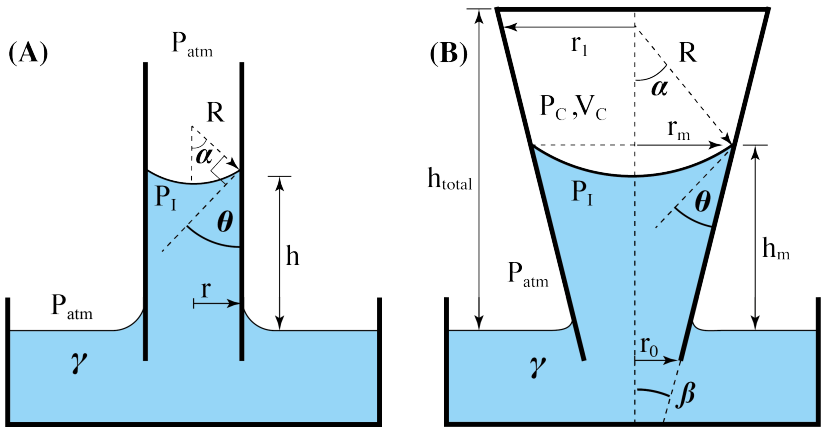


Figure 5.2: *Two different scenarios of capillary rise. In general, the liquids will rise in the capillaries until the capillary pressure is counteracted by an opposing force. In (A) this opposing force can be gravity, but this is assumed negligible at the microscale. In (B), the rising column causes the pressure of the trapped gas to rise until an equilibrium is met. The slanted walls represent a more realistic geometry for the nozzle of a femtopipette. The radius of the rising liquid meniscus thus increases with height, effectively lowering the capillary pressure.*

pressure $\Delta P = \frac{2\gamma}{R}$ comes into effect that works to minimize the surface area of the meniscus. The total capillary pressure also depends on the surface tension $\gamma$ of the liquid, and is given by the Young-Laplace equation

$$\Delta P = P_{atm} - P_l = \frac{2\,\gamma}{R}, \tag{5.9}$$

where $P_l$ is the pressure on the liquid-side of the meniscus. The spherical radius $R$ can in turn be expressed in terms of the wetting angle $\theta$ and the radius of the capillary $r$ as depicted in figure 5.2. According to simple geometry, $\cos(\theta) = \frac{r}{R}$, so that equation (5.9A) becomes

$$\Delta P = P_{atm} - P_l = \frac{2\,\gamma\,\cos(\theta)}{r}. \tag{5.10}$$

From this equation we can see that the capillary pressure increases for increasing surface tension $\gamma$, decreasing wetting angle $\theta$ and decreasing capillary radius $r$. The scenario can be expanded to accommodate for slanted walls such as in figure 5.2B. Here, it is best to define an angle $\alpha$ that describes the arc of the meniscus and is given as $\alpha = 90° - \theta - \beta$. Then, adjusting equation (5.10) yields

$$\Delta P = P_{atm} - P_l = \frac{2\,\gamma\,\sin(\alpha)}{r_m}, \tag{5.11}$$

with $r_m$ the effective radius of the meniscus, dependent on the height $h_m$.

Now in principle the capillary pressure causes the liquid to rise until it is being counteracted by an opposing force or geometrical change. Two different scenarios that are depicted in figure 5.2. In figure 5.2A, a classical capillary is depicted where the liquid will generally continue to rise until a hydrostatic equilibrium is reached, balanced by the gravitational force on the liquid column. However, in view of the dimensions of this concept (capillaries in the order of 20µm), the increase in hydrostatic pressure as a consequence of capillary rise are negligible. In figure 5.2B, the top of the capillary is closed, so that the rising column will increase the pressure in the upper chamber, eventually balancing the capillary pressure.

The scenario in figure 5.2(B) resembles the simplified situation of a femtopipette with an embedded membrane. In order to quantify this scenario, an ideal gas is assumed to be present inside the void volume at atmospheric pressure, just before the capillary is filled. Assuming the temperature will remain constant, the ideal gas law can be used to calculate the increasing gas pressure in the capillary, $P_C$, based on the advancing liquid meniscus. For simplicity, the membrane is assumed infinitely rigid. The volume of the liquid column can be approached as a truncated cone

$$V_{cone}(h_m) = \frac{\pi h_m}{3}\left(r_0^2 + r_0 r_m + r_m^2\right), \tag{5.12}$$

where $r_m$ is a function of $h_m$. From this truncated cone, a spherical cap can be subtracted to better approximate the liquid volume:

$$V_{cap}(h_m) = \frac{\pi R^3}{3}(2 + \cos(\alpha))(1 - \cos(\alpha))^2, \tag{5.13}$$

where $R$ is dependent on $h_m$. The steady-state pressure can then be calculated, together with the initially empty volume $V_{empty}$

$$P_C(h_m) = \frac{P_{atm} V_{empty}}{V_{empty} - V_{cone} + V_{cap}}. \tag{5.14}$$

Due to the expanding walls, the radius of the liquid meniscus will increase and therefore the capillary pressure will decrease. At some point, the internal gas pressure will reach equilibrium with the capillary pressure. This point can be calculated by expressing both the entering volume and the decreasing capillary pressure in terms of meniscus height $h_m$.

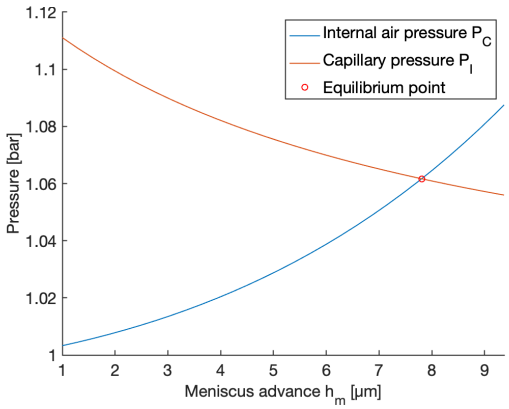


Figure 5.4: *Equilibrium pressure for a conical nozzle ($r_0$ = 2µm) with a closed membrane ($r_1$ = 10µm) and height ($h_{total}$ = 30µm), thus having slanted walls with $\beta$ = 14.93°. A spherical cap is subtracted from the liquid volume for better approximation to the internal pressure $P_C$.*

The calculations presented above give an estimation of how much volume will have entered into the nozzle-chamber before actuation, by means of capillarity. This initial volume can be altered by changing the geometry of the nozzle. Once

the liquid is inside the nozzle-chamber, the membrane could be actuated to have control over the amount of liquid that is enclosed. Note that this initial uptake volume is crucial to the working of this concept and therefore this concept will only work properly when the material is hydrophilic.

## 5.3. Methods

### 5.3.1. Fabrication methods

The whole system was made up of a combination of two parts that are both additively manufactured.

A multi-scale 3D printing method was applied to the production of the entire system, comprising the 2PP printed elements and their fluid interface. This method allowed for considerable design freedom and was based on the protocol developed by Kramer et al. [11] which was further refined by Altena et al. [16]. The functional parts of the system, the 2PP printed elements, are 3D printed on the micro-scale using two-photon-polymerization (2PP) (Photonic Professional GT Laser Lithography System, Nanoscribe GmbH). Different types of 2PP printed elements were made. First, dome shaped devices were printed to expose and characterize the 2PP printed membrane. Later, also femtopipettes with embedded membranes were 2PP printed using the same methodology. To be able to handle these 2PP printed elements, they were printed on top of the so called 'fluid-interface', which were also 3D printed but at the macro scale using a digital light processing (DLP) printer (EnvisionTEC Micro Plus HiRes, EnvisionTEC GmbH). Both parts will be treated in detail below.

**Fluid interface**

The fluid interface allows the 2PP printed elements to be easily handled and connected to a pressure source. An overview is shown in figure 5.5. The fluid interface comprises a plug-type connector to which a flexible tube (Masterflex Transfer Tubing, Tygon® ND-100-80 Microbore, ID 1.02mm, OD 1.78mm) can be connected (figure 5.5(1)); an internal channel that leads to the femtopipette location; a purge channel to facilitate development during fabrication (figure 5.5(3)) (to be plugged later). The top of the fluid interface serves as the substrate for 2PP printing (figure 5.5(2)). Geometrical rim features were designed to facilitate targeting the print location in the 2PP process, as well as to help retain the droplet of 2PP resin on the printing site (figure 5.5(4)). The fluid interface was designed to be symmetrical around the axis of the plug (fig. 5.5F), such that the interface could be easily rotated. This enabled either the horizontal or the vertical membrane to be analysed (illustrated with purple and blue arrow, fig. 5.5F). The aperture was designed to be close to the edge so that the membrane printed in the vertical orientation would be nearly flush with the side edge.

The fluid interfaces were printed on sacrificial supports inside a specially designed sample cup that fits the sample holder (25mm X 25mm) of the 2PP printer. The supports were automatically generated using the proprietary DLP slicing software (Perfactory Slicer, EnvisionTEC GmbH). The top surfaces of the fluid interfaces are level with the edges of the sample cup, minimizing the risk of damage to the objective of the 2PP printer.

The assembly of fluid interfaces and sample cups was printed with a layerheight of 35µm using a standard recipe (HTM140v2, EnvisionTEC GmbH) in combination with a transparent methacrylate/ acrylate-based photoresist (3DM Tough Clear, ADMAT SASU). Prints were cleaned with IPA (99.8% Honeywell, Riedel-de-Haën™) and UV post-cured (Photopol A5406, Dentalfarm) according to the standard development process (see appendix B for more details).

Before 2PP printing, the fluid interfaces were briefly sputtered with a 3nm gold layer (JEOL JFC1300 sputter coating system, five seconds at 10mA with a 20mm distance between the target and the substrate). This step enhanced the reflectivity of the surface, which made it possible to automate the interface finding in the 2PP printer.

After successfully printing and developing the 2PP printed elements (see following section), the individual fluid interfaces could be removed from their sacrificial supports with tweezers. The purge channel was then plugged by applying a small amount of 3DM Tough Clear resin with a dipped needle. This small droplet was cured for five minutes in the UV oven.

**2PP printed elements**

The 2PP printed elements were 3D printed on top of the fluid interface with extremely high resolution using the Nanoscribe. In the first stage, only the membrane was printed in order to characterize its functioning. Later, this membrane was printed inside a suspended cantilever femtopipette, following a similar approach as previous works [11], [16].

To make the connection between the fluid interface and the 2PP printed elements, a 'dome' was printed that covered the entire aperture of the fluid interface. The dome was designed to have a broad rim for better adhesion and relatively thick walls to provide structural rigidity. A membrane could be positioned on top of the dome for a hori-

zontal orientation (fig. 5.5B-C) or to the side for a vertical orientation (fig. 5.5D-E). Membranes with different diameters and thicknesses were printed.

CAD files of the parts were imported into the proprietary slicing software (DeScribe V2.5.7, Nanoscribe GmbH) where the printing parameters could be programmed. The dip-in-laser-lithography (DiLL) configuration was used in combination with the highest magnifying objective (63x) and the resin IP-Dip (Nanoscribe GmbH). The domes were printed slightly deeper than the found interface, to ensure good attachment and prevent leakage. Later, when the cantilever was printed, it was attached to a slanted channel wall at the dome. The cantilever was printed in subsequent overlapping slabs at a 45°angle to prevent sagging of the bottom layers, as well as to enable printing cantilevers with dimensions greater than the writing field. The main parameters of influence are the laser power and the writing speed, the combination of which determines the dose received by the resin. The domes were printed with a laser power of 60% (of the total power of 50mW); scanning speed of 70 mm $s^{-1}$.

The gold sputtered fluid interfaces in their respective sample cup were secured onto the Nanoscribe sampleholder with tape. Droplets of IP-Dip were applied with the resin cartridge-syringe to the areas of interest on the fluid interfaces. The samples were then loaded into the Nanoscribe, upon which the objective approached the sample and made contact with the resin droplet. The global coordinates of each individual fluid interface were known and programmed, but a manual alignment step was still necessary to pinpoint the exact printing location for each fluid interface. Due to the thin sputtered gold layer, the interface could be detected automatically by the Nanoscribe.

Upon finishing the last 2PP printed elements, the samples could be unloaded from the Nanoscribe. The samples were developed by first submerging them in propylene-glycol-methyl-ether-acetate (PGMEA, Sigma-Aldrich) for 30 minutes, then in isopropanol (IPA, Sigma-Aldrich) for 5 minutes, and lastly in Methyl perfluoropropyl ether, 1-Methoxy-heptafluoropropane (Novec™, Sigma-Aldrich) for 3 minutes—with gentle compressed air blow-drying in between each step. The samples were then inspected with an optical microscope to ensure all channels were cleared. If this was not the case, an additional development cycle could be employed.

## 5.3.2. Characterization

The fluid interfaces were inspected for obvious defects before continuing the process. The printed apertures were inspected and measured with an optical microscope (Keyence Digital Microscope VHX-600). After 2PP printing, the internal channel dimensions of the 2PP printed cantilevers could also be inspected with this microscope, due to the transparency of the cured IP-Dip resin. For observing the smallest features, a scanning electron microscope (SEM, Jeol JSM6010LA) was used.

To quickly assess the functioning of each device after developing and plugging the purge channel, the individual devices were connected to a 10mL syringe with Tygon™ tubing, and submerged into IPA. Pressure was then applied manually with the syringe to see if bubbles occurred indicating leakage.

### Membrane deflection

The 2PP printed membranes on top of the fluid interfaces could be supplied with gas pressure through the plug connector. As a pressure source, a syringe (60mL, BD Plastipak) on a syringe-pump (KDS legato 111, KD Scientific Inc.)

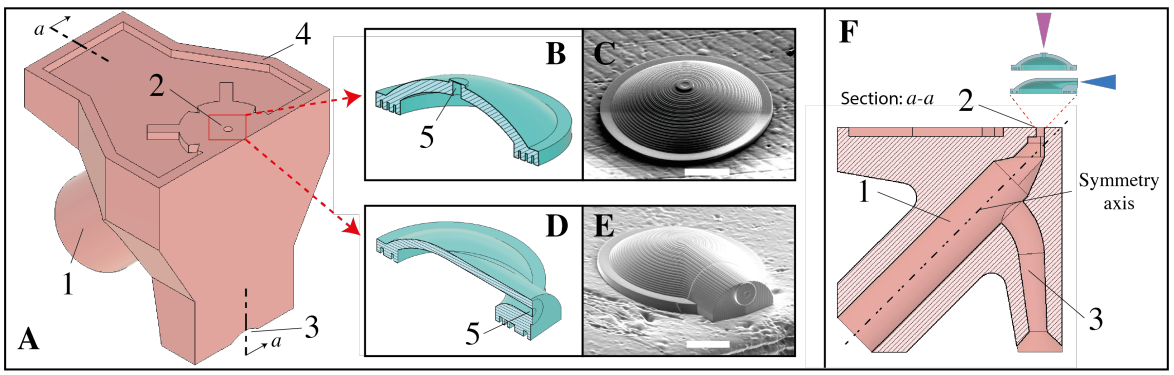


Figure 5.5: *Overview of fluid interface used for development of membrane concept. A small aperture is printed in the fluid interface (2) on top of which the 2PP printed elements are created with the Nanoscribe. Both horizontal (B-C) and vertical (D-E) orientations of membranes could be tested. The fluid interface is designed symmetrical around a 45° axis (F), to allow for easy positioning in both horizontal (purple arrow) and vertical (blue arrow) test orientations. Scalebar in SEM images: 100*µm.

was used. The pressure was measured by a digital pressure sensor (Gems 3500, 0-4 bar ± 10 mbar, Gems Sensors Inc.) in series with the pressure source.

To measure the deflection of the membranes under pressure, a white-light interferometer (ContourGT-X, Bruker) was used. First, the neutral position of each membrane was scanned. Then, in incremental steps, the pressure was increased and the deformation was measured at different static pressure levels, ranging up to 3.5 bars.

For easy installation of fluid interfaces into the whitelight interferometer setup, a special clamp was 3D printed that could hold the fluid interface in place. This made interchanging of different devices straightforward and simplified the alignment procedure of the whitelight interferometer. Scans were made using the green-narrowband light source and a magnification objective of 20X.

**Femtopipette with embedded membrane**

When the membrane was characterized, the next step was to print femtopipettes with embedded membranes. To test the working of these devices, the fluid interfaces together with the attached cantilevers were submerged in a droplet of DI-water and placed under an optical microscope. Then it was observed whether the liquid-air meniscus could be controlled by applying pressure to the back of the membrane.

## 5.4. Results & Discussion

### 5.4.1. Fabrication

**Fluid Interface**

Two sample cups holding up to 16 fluid interfaces each were 3D-printed with a layer-height of 35 µm in 80 minutes. For a DLP printer, the used print area does not influence print time, but the part-height does. The height of the fluid interfaces was kept intentionally low, to be able to fit the sliding sample-holder with loaded samples into the Nanoscribe. The fluid interfaces were very rarely clogged, and were not difficult to clean using the standard cleaning protocol (see Appendix B).

The printed apertures had a nominal diameter of ∼ 150 µm. However, the edges of apertures were not very smooth and rounded inwards, resulting in an effective diameter that was more in the order of ∼ 200 µm.

**2PP printed elements**

The sputtered 3nm gold layer provided enough reflectivity to allow automatic interface finding. The interface finding command could be executed at the location of the aperture, without needing to move to the side of the aperture first. This is because the interface is not found exactly in the middle of the writing field, and the aperture was sufficiently small. The relative coordinates of each fluid interface were known, but due to small variances in alignment of the sample cup and minor deformations due to handling, each aperture still needed a final manual alignment step.

The printing was programmed to start up to 20 µm below the found interface. This ensured a secure, leak-free attachment of the dome in most cases—tested to withstand at least 4.5 bar. When the 2PP laser reached the surface, tiny bubbles could be observed through the process-camera feed, confirming contact with the interface.

The domes were designed with an outer diameter of 400 µm, and because the writing field

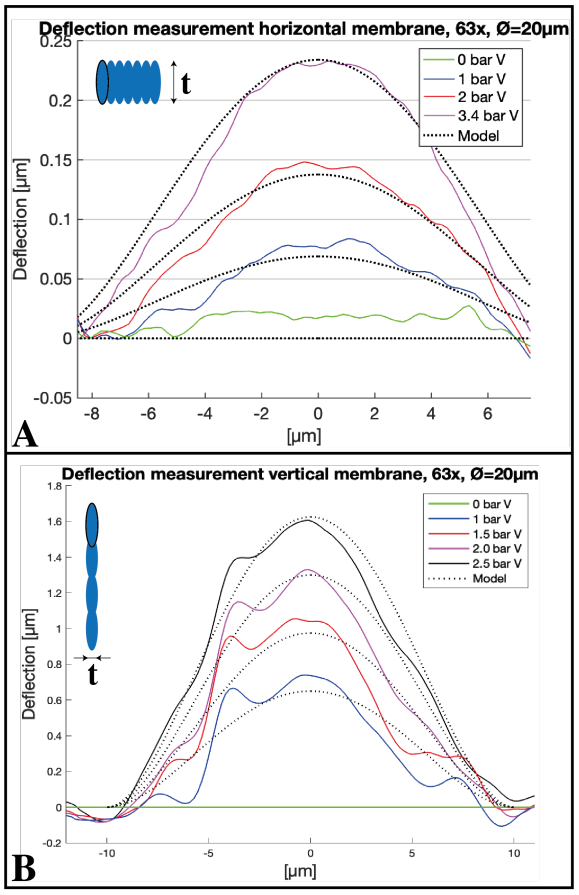


Figure 5.6: *Deflection measurements for different static pressures compared to deflection model (eqn.* (5.1)*). Schematic representations of the voxel orientation and resulting membrane thickness $t$ are shown for illustrative purposes. A: Horizontally-printed membrane with* 20 µm *diameter. The model is plotted for a thickness of 930 nm, resulting in a maximum volume displacement of 24.51 fL. B: Vertically-printed membrane with* 20 µm *diameter. The model is plotted for a thickness of 440 nm resulting in a maximum volume displacement of 170.2 fL.*

of the 63x Nanoscribe objective is only 200 µm in diameter, block stitching was needed to create the entire dome. Hexagonal blocks were chosen and care was taken to keep the membrane free of block-stitching lines (see appendix B). Domes with horizontally-oriented membranes were printed in ~58 minutes and domes with vertically-oriented membranes in ~70 minutes.

### 5.4.2. Membrane deflection

The topological measurement data of the white-light interferometer scan was recorded and saved for each static pressure step. A scan depth of 20 µm was used to capture not only the membrane itself, but also the edges enabling better alignment of the data in postprocessing.

The data was imported into topological post-processing software (Gwyddion V2.6, open source). Here, the data was levelled and zeroed with respect to the membrane perimeter. Then, both a horizontal and a vertical cross-sectional profile was extracted, crossing in the centre of the membrane. This data was then imported into Matlab (R2019b, Mathworks Inc.) where each measurement was further aligned, trimmed to the region of interest, and compared to the deflection model (eqn. (5.1)). Results of a horizontally-printed and a vertically-printed membrane are shown in figure 5.6.

The measured deflection profiles are compared to the model using the same geometrical parameters and material properties summarized in section 5.2.1 leaving only the membrane thickness as free parameter to fit the model. It can be seen that the vertically-printed membrane deflects significantly more than the horizontally-printed membrane for similar pressure levels. This is because the thickness of the vertically-printed membrane can be less due to the voxel orientation. For the horizontally-printed membrane, the best fit was achieved for a thickness $t$ of 930 nm; for the vertically-printed membrane $t$ was found to be 440 nm. These values for $t$ are well within the range of expectation: for the 63 objective and the used resin, the minimum theoretical voxel size is reported as 830 nm in the axial direction, and 340 nm in the lateral direction [22]. Schematic representations of the voxel orientations are included in figure 5.6.

From this deflection measurement, the displaced volume can be approximated by applying equation (5.6) to the fitted model. For the displayed horizontally-printed and vertically-printed membrane in figure 5.6, this results in a maximum deflected volume of 24.51 fL and 170.2 fL, at 3.4 bar and 2.5 bar respectively.

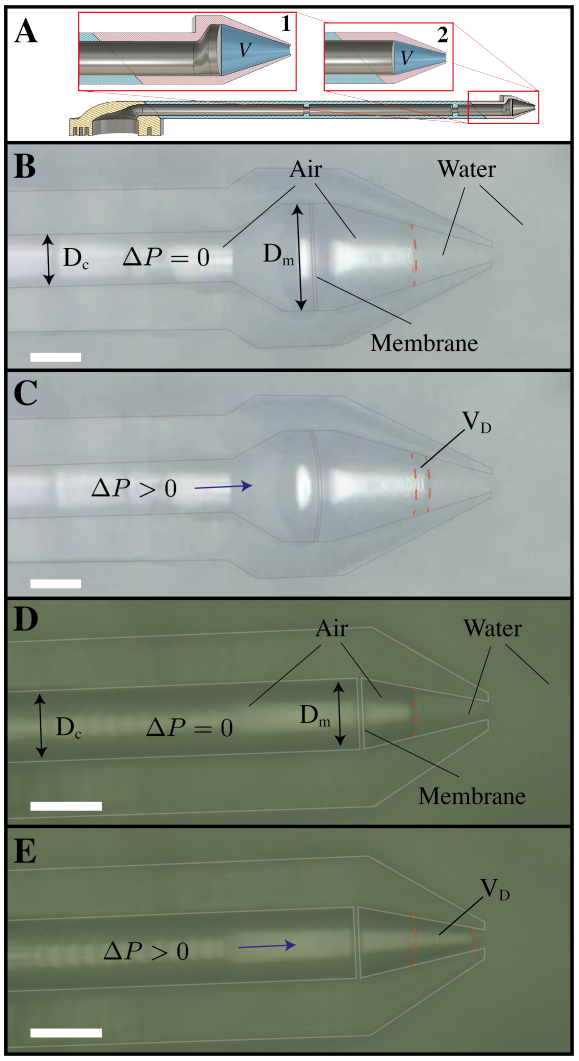


Figure 5.7: *Femtopipettes with embedded membrane. A: CAD model of the 2PP printed dome, cantilever and membrane. Two different diameters are shown in the insets, where (1) presents a* 30 µm *membrane and (2) presents a* 20 µm *membrane. The total volume of the nozzle-chamber is shaded blue and indicated with* $V$*. B-E: Topview of experiment with submerged membrane cantilevers, shown for both neutral and actuated position. A pressure* $\Delta P$ *is applied from the left. Subtle line overlays are inserted for clarity. Red-dotted lines indicate the liquid-air meniscus. B-C: Membrane with diameter* $D_m$ *of* 30 µm*. The displaced volume* $V_D$ *in B is evaluated at 1.42 pL. D-E: Membrane with diameter* $D_m$ *of* 20 µm*. Displaced volume* $V_D$ *is 1.27 pL. Scalebar and channel diameter* $D_c$ *are* 20 µm *in all images.*

### 5.4.3. Femtopipette with embedded membrane

Different cantilevers with embedded membranes were printed and tested. To evaluate their performance, each cantilever was submerged in DI-water and observed from the top. Then, either negative or positive pressure was applied to the membrane through the cantilever channel. It was observed whether the liquid-air meniscus could be controlled in this manner.

Some cantilevers with embedded membranes were able to control the liquid meniscus by applying pressure to the membrane. Two of such membranes are shown in figure 5.7, for both neutral and actuated positions. The images are frames taken from movies recorded with an optical microscope [23].

However, the analysed resulting volume displacement was not in agreement with the estimated values based on the deflection measurement. The observed difference between two extreme positions of the liquid meniscus allowed to calculate the actuated volume by approximating it as a truncated cone. For the devices displayed in figure 5.7, the actuated volumes $V_D$ were evaluated at 1.42 pL (A-B) and 1.27 pL (C-D) respectively. This was unexpected, since these volumes are much higher than the displaced volumes approximated from the measured deflection of the membranes—roughly 200 fL for a vertically-printed membrane, see section 5.4.2. Furthermore, for displaced volumes in the order of picolitres, the deflection of the membrane should have been visible in figure 5.6, but no clear deflection was observed.

Furthermore, it turned out difficult to get the fabrication of the cantilevers right. Most of the time, no liquid movement was visible at all, leading to the suspicion that the membrane was too thick to produce noticeable displacement. Other times, the liquid would just burst past the location of the membrane inwards, clearly indicating a 'leaking' membrane. The unreliability of the membrane fabrication is thought to originate for a substantial part from the development process: because the channel is physically barred by the membrane, the liquid developing agents are less likely to sufficiently reach all the surface area needed for proper development. Dose-tests and SEM inspections of vertically printed, exposed membranes are included in appendix B, revealing the difficulties in finding the right printing parameters for thin membranes.

The discrepancy between the measurements of the volume deflected by the membrane and the volume measured from the liquid menisci positions is significant. This lead to the suspicion that the membranes were in fact faulty: likely leaking air through tiny, unintended pores in the membrane. This porosity may have already been present in the membranes printed for the deflection measurement, but these pores may be so small that they were not visible in either of the inspection methods. Also, such small pores likely do not decrease the internal pressure within the sensitivity limits of the pressure sensor.

## 5.5. Conclusion

In this paper, a new concept for improving the volume dosing resolution of a pressure actuated femtopipette is proposed and tested. The concept is the first to embed a physical barrier into the femtopipette in the form of a flexible membrane. Based on the presented theory, it was expected that the concept could improve upon the volume dosing resolution found in the state of the art, set at 100 fL. A multi-scale 3D printing methodology was successfully applied to the production of 2PP printed functional elements. This methodology allowed for a high level of design freedom and enabled fast iteration of concepts.

Thin, flexible membranes were 2PP printed and their pressure induced deformation was characterized and compared to an analytical model. The resulting deflection compared well to the model, and the fitted membrane thickness was in the range of expectation. The volume that was deflected by the deformation of the membrane could be approximated and was in the range of 100 fL, aligned with the target volume found as the state of the art.

Repeatability issues were encountered in the production of femtopipettes with embedded membranes, likely originating from the development process and the inherent difficulties of developing closed 2PP printed channels. To some extent, the resulting femtopipettes were able to control liquid volumes on the microscale: volumes in the order of 1 picolitre were controlled. However, the actuated volume range that was measured by observing the position of the liquid meniscus inside the femtopipette, was not in line with expectation. The actuated liquid portion was significantly larger than the volume deflected by measuring the deforming membrane. This led to the suspicion that the membranes were slightly porous, but this suspicion was difficult to confirm by inspection or with the resolution of the used pressure sensor.

In all, the proposed concept did allow control over volumes in the order of single picolitres, even by manual operation. This is a feat that is still noteworthy, but it is ambiguous whether this can be claimed as a 'proof of concept'.

Perhaps with further optimisation of the presented production techniques—2PP printing parameters or changing to a different photoresist—, membranes could be fabricated that better serve the purpose of this concept.

## References

[1] S. Lindström and H. Andersson-Svahn, "Overview of single-cell analyses: Mi-

crodevices and applications", *Lab on a Chip*, vol. 10, no. 24, pp. 3363–3372, 2010.

[2] J. R. Heath, A. Ribas, and P. S. Mischel, "Single-cell analysis tools for drug discovery and development", *Nature Reviews Drug Discovery*, vol. 15, no. 3, pp. 204–216, 2016.

[3] P. Actis, "Sampling from Single Cells", *Small Methods*, vol. 2, no. 3, p. 1 700 300, Mar. 2018.

[4] M. P. Stewart, R. Langer, and K. F. Jensen, "Intracellular delivery by membrane disruption: Mechanisms, strategies, and concepts", *Chemical Reviews*, vol. 118, no. 16, pp. 7409–7531, 2018.

[5] G. Bulbul, G. Chaves, J. Olivier, R. Ozel, and N. Pourmand, "Nanopipettes as Monitoring Probes for the Single Living Cell: State of the Art and Future Directions in Molecular Biology", *Cells*, vol. 7, no. 6, p. 55, 2018.

[6] A. Meister, M. Gabi, P. Behr, P. Studer, J. Vörös, P. Niedermann, J. Bitterli, J. Polesel-Maris, M. Liley, H. Heinzelmann, and T. Zambelli, "FluidFM: Combining atomic force microscopy and nanofluidics in a universal liquid delivery system for single cell applications and beyond", *Nano Letters*, vol. 9, no. 6, pp. 2501–2507, 2009.

[7] O. Guillaume-Gentil, E. Potthoff, D. Ossola, P. Dörig, T. Zambelli, and J. A. Vorholt, "Force-controlled fluidic injection into single cell nuclei", *Small*, vol. 9, no. 11, pp. 1904–1907, 2013.

[8] O. Guillaume-Gentil, R. V. V. Grindberg, R. Kooger, L. Dorwling-Carter, V. Martinez, D. Ossola, M. Pilhofer, T. Zambelli, and J. A. A. Vorholt, "Tunable Single-Cell Extraction for Molecular Analyses", *Cell*, vol. 166, no. 2, pp. 506–516, 2016.

[9] E. Potthoff, O. Guillaume-Gentil, D. Ossola, J. Polesel-Maris, S. LeibundGut-Landmann, T. Zambelli, and J. A. Vorholt, "Rapid and Serial Quantification of Adhesion Forces of Yeast and Mammalian Cells", *PLoS ONE*, vol. 7, no. 12, 2012.

[10] P. Dörig, P. Stiefel, P. Behr, E. Sarajlic, D. Bijl, M. Gabi, J. Vörös, J. A. Vorholt, and T. Zambelli, "Force-controlled spatial manipulation of viable mammalian cells and micro-organisms by means of FluidFM technology", *Applied Physics Letters*, vol. 97, no. 2, pp. 1–4, 2010.

[11] R. C. L. N. Kramer, E. J. Verlinden, L. Angeloni, A. van den Heuvel, L. E. Fratila-Apachitei, S. M. van der Maarel, and M. K. Ghatkesar, "Multiscale 3D-printing of microfluidic AFM cantilevers", *Lab on a Chip*, vol. 20, no. 2, pp. 311–319, Jan. 2020.

[12] M. Knoblauch, J. M. Hibberd, J. C. Gray, and A. J. Van Bel, "A galinstan expansion femtosyringe for microinjection of eukaryotic organelles and prokaryotes", *Nature Biotechnology*, vol. 17, no. 9, pp. 906–909, 1999.

[13] K. T. Rodolfa, A. Bruckbauer, D. Zhou, A. I. Schevchuk, Y. E. Korchev, and D. Klenerman, "Nanoscale pipetting for controlled chemistry in small arrayed water droplets using a double-barrel pipet", *Nano Letters*, vol. 6, no. 2, pp. 252–257, 2006.

[14] Y. T. Chow, S. Chen, R. Wang, C. Liu, C. W. Kong, R. A. Li, S. H. Cheng, and D. Sun, "Single cell transfection through precise microinjection with quantitatively controlled injection volumes", *Scientific Reports*, vol. 6, no. April, pp. 1–9, 2016.

[15] H. H. Perez Garza, M. K. Ghatkesar, P. Lothman, A. Manz, and U. Staufer, "Enabling local deposition and controlled synthesis of Au-nanoparticles using a femtopipette", *9th IEEE International Conference on Nano/Micro Engineered and Molecular Systems, IEEE-NEMS 2014*, pp. 323–328, 2014.

[16] P. F. J. Altena van, "Multiscale 3D printed polymer probes for single cell experiments", Master's thesis, TU Delft, Delft, 2021.

[17] S. P. Timoshenko and S. Woinowsky-Krieger, *Theory of plates and shells*. McGraw-hill, 1959.

[18] W. P. Eaton and J. H. Smith, "Micromachined pressure sensors: Review and recent developments", *Smart Materials and Structures*, vol. 6, no. 5, pp. 530–539, 1997.

[19] A. DeHennis and J. Chae, "2.04 - pressure sensors", in *Comprehensive Microsystems*, Y. B. Gianchandani, O. Tabata, and H. Zappe, Eds., Oxford: Elsevier, 2008, pp. 101–133.

[20] E. D. Lemma, F. Rizzi, T. Dattoma, B. Spagnolo, L. Sileo, A. Qualtieri, M. De Vittorio, and F. Pisanello, “Mechanical Properties Tunability of Three-Dimensional Polymeric Structures in Two-Photon Lithography”, *IEEE Transactions on Nanotechnology*, vol. 16, no. 1, pp. 23–31, 2017.

[21] I. S. Ladner, M. A. Cullinan, and S. K. Saha, “Tensile properties of polymer nanowires fabricated: Via two-photon lithography”, *RSC Advances*, vol. 9, no. 49, pp. 28 803–28 813, 2019.

[22] Nanoscribe GmbH, *Nanoguide: 63x objective*, https://support.nanoscribe.com/hc/en-gb/articles/360002471754-63x-Objective, 2022.

[23] M. Blankespoor, *Cantilevers with embedded membranes*, https://vimeo.com/692217196, 2022.

# 6

# Phaseguide controlled pipetting

# Discrete femtolitre dosing with axisymmetrical phaseguides

**Abstract**

Femtopipettes are tools that are used to aspirate and dispense liquids on the microscale with high positional accuracy. When combined with Atomic Force Microscopy (AFM), these microfluidic devices form a powerful means to perform research on the single-cellular level. Pressure is the most common way to actuate femtopipettes. The smallest volumes are achieved by applying a short pressure pulse, but the resulting dosing resolution is limited. In this work, a new femtopipette concept is proposed that makes use of axisymmetrical phaseguides to dose liquid in discrete steps of known volume, backed by an analytical model. Using a multi-scale 3D printing strategy combining stereolithography and two-photon-polymerization, three different variants are fabricated with respective dosing resolutions of 10 picolitre, 200 femtolitre and 60 femtolitre. As a demonstration, controlled amounts of a water-glycerol mixture were first aspirated and then dispensed into a mineral oil droplet with unprecedented resolution.

## 6.1. Introduction

Understanding the functioning of cells is of paramount importance for biology and medicine. The research of individual cells is a topic of increasing scientific efforts. Classical methods usually involve steps to sort and/or isolate the cells of interest, after which the cell is opened by lysis or microdissection to gain access to the cell content [1], [2]. Although a lot of insight can be gained this way, obvious disadvantages in most such methods are that the cells are analysed away from their natural environment and are often killed in the process. New and innovative methods have been proposed more recently, that study the contents of cells while they stay alive [3]. An important factor for this way of analysis is the controlled transport of substances of interest through the cell membrane and many methods have been invented for this purpose [4]. Among these methods, the so called femtopipette is a very promising and versatile technique due to its positional accuracy and the possibility for both extraction and delivery of substances in a single living cell [5].

Classically, femtopipettes are fabricated by heating and pulling a glass tube, and modern methods can achieve apertures of several tens of nanometers. Positioning such femtopipettes often relies on optical feedback, and it is difficult to asses whether the targeted cell is indeed penetrated or not.

An interesting extension to the functionality of the femtopipette was proposed by Meister et al. when they made a hollow cantilever for an atomic force microscope (AFM) [6]. They were the first to connect the cantilever to a pressure source such that liquid could be flown through the tip, yielding the appropriate name ‘FluidFM’. The additional gained force feedback provided by the AFM system proved useful to detect contact with the cell surface and even penetration of the cell membrane. Successful injection as well as aspiration was established on living cells [7], [8]. Moreover, cell adhesion force measurements and pick-and-place functionality have been demonstrated using the FluidFM system [9], [10].

Different experiments often require a specific cantilever and/or tip shape design, but since most AFM cantilevers are fabricated by means of photolithography steps, customization is lengthy and costly. An interesting advancement was provided by Kramer et al. when they made a fully functional microfluidic AFM cantilever by means of additive manufacturing [11]. Using digital light processing (DLP) combined with two-photon-polymerization (2PP) allowed for more design freedom whilst also significantly reducing the production time.

For controlling the amount of liquid that is pipetted within a liquid environment, three different actuation methods have been reported: thermally driven, electrochemically driven and pressure driven. Respectively, the first two have been able to obtain volume resolutions down to the attolitre level (1 aL = $10^{-18}$L) [12], [13], but the disadvantage is that these techniques limit the choice of working liquids. Pressure remains the most straightforward actuation method and allows for the widest range of substances to be handled—a useful aspect, especially concerning cell biology. However, the resolution of pressure driven methods is relatively low, with the best results in literature coming down to approximately 100 femtolitre (1 fL = $10^{-15}$L), albeit, with substantial uncertainty [7], [8], [14].

Being able to easily control the volume dosing with higher resolution could be a major enabling factor for single-cell research. Firstly, smaller

samples being injected or aspirated interfere less with the natural functioning of the cell. Secondly, higher specificity in targeting may result in more detailed cell analysis. Finally, supplying cells with an accurate dose could be important for small scale drug testing.

Other envisaged applications in nanotechnology can also greatly benefit from high resolution liquid dosing. For example, delivery of small amounts of substances to nano-sensors or transmission-electron-microscope (TEM) windows could also benefit from increased resolution [15].

Therefore, the goal of this research is aimed to increase the resolution of pressure driven femtopipetting systems. A new femtopipette concept is proposed based on the design and production methods of Kramer et al. [11]. This way, the femtopipette may also benefit from the AFM functionality that was demonstrated by Kramer et al. and Van Altena et al. [11], [16]. The concept makes use of capillary pinning locations, otherwise known as 'phaseguides' [17] or 'capillary valves' [18], where the meniscus formed at the liquid-air interface pins predictably to designated locations. This phenomenon is used to provide discrete steps of known volume, adjustable by the designer.

In the following section, the theory behind these capillary pinning locations is treated, accompanied by an analytical model. Then, in section 6.3, the production methods as well as the experimental methods are described. The results are elaborated and discussed in section 6.4. Finally, the conclusions of this work are stated in section 6.5.

## 6.2. Theory

The geometry of channels on the micro scale is influential for the behaviour of the fluid inside, especially when an interface is involved between different fluid regions. Such an interface can exist between two immiscible liquids or between fluid phases. For the purpose of clarity—and with respect to the intended application—the following section will treat an interface between liquid and gas.

At the interface, an interfacial tension will exist that forms a meniscus: the origin of capillarity. Capillarity can be exploited in microfluidics to alter the behaviour of the liquid, which is also the purpose of the capillary pinning locations [19]. The behaviour is slightly different in the case of liquid advancement versus liquid compelling (gas advancement), and both will be treated below. The capillary pressure of a liquid inside a straight-walled channel is caused by the so called *Laplace pressure*, which acts on the curved surface of the meniscus. The Laplace pressure is given relative to the atmospheric pressure as

$$\Delta P = \frac{2\gamma}{R}, \tag{6.1}$$

where $\gamma$ is the surface tension, and $R$ is the radius of curvature of the meniscus. The radius of curvature $R$ can be deduced from the diameter of the channel $d$ and the contact angle $\theta$ according to $R = \frac{d/2}{\cos(\theta)}$ (see figure 6.1), yielding the convenient expression for capillary pressure

$$\Delta P = \frac{4\gamma\cos(\theta)}{d}. \tag{6.2}$$

Then, depending on whether the contact angle $\theta < 90°$ (hydrophilic) or $\theta > 90°$ (hydrophobic), the relative capillary pressure will be either positive or negative with respect to the atmospheric pressure.

### 6.2.1. Liquid advancement

Equation (6.2) describes the relative pressure inside the liquid adjacent to the meniscus, which is the driving force behind capillary action.

When dealing with changes in channel geometry, it becomes useful to define an angle $\alpha$, which describes the angle of half the meniscus

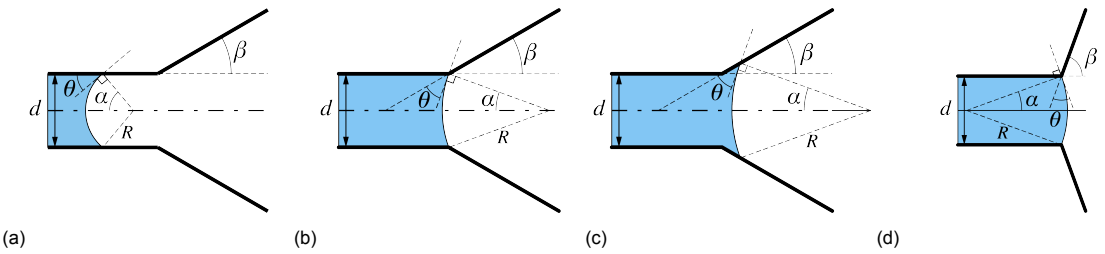


Figure 6.1: *Capillary advance of liquid inside a hydrophilic channel. (a): Meniscus in straight-walled channel with constant diameter $d$, where $\alpha = 90° - \theta$. (b): Meniscus reaching the corner point, the contact angle re-establishes on the slanted walls such that $\alpha = 90° - \theta - \beta$. (c): For $\beta < \beta_c$, the meniscus will continue to advance, but the capillary pressure decreases. (d): For $\beta > \beta_c$, the meniscus changes shape, $\alpha < 0$, and stops advancing.*

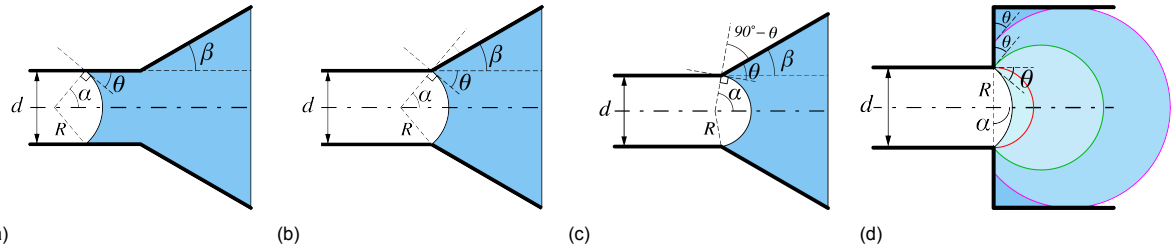


Figure 6.2: *Gas advancement in liquid-filled hydrophilic channel. (a): Situation comparable to figure 6.1(a), meniscus in straight-walled capillary. (b): Here, $\alpha$ remains the same until the pressure is increased in (c). (c): Liquid is compelled back and $\alpha$ will be defined as $\alpha = 90° - \theta + \beta$. (d): At angles $\beta > \beta_{c,air}$, increasing pressure will cause the meniscus to burst when $\Delta P_{burst} = \frac{4\gamma}{d}$.*

arc and is by definition perpendicular to the contact angle $\theta$, see figure (6.1a). Thus, when the meniscus remains within a straight-walled channel with constant diameter $d$, $\alpha = 90° - \theta$. Equation (6.2) can then be re-written as

$$\Delta P = \frac{4\gamma \sin(\alpha)}{d}. \tag{6.3}$$

When the meniscus reaches a point where the channel expands axisymmetrically with a certain expansion angle $\beta$, the edges of the meniscus will pivot around the corner edge to re-establish the contact angle between the liquid and the slanted walls (6.1b,c). The radius of curvature $R$ therefore increases, and the capillary pressure will decrease according to eq. (6.1). In this situation, $\alpha = 90° - \theta - \beta$. The liquid will be able to advance for expansion angles $\beta$ below a critical value $\beta_c = 90° - \theta$. Beyond this critical angle $\beta_c$, the contact angle $\theta$ forces the meniscus to change from concave to convex, causing $\alpha$ to become negative (6.1d). At the critical angle $\beta_c$, $\alpha = 0$, and the meniscus is flat ($R = \infty$). From this point, the relative capillary pressure becomes negative and the liquid has no force driving it forwards. Such a point is called a phaseguide.

### 6.2.2. Gas advancement

In the case when liquid is compelled back by an opposing gas pressure, the scenario becomes slightly different, as illustrated in figure (6.2). It is assumed that liquid has filled the entire channel and a positive gas pressure is needed to force the meniscus back. When the meniscus is inside the straight-walled part with constant diameter $d$, the pressure is once again given by equations (6.2, 6.3), with $\alpha$ being the same as before. This relation still holds when the meniscus comes to the corner of the expansion (fig. 6.2b).Then, when the gas pressure is increased, the liquid will be forced to pivot around the corner to re-establish its contact angle $\theta$, and $\alpha$ is defined: $\alpha = 90° - \theta + \beta$ (see figure 6.2c).

The maximum Laplace pressure inside the liquid occurs when the radius of curvature $R$ is minimal. A minimum radius of curvature is achieved when $R = d/2$, with $\alpha = 90°$. Here, a new 'critical angle' is defined as $\beta_{c,air} = \theta$.

When the pressure is increased beyond $\beta_{c,air}$, the radius of curvature $R$ will increase again, decreasing the required pressure, and thus resulting in an unstable bubble bursting into the channel. This scenario is depicted in figure 6.2d, where the critical radius $R$ is indicated with a red line, progressing to an unstable bubble indicated with green, which will grow until the next channel diameter is reached (pink). The development of the burst pressure (relative to the atmospheric pressure) can be expressed as:

$$\Delta P = \begin{cases} \frac{4\gamma \sin(\alpha)}{d} & \text{for } \alpha < 90°,\ \beta < \beta_{c,air}. \\ \frac{4\gamma}{d} & \text{for } \alpha \geq 90°,\ \beta \geq \beta_{c,air}\ . \end{cases} \tag{6.4}$$

Here, the burst pressure can be related to the so-called 'bubble point pressure' in literature [20]. Equation 6.4 predicts that the burst pressure will plateau from the critical angle $\beta_{c,air}$ onwards.

## 6.3. Methods

### 6.3.1. Fabrication methods

A multi-scale 3D printing method was applied that allowed for considerable design freedom, based on the protocol developed by Kramer et al. [11] —further refined by Altena et al. [16]. The femtopipette system consists of a combination of two parts that are both 3D printed. The functional part of the device, the femtopipette, is 3D printed on the microscale using two-photon-polymerization (2PP) (Photonic Professional GT Laser Lithography System, Nanoscribe GmbH). To handle this part, it is printed on top of the so-called 'fluid-interface', which is 3D printed at the macro-scale using a digital light processing (DLP) printer (Micro Plus HiRes, EnvisionTEC GmbH). Both parts will be treated below.

**Fluid interface**

The fluid interface allows the femtopipette to be easily handled and connected to a pressure source. An overview is shown in figure 6.3. The fluid interface comprises a plug-type connector to which a flexible tube (Masterflex Transfer Tubing, Tygon® ND-100-80 Microbore, ID 1.02mm, OD 1.78mm) can be connected (figure 6.3A, 3); an internal channel that leads to the femtopipette location (figure 6.3B, 1); a purge channel to facilitate development during fabrication (figure 6.3B, 4)—to be plugged later—and a notch to accommodate a fit to the AFM holder (BioAFM holder of the JPK BioAFM Nanowizard 4, JPK Instruments AG)(figure 6.3A, 4). The top of the fluid interface serves as the substrate for 2PP printing (figure 6.3B, 3). Geometrical rim features were designed to facilitate targeting the print location in the 2PP process, as well as to help retain the droplet of 2PP resin on the printing site.

In order to reduce the 2PP printing time, an aperture of minimal size is needed to connect the internal channels of the fluid interface to the femtopipette. The capacity of the DLP printer to print small apertures was decided to be insufficient with tested minimal aperture sizes coming down to ~160µm for the chosen printing recipe. Instead, the top surface was printed closed, and an aperture was later 'drilled' with a high resolution lasercutter (figure 6.3B2 and 6.3E).

The fluid interfaces were printed on sacrificial supports inside a specially designed sample cup (figure 6.3C), that fits the sample holder (25mm X 25mm) of the 2PP printer. The supports were automatically generated using the proprietary DLP slicing software (Perfactory Slicer, EnvisionTEC GmbH). The top surfaces of the fluid interfaces are level with the edges of the sample cup, minimizing the risk of damage to the objective of the 2PP printer. Five fluid interfaces fit in one sample cup. The sample cup has a cut-out corner to optimally make use of the real estate of the DLP buildplate (27.5mm X 44mm), allowing for a second sample cup to be placed when rotated 180°(figure 6.3D).

The assembly of fluid interfaces and sample cups was printed with a layerheight of 35µm using a standard recipe (HTM140v2, EnvisionTEC GmbH) in combination with a transparent methacrylate/ acrylate-based photoresist (3DM Tough Clear, ADMAT SASU). Prints were cleaned with IPA (99.8% Honeywell, Riedel-de-Haën™) and UV post-cured (Photopol A5406, Dentalfarm) according to the standard development process (see appendix B for more details).

Next, the apertures were created with a high resolution lasercutter (WS Starter micro-machining laser system, Optec S.A.) employing a laser power of 15W at 50kHz with a writing speed of 15mm $s^{-1}$ and 15 repetitions.

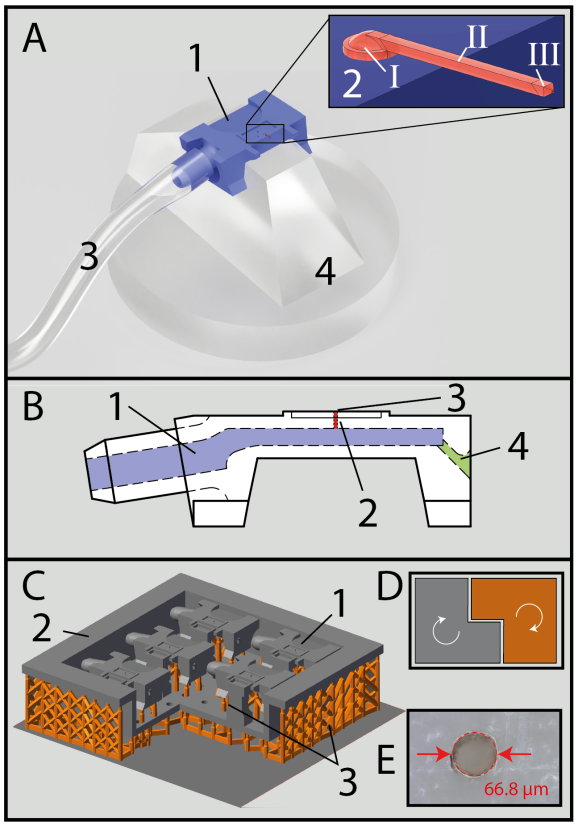


Figure 6.3: *Fluid interface. A: Overview of the device setup with the fluid interface (1) attached to the JPK AFM holder (4) and connected to a pressure source with a flexible tube (3). Inset shows a CAD image of the actual femtopipette with its dome (I), cantilever (II) and nozzle (III). B: Schematic cross-sectional view of the fluid interface showing the internal channel (1) connecting to the laser-drilled aperture (2) which leads to the 2pp printing site (3). The purge channel (4) can be plugged later. C: DLP printing software showing five fluid interfaces (1) in their respective sample-cup (2) with automatically generated support structure (3) to be removed later. D: Two sample cups can fit on the DLP printbed when rotated 180°with respect to each other. E: Optical micrograph of the laser drilled aperture.*

The last step before 2PP printing was to briefly sputter the fluid interfaces with a 3nm gold layer (JEOL JFC1300 sputter coating system, 5 seconds at 10mA with 20 mm target-substrate distance). This step enhanced the reflectivity of the surface, which enables automatic interface finding in the 2PP printer.

After successfully 2PP printing and developing the femtopipette (see following section), the individual fluid interfaces could be removed from their sacrificial supports with tweezers. The purge channel was then plugged by applying a small amount of 3DM Tough Clear resin with a dipped needle. This small droplet was cured for 5 minutes in the UV oven.

**Femtopipette**

The femtopipette was 3D printed on top of the fluid interface with extremely high resolution using two-photon-polymerization (2PP). The femtopipette was designed as a suspended hollow cantilever that protrudes over the edge of the fluid interface (see figure 6.3A, 2). This protrusion allows for imaging and targeting, but moreover, the suspended hollow cantilever is shown to be capable of acting as a probe for AFM functionality [11], [16].

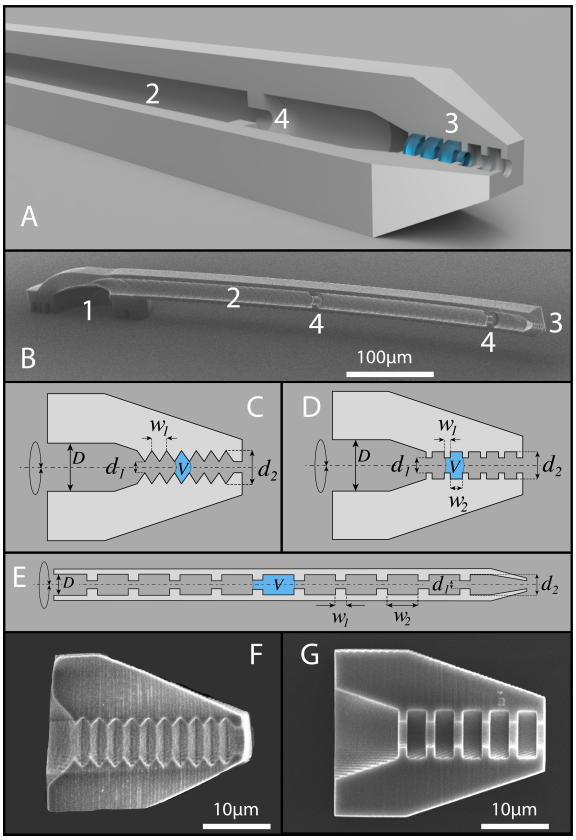


Figure 6.4: *Overview of the femtopipette cantilever and three different axisymmetrical phaseguide geometries. A: Cut out section of cantilever CAD model with exposed internal channel (2) connecting to the pressure source; a nozzle (3) with fine phaseguides, of which three are shown 'filled'; a large 'back-up' phaseguide (4) to better control aspiration volume. B: SEM image of device, including dome (1), printed half to reveal internals. C-E: Schematic representation of three axisymmetrical phaseguide geometries with definition of used dimensions. F-G: SEM images of two half-printed nozzle designs. SEM measurements of the dimensions of $d_1, d_2, w_1$ and $w_2$ are tabulated in table 6.1.*

The femtopipette consists of three parts that are merged together in the 2PP process: (1) the 'dome'—which connects the fluid interface to the femtopipette and seals the aperture; (2) the hollow cantilever that is suspended horizontally to protrude over the edge of the fluid interface; and (3) the nozzle in which stepped, axisymmetrical phaseguides are embedded (figure 6.4B). Note that the third part (3) is only necessary when sub picolitre (pL, $10^{-12}$L) volumes are dosed, otherwise larger axisymmetrical phaseguides could also be embedded in the suspended hollow cantilever (figure 6.4E). Distinguishing between these parts also permits to set specific parameters separately, which facilitates print optimization. The separate CAD files of the parts were imported into the proprietary slicing software (DeScribe V2.5.7, Nanoscribe GmbH) where the printing parameters could be programmed, see table 6.2.

Different variants and sizes of axisymmetrical phaseguides were designed and tested. The design freedom gained by employing the 2PP printing technique enables to adjust the desired dosing volume by reshaping the phaseguide geometry. The volume of one dosing step is determined by the void-volume between two successive channel expansions. These expansions can take different forms as long as the expansion angle $\beta$ remains larger than the critical angle $\beta_{c,air}$. In this research, two such geometrical variants are treated: 1) triangular axial revolutions (figure 6.4C) where the volume per step is given as

$$V_{step} = \frac{1}{12}\pi w_1 (d_1^2 + d_1 d_2 + d_2^2), \qquad (6.5)$$

and 2) rectangular axial revolutions (6.4D-E) where the volume is simply

$$V_{step} = \frac{1}{4}\pi (d_1^2 w_1 + d_2^2 w_2), \qquad (6.6)$$

with different values for $d_1, d_2, w_1$ and $w_2$ tabulated in table 6.1.

The dip-in-laser-lithography (DiLL) configuration was used in combination with the highest magnifying objective (63x) and the resin IP-Dip (Nanoscribe GmbH). The dome was printed slightly deeper than the found interface, to ensure good attachment and prevent leakage. The dome was designed such that it could be printed within the writing field (200µm diameter) without block stitching—as opposed to previous work [16]. The cantilever was printed second, and attached to the slanted channel of the dome. The cantilever was printed in subsequent overlapping slabs at a 45°angle to prevent sagging of the bottom layers, as well as to enable printing cantilevers with dimensions greater than the writing field. The nozzle was printed in a similar way, with parameters optimized for small cross-sectional channels (table 6.2).

The gold-sputtered fluid interfaces in their respective sample cup were secured onto the Nanoscribe sample holder with tape. Droplets of IP-Dip were applied with the resin cartridge-syringe

| | Design: | | | | | | SEM measurement: | | | | Actual: | | |
|---|---|---|---|---|---|---|---|---|---|---|---|---|---|
| | $V_{step}$ | $V_{total}$ | $d_1$ | $d_2$ | $w_1$ | $w_2$ | $d_1$ | $d_2$ | $w_1$ | $w_2$ | $V_{step}$ | $V_{total}$ | Shrinkage % |
| Rectangular picoltre phaseguides (fig. 6.4E) | 10 pL | 100 pL | 8 | 20 | 10 | 30.23 | 8.27 | 19.81 | 9.00 | 30.52 | 9.89 pL | 98.9 pL | 1.10% |
| Rectangular femtolitre phaseguides (fig. 6.4D) | 200 fL | 2 pL | 4 | 8 | 7.958 | 1.989 | 4.20 | 7.86 | 6.32 | 1.93 | 181.1 fL | 1.81 pL | 9.45% |
| Triangular femtolitre phaseguides (fig. 6.4C) | 60 fL | 600 fL | 3.6 | 7 | 2.63 | — | 3.73 | 6.77 | 2.41 | — | 53.6 fL | 535.6 fL | 10.73% |

Table 6.1: *Dimensions of three different variants of axisymmetrical phaseguides. All values for $d_1, d_2, w_1, w_2$ are in* µm. *Shrinkage values are calculated with respect to designed volume.*

to the areas of interest on the fluid interfaces. The samples were then loaded into the Nanoscribe, upon which the objective approached the sample and made contact with the resin droplet. The global coordinates of each individual fluid interface were known and programmed, but a manual alignment step was still necessary to pinpoint the exact printing location for each fluid interface (see appendix B). Due to the thin sputtered gold layer, the interface could be detected automatically by the Nanoscribe. This was programmed to occur only once for each complete femtopipette.

| | Dome | Cantilever | Nozzle |
|---|---|---|---|
| Laser power* | 60% | 50% | 40% |
| Scanning speed [mm/s] | 70 | 40 | 50 |
| Slicing distance [$\mu$m] | 0.35 | 0.2 | Adaptive (0.05-0.3) |
| Hatching distance [$\mu$m] | 0.25 | 0.2 | 0.15 |
| Galvo acceleration [V/m$s^2$] | 6 | 6 | 2 |
| Find interface at [$\mu$m] | 5 | - | - |

Table 6.2: *Parameters of the two-photon-polymerization printing process. *Laser power is given as percentage of total laser power, which is 50mW for the used system.*

Upon finishing the last femtopipette print, the samples could be unloaded from the Nanoscribe. The samples were developed by first submerging them in propylene-glycol-methyl-ether-acetate (PGMEA, Sigma-Aldrich) for 30 minutes, then in isopropanol (IPA, Sigma-Aldrich) for 5 minutes, and lastly in Methyl perfluoropropyl ether, 1-Methoxy-heptafluoropropane (Novec™, Sigma-Aldrich) for 3 minutes—with gentle compressed air blow-drying in between each step. The samples were then inspected with an optical microscope to ensure all channels are cleared. If this was not the case, an additional development cycle could be employed.

## 6.3.2. Characterization

The fluid interfaces were inspected for obvious defects before continuing the process. Then, after laser drilling, the created apertures were inspected and measured with an optical microscope (Keyence Digital Microscope VHX-600). After 2PP printing, the internal channel dimensions of the 2PP printed femtopipettes could also be inspected optically, due to the transparency of the cured IP-Dip resin. However, for measuring the smallest features such as the individual axisymmetrical phaseguides, a scanning electron microscope (SEM, Jeol JSM6010LA) was used on models with an exposed cross-section, printed with the same parameters (fig. 6.4F-G).

To quickly assess the functioning of each device after developing and plugging the purge channel, the individual devices were connected to a 10mL syringe with Tygon™ tubing, and submerged into IPA. Pressure was then applied manually with the syringe to see if bubbles occurred, confirming a cleared femtopipette or indicating leakage in other areas.

**Burst pressure measurement**

When a device passed the initial assessment, it was ready for more detailed testing. The device could then be connected to a pressure sensor (Gems 3500, 0-2.5 bar $\pm$ 6.25 mbar, Gems Sensors Inc.) in series with a pressure source —in this case a syringe (60mL, BD Plastipak) on a syringe-pump (KDS legato 111, KD Scientific Inc.). The connected device could then be positioned under an optical microscope. Next, the top-surface of the device, including the femtopipette, could be submerged in a droplet of DI-water (ELGA Purelab Flex 3, Veolia).

For the purpose of validating the proposed analytical model, a special cantilever was designed with successive axisymmetrical expansions with increasing expansion angles $\beta$, schematically shown in figure 6.5A. The expansion angles $\beta$ were varied for both inwards and outwards direction. After letting the liquid enter due to capillary action, the settling point of the meniscus under neutral pressure was observed as an indication of the static contact angle $\theta$. Then, negative pressure was applied to fill the remaining cantilever. Lastly, positive pressure was slowly increased, allowing the pressure to equalize over the system of tubes for accurate pressure measurement. While compelling the liquid-air meniscus outwards, the burst pressure as function of expansion angle $\beta$ was recorded for each expanding step. The meniscus position was observed by optical microscope.

**Controlled dosing**

The method described above (even without pressure sensor) also provided a simple way to quickly assess the dosing capability of different concept designs. Submerged in the water

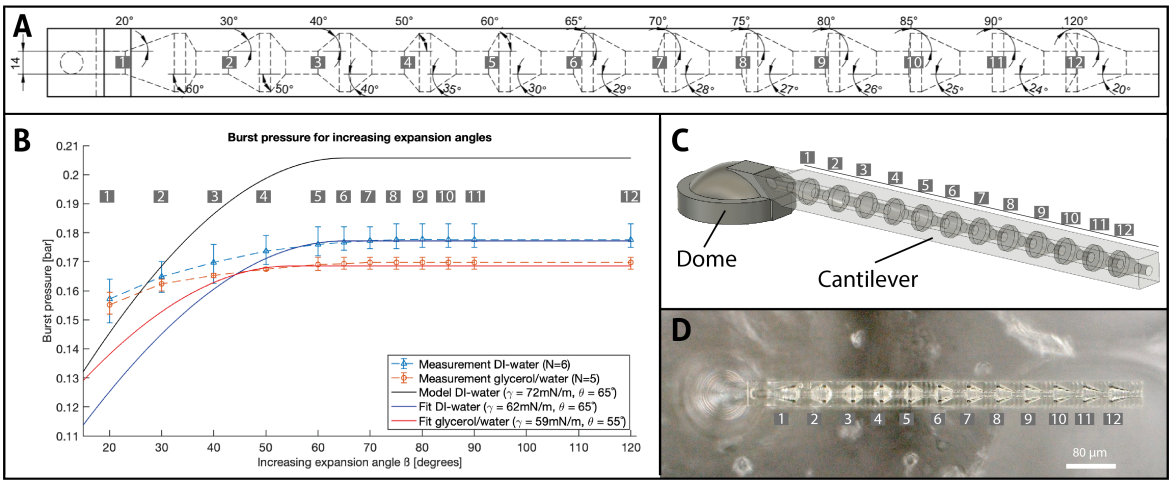


Figure 6.5: *Burst pressure measurement. A: Schematic of cantilever with 12 successive expansions with increasing expansion angle β (ltr). B: Plot of burst-pressure measured at each step, compared to analytical model prescribed by equation 6.4. C: CAD model showing 3D representation of axisymmetrical expansions. D: Optical micrograph showing 2PP printed device on top of fluid interface.*

droplet, an empty cantilever with axisymmetrical phaseguides could be filled in steps by applying a negative pressure with a handheld syringe. Next, the water could be compelled back out in subsequent steps, while observing whether the liquid-air meniscus caught on each axisymmetrical phaseguide step.

To consolidate the ability to dose liquid-in-liquid with the axisymmetrical phaseguides, an experiment was devised where one liquid would be dosed inside another (immiscible) liquid. As an approach to a more realistic application, the experiment was performed on an AFM system (JPK BioAFM Nanowizard 4, JPK Instruments AG). Two separate droplets were pipetted on a glass microscope slide: 1) 50:50 wt% DI-water:Glycerol (Sigma Aldrich) and 2) filtered mineral oil (BioReagent light oil, Sigma Aldrich). To prevent spreading of the droplets, the glass microscope slide was first treated with siliconizing reagent (Sigmacote®, Sigma Aldrich) in a desiccator for 1 hour (see appendix C for more details). The experiment could be monitored with an embedded inverted microscope (Zeiss Axio Observer 3, Carl Zeiss Microscopy GmbH). The device was attached to the probe holder of the AFM system whilst being connected to a pressure source (syringe, either manual or on the syringe-pump). The femtopipette was then brought within view, and lowered until sufficiently close to the microscope slide, determined by the optical focus of the inverted microscope. The microscope slide could then be moved in the XY plane using a motorized stage in order to position the droplets. An impression of the experiment is provided in figure 6.6D. First, the water/glycerol droplet was approached and entered with the femtopipette upon which negative pressure was applied with the syringe to aspirate a controlled amount of liquid. Then, the femtopipette was brought to the mineral oil droplet, where the water/glycerol mixture was dispensed in discrete steps, according to the volume contained within each step between two successive axisymmetrical phaseguides. The diameter of the resulting droplet was measured to determine its volume.

## 6.4. Results & Discussion

### 6.4.1. Fabrication

#### Fluid Interface

Two sample cups with five fluid interfaces each could be 3D-printed with a layer-height of 35µm in 80 minutes. For a DLP printer, the used print area does not influence print time, but the part-height does. The height of the fluid interfaces was kept intentionally low, to be able to fit the sliding sample-holder with loaded samples into the Nanoscribe. The fluid interfaces were very rarely clogged, and were not difficult to clean using the standard cleaning protocol (see Appendix B).

Aligning the laser was straightforward using the system's embedded alignment camera. After double-checking the position of the fluid interfaces, all the five apertures could be drilled in one run, taking less than 30 seconds. Since the fluid interfaces are composed of thermosetting methacrylate/acrylate based resin, it is assumed that the laser completely ablates the material without melting the surrounding areas. By focussing the laser at the top surface and not varying the focal depth of the laser during the operation, the

laser only drilled the connecting aperture to the microchannel—not all the way through the bottom of the fluid interface.

Upon inspection with the optical microscope, the diameter of the apertures was measured, giving 60µm $\pm$ 10µm. Sometimes small cracks could be seen around the aperture, likely due to the heat stress. Overall, the apertures looked clean (see figure 6.3E): without the rounded edges observed when DLP printing the apertures (as seen in previous work [16]).

**Femtopipette**

Due to the decreased aperture size compared to previous work, the dome needed no block stitching and was printed in one writing field in 7 minutes (compared to ∼60 minutes [11], [16]). Cantilevers were 600µm long and printed in 18 minutes. The nozzle printed in ∼5-8 minutes, depending on the chosen phaseguide-geometry.

The sputtered 3nm gold layer provided enough reflectivity to allow automatic interface finding. The interface finding command could be executed at the location of the aperture, without needing to move to the side of the aperture first. This is because the interface is not found exactly in the middle of the writing field, and the aperture was sufficiently small. The relative coordinates of each fluid interface were known, but due to small variances in alignment of the sample cup and minor deformations due to handling, each aperture still needed a final manual alignment step.

The printing started 5µm below the found interface, which ensured a secure, leak-free attachment of the dome in most cases—tested to withstand at least 4.5 bar. When the 2PP laser reached the surface, tiny bubbles could be observed through the process-camera feed, confirming contact with the interface.

Printing the nozzle required delicate fine-tuning of the process parameters as the small diameter sections were prone to clogging. The feature sizes in the smallest axisymmetrical phaseguides come near the resolution limit of the Nanoscribe. To prevent unwanted polymerization of the void channel regions, the dose was lowered when printing the nozzle section. The lower dose did result in higher shrinkage during development, reducing the void volume up to 10.73% with respect to the designed void volume, depending on the dose (see table 6.1).

## 6.4.2. Characterization with liquid

**Contact angle measurement**

An important unknown property for the characterization of the femtopipettes was the contact angle $\theta$ between the liquid (water) and the cantilever material (cured IP-Dip). From literature, the static contact angle between water and cured IP-Dip was suggested to be in the range of 72° [21] to 80.5° [22]. As an extra reference, a macro-scale contact angle measurement was performed on spincoated IP-Dip (WS-400E-6NPP-LITE, Laurell) which was cured with a UV spot source (Bluepoint 4 Ecocure, Honle UV technology) for 10 minutes at 50mm and then developed using PGMEA and IPA according to the standard protocol (App. B). Contact angles were measured using an optical tensiometer (Theta Lite, Biolin scientific) with DI-water (MilliQ). This resulted in a measured macro-scale contact angle $\theta$ of $62.3° \pm 4.8°$ (N=18).

However, to ascertain that this contact angle would also hold for microscale structures, an additional test was devised where the capillary filling of a cantilever with varying expansion angle $\beta$ was observed. The cantilever would be submerged in DI-water without applying pressure. Liquid would enter the cantilever by itself by means of capillary action, until the critical angle $\beta_c$ was met—depending on the contact angle $\theta$ of the liquid with the cantilever walls (section 6.2.1). The point where the liquid stopped thus gave an indication of the static contact angle according to $\theta = 90° - \beta_c$. Pinning was observed at expansion angles $\beta$ from 24° to 30° (for N=5 different cantilevers) yielding an approximate static contact angle $\theta$ between 66° and 60° respectively. This is well in the range of the macro-scale measurement.

Precise measurement of the contact angle is limited by the 2PP printing resolution and resulting microscopic irregularities near the edges of the expansions.

**Burst pressure measurement**

After filling the remaining cantilever sections using negative air pressure, the liquid-air meniscus was compelled outwards by slowly increasing the pressure. The meniscus was observed to pin to each expansion site, as expected. Then, when the air pressure was sufficient, the meniscus would burst through, and pin to the next expansion site with increased expansion angle $\beta$.

The burst pressures were recorded and are shown in figure 6.5B. In this figure, the analytical model prescribed by equation 6.4 is plotted and compared to measured burst pressures of DI-water (blue) and a 50% glycerol/water mixture (orange). As was predicted by the model, a plateau in the burst pressure can be observed for expansion angles $\beta$ greater than the critical angle $\beta_{c,air}$. Note that in this scenario the contact angle $\theta$ is equal to the critical angle $\beta_{c,air}$ (see section

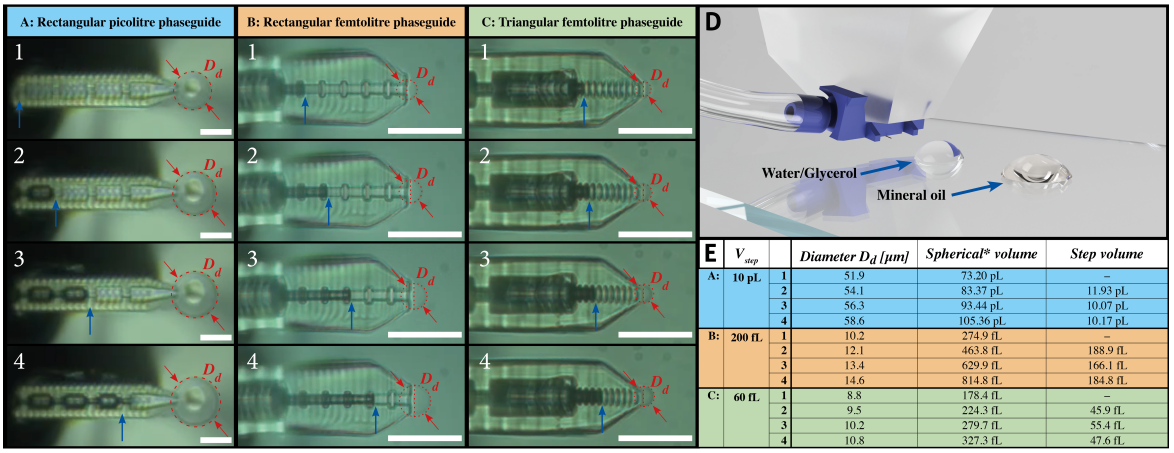


| E | $V_{step}$ | | Diameter $D_d$ [µm] | Spherical* volume | Step volume |
|---|---|---|---|---|---|
| A: | 10 pL | 1 | 51.9 | 73.20 pL | – |
| | | 2 | 54.1 | 83.37 pL | 11.93 pL |
| | | 3 | 56.3 | 93.44 pL | 10.07 pL |
| | | 4 | 58.6 | 105.36 pL | 10.17 pL |
| B: | 200 fL | 1 | 10.2 | 274.9 fL | – |
| | | 2 | 12.1 | 463.8 fL | 188.9 fL |
| | | 3 | 13.4 | 629.9 fL | 166.1 fL |
| | | 4 | 14.6 | 814.8 fL | 184.8 fL |
| C: | 60 fL | 1 | 8.8 | 178.4 fL | – |
| | | 2 | 9.5 | 224.3 fL | 45.9 fL |
| | | 3 | 10.2 | 279.7 fL | 55.4 fL |
| | | 4 | 10.8 | 327.3 fL | 47.6 fL |

Figure 6.6: *Discrete dispensing of water/glycerol droplet into mineral oil. A-C: The meniscus is indicated with a blue arrow. The droplets are created with a manually operated syringe which connected to the femtopipette. The droplets are denoted $D_d$ and marked with a red-dotted circle. The scale bar (white) is 40*µm*. Four incremental steps are shown (Note that for A, the last 4 steps out of 10 are shown). D: Impression of the experiment. The femtopipette is installed on the JPK AFM and first approaches the water/glycerol droplet to aspirate a small amount, which is then dispensed into the mineral-oil droplet. Images are taken with an inverted microscope below the sample. E: Tabulated results. *Droplets were assumed spherical (A) or half spherical (B-C).*

6.2.2). The level of the plateau is determined by the ratio of the surface tension $\gamma$ over the channel diameter $d$, of which the latter is fixed at 14 µm—confirmed by optical measurement. The reference model (black) is plotted for the surface tension $\gamma$ of DI-water at 72 mN m$^{-1}$, with the contact angle $\theta$ taken as 65°. The measurement data is fitted with the model by setting the surface tension $\gamma$ and contact angle $\theta$ as fitting parameters. It becomes clear that the plateauing level of the measured DI-water data is lower than the reference, but the critical angle $\beta_{c,air}$ seems to correspond. The experiment was repeated with a glycerol/water mixture to strengthen the observation of the plateauing behaviour. A slightly lower plateau is observed, together with a lower critical angle. This is expected because the surface tension as well as the contact angle of a glycerol/water mixture is known to be lower than that of water [23].

It is difficult to say with certainty why the resulting burst pressures are lower than expected, but it could be argued that in practice, the surface tension of the liquid inside the channel is lowered due to contaminants left over from the chemical development process that act as surfactants. Another explanation could be that the air adjacent to the meniscus has a higher relative humidity, which could effectively lower the surface tension [24].

### Controlled dosing

The liquid pinning behaviour proved predictable and controllable, so as a step in the direction of functionality, the liquid dosing capabilities of axisymmetrical phaseguides were investigated. Several concepts were designed and tested (see figure 6.4) with the goal of minimizing the dosing volume beyond the state of the art of 100fL. The working of each concept was first confirmed while observing the liquid pinning when the femtopipette was submerged in DI-water and actuated with a manually operated syringe. These observations were consolidated with an experiment where a femtopipette first aspirated an amount of water/glycerol which was then dispensed in discrete steps inside a droplet of mineral oil (videos available: [25], [26]). Glycerol was added to the water to reduce evaporation of the aspirated amount when moving the femtopipette out of the droplet.

The used JPK AFM platform proved useful for this experiment due to its straightforward use and accuracy in positioning the femtopipette. Droplets that were created within the mineral oil could be observed due to the difference in refractive index. The diameter of these droplets was then measured using the proprietary ZEN software (ZEN Blue, Carls Zeiss Microscopy GmbH). Images of the resulting droplets are shown in figure 6.6A-C.

The volume was then calculated based on the assumption that the droplet formed a perfect sphere (in the case of the 10pL steps, fig. 6.6A) or a perfect half sphere (in the cases of the 200fL and 60fL steps where the droplet was still partly adhered to the surface of the femtopipette, fig. 6.6B-C). Due to the hydrophilic properties of the cured IP-Dip, the droplet remained adhered to the femtopipette.

The diameter measurement was performed manually three times for each liquid step, resulting in a small measurement uncertainty of 0.3 µm on average. This measurement uncertainty propagates according to $\Delta V = \frac{1}{2}\pi D^2 \cdot \Delta D$ when determining the volume of the sphere, and it is further worsened by adding the uncertainties when determining the step volume. As the dosed volume gets smaller, the measurement uncertainties gain in relative size, becoming exorbitantly large for the femtolitre steps (averaging at 38.1 fL, nearly as big as the stepped volume). It is therefore a point of discussion whether the used measurement method is suited for the intended purpose, especially on the femtolitre level. However, looking at the low dispersion of measured step volumes and comparing them to the intended dosing volume, it is reasonable to argue that the measurement uncertainty is very conservative.

It was also observed that when exiting the water/glycerol droplet, a small amount of liquid adhered to the outside of the femtopipette. This amount then beaded up when entering the oil, so that a small initial droplet was observed at the nozzle before the first step was taken. This explains the small initial volume offset which is especially visible in the 200fL and 60fL results (fig. 6.6E(B-C)).

## 6.5. Conclusion

In this work, a new type of femtopipette has been developed that is able to control discrete amounts of liquid. To the best of the authors' knowledge, it is the first time that pressure actuated in-liquid dosing has reached a resolution beyond 100fL. The use of axisymmetrical phaseguides allows for controllable and repeatable in-liquid dosing that is straightforward to use with different kinds of pressure sources —even manually.

The application of multi-scale 3D printing has proven valuable for concept iterations, design freedom and production time. A functional device can be fabricated and tested over the course of merely 2 days. The introduction of a laser drilled aperture in the fluid interface significantly reduced 2PP printing time compared to previous works.

The existing analytical model for capillary pressure has been extended for predicting the geometry-dependent burst pressure when compelling liquid past axisymmetrical phaseguides. A special type of hollow cantilever was devised to test this theory. In line with the prediction, the burst-pressure saturated from the critical angle $\beta_c$ onwards.

Three variants of axisymmetrical phaseguide geometry were fabricated and tested, each with a different void volume (10 pL, 200 fL and 60 fL), specified by design. As a step towards future applications, a demonstration experiment was performed: a controllable amount of water/glycerol was first aspirated from one droplet, and then transported and dispensed with discrete steps into another droplet consisting of mineral oil. The demonstrated step-sizes cover a wide volume-range and have proven an increased resolution compared to the state of the art.

These demonstrations prove the concept of axisymmetrical phaseguides as a way to discretely dose liquid with unprecedented resolution. In principle, the achievable volume dosing resolution is only limited by the fabrication method, as it has been shown that the Laplace equations are still valid on a molecular scale [27]. Axisymmetrical phaseguides should also show meniscus pinning behaviour when the system is hydrophobic [28], which extends the range of possible applications.

The optical method used to check the volume of the created droplets shows large measurement uncertainty, especially for the smallest volumes. However, SEM measurements of the fabricated geometries, together with the observed pinning behaviour and consistency in measured step volumes, confirm the controlled dosing with high resolution.

The application of axisymmetrical phaseguides to femtopipettes holds great promise as a multifunctional tool in micro-engineering, micro-chemistry and micro-biology. The provided designs are well suited to be complemented with AFM functionality, opening the door to exciting next steps in single-cell research.

## References

[1] S. Lindström and H. Andersson-Svahn, "Overview of single-cell analyses: Microdevices and applications", *Lab on a Chip*, vol. 10, no. 24, pp. 3363–3372, 2010.

[2] J. R. Heath, A. Ribas, and P. S. Mischel, "Single-cell analysis tools for drug discovery and development", *Nature Reviews Drug Discovery*, vol. 15, no. 3, pp. 204–216, 2016.

[3] P. Actis, "Sampling from Single Cells", *Small Methods*, vol. 2, no. 3, p. 1 700 300, Mar. 2018.

[4] M. P. Stewart, R. Langer, and K. F. Jensen, "Intracellular delivery by mem-

brane disruption: Mechanisms, strategies, and concepts", *Chemical Reviews*, vol. 118, no. 16, pp. 7409–7531, 2018.

[5] G. Bulbul, G. Chaves, J. Olivier, R. Ozel, and N. Pourmand, "Nanopipettes as Monitoring Probes for the Single Living Cell: State of the Art and Future Directions in Molecular Biology", *Cells*, vol. 7, no. 6, p. 55, 2018.

[6] A. Meister, M. Gabi, P. Behr, P. Studer, J. Vörös, P. Niedermann, J. Bitterli, J. Polesel-Maris, M. Liley, H. Heinzelmann, and T. Zambelli, "FluidFM: Combining atomic force microscopy and nanofluidics in a universal liquid delivery system for single cell applications and beyond", *Nano Letters*, vol. 9, no. 6, pp. 2501–2507, 2009.

[7] O. Guillaume-Gentil, E. Potthoff, D. Ossola, P. Dörig, T. Zambelli, and J. A. Vorholt, "Force-controlled fluidic injection into single cell nuclei", *Small*, vol. 9, no. 11, pp. 1904–1907, 2013.

[8] O. Guillaume-Gentil, R. V. V. Grindberg, R. Kooger, L. Dorwling-Carter, V. Martinez, D. Ossola, M. Pilhofer, T. Zambelli, and J. A. A. Vorholt, "Tunable Single-Cell Extraction for Molecular Analyses", *Cell*, vol. 166, no. 2, pp. 506–516, 2016.

[9] E. Potthoff, O. Guillaume-Gentil, D. Ossola, J. Polesel-Maris, S. LeibundGut-Landmann, T. Zambelli, and J. A. Vorholt, "Rapid and Serial Quantification of Adhesion Forces of Yeast and Mammalian Cells", *PLoS ONE*, vol. 7, no. 12, 2012.

[10] P. Dörig, P. Stiefel, P. Behr, E. Sarajlic, D. Bijl, M. Gabi, J. Vörös, J. A. Vorholt, and T. Zambelli, "Force-controlled spatial manipulation of viable mammalian cells and micro-organisms by means of FluidFM technology", *Applied Physics Letters*, vol. 97, no. 2, pp. 1–4, 2010.

[11] R. C. L. N. Kramer, E. J. Verlinden, L. Angeloni, A. van den Heuvel, L. E. Fratila-Apachitei, S. M. van der Maarel, and M. K. Ghatkesar, "Multiscale 3D-printing of microfluidic AFM cantilevers", *Lab on a Chip*, vol. 20, no. 2, pp. 311–319, Jan. 2020.

[12] M. Knoblauch, J. M. Hibberd, J. C. Gray, and A. J. Van Bel, "A galinstan expansion femtosyringe for microinjection of eukaryotic organelles and prokaryotes", *Nature Biotechnology*, vol. 17, no. 9, pp. 906–909, 1999.

[13] K. T. Rodolfa, A. Bruckbauer, D. Zhou, A. I. Schevchuk, Y. E. Korchev, and D. Klenerman, "Nanoscale pipetting for controlled chemistry in small arrayed water droplets using a double-barrel pipet", *Nano Letters*, vol. 6, no. 2, pp. 252–257, 2006.

[14] Y. T. Chow, S. Chen, R. Wang, C. Liu, C. W. Kong, R. A. Li, S. H. Cheng, and D. Sun, "Single cell transfection through precise microinjection with quantitatively controlled injection volumes", *Scientific Reports*, vol. 6, no. April, pp. 1–9, 2016.

[15] H. H. Perez Garza, M. K. Ghatkesar, P. Lothman, A. Manz, and U. Staufer, "Enabling local deposition and controlled synthesis of Au-nanoparticles using a femtopipette", *9th IEEE International Conference on Nano/Micro Engineered and Molecular Systems, IEEE-NEMS 2014*, pp. 323–328, 2014.

[16] P. F. J. Altena van, "Multiscale 3D printed polymer probes for single cell experiments", Master's thesis, TU Delft, Delft, 2021.

[17] P. Vulto, S. Podszun, P. Meyer, C. Hermann, A. Manz, and G. A. Urban, "Phaseguides: A paradigm shift in microfluidic priming and emptying", *Lab on a Chip*, vol. 11, no. 9, pp. 1596–1602, 2011.

[18] A. Glière and C. Delattre, "Modeling and fabrication of capillary stop valves for planar microfluidic systems", *Sensors and Actuators, A: Physical*, vol. 130-131, no. SPEC. ISS. Pp. 601–608, 2006.

[19] E. Yildirim, S. J. Trietsch, J. Joore, A. Van Den Berg, T. Hankemeier, and P. Vulto, "Phaseguides as tunable passive microvalves for liquid routing in complex microfluidic networks", *Lab on a Chip*, vol. 14, no. 17, pp. 3334–3340, 2014.

[20] I. Wenten, K. Khoiruddin, A. Hakim, and N. Himma, "The Bubble Gas Transport Method", in *Membrane Characterization*, Elsevier, 2017, pp. 199–218.

[21] A. D. Lantada, S. Hengsbach, and K. Bade, "Lotus-on-chip: Computer-aided design and 3D direct laser writing of bioinspired surfaces for controlling the wettability of materials and devices", *Bioinspiration and Biomimetics*, vol. 12, no. 6, 2017.

[22] M. F. Berwind, A. Hashibon, A. Fromm, M. Gurr, F. Burmeister, and C. Eberl, “Rapidly prototyping biocompatible surfaces with designed wetting properties via photolithography and plasma polymerization”, *Microfluidics and Nanofluidics*, vol. 21, no. 9, pp. 1–7, 2017.

[23] K. Takamura, H. Fischer, and N. R. Morrow, “Physical properties of aqueous glycerol solutions”, *Journal of Petroleum Science and Engineering*, vol. 98-99, pp. 50–60, 2012.

[24] J. L. Pérez-Díaz, M. A. Álvarez-Valenzuela, and J. C. García-Prada, “The effect of the partial pressure of water vapor on the surface tension of the liquid water-air interface”, *Journal of Colloid and Interface Science*, vol. 381, no. 1, pp. 180–182, 2012.

[25] M. Blankespoor, *Experiment demonstrating dosing capability of 2pp printed cantilevers with axisymmetrical phaseguides*, https://vimeo.com/692216865, 2022.

[26] ——, *Discrete femtolitre liquid dosing using axisymmetrical phaseguides*, https://vimeo.com/692222490, 2022.

[27] J.-C. Fernandez-Toledano, T. Blake, P. Lambert, and J. De Coninck, “On the cohesion of fluids and their adhesion to solids: Young’s equation at the atomic scale”, *Advances in colloid and interface science*, vol. 245, pp. 102–107, 2017.

[28] J. M. Chen, C. Y. Chen, and C. H. Liu, “Pressure barrier in an axisymmetric capillary microchannel with sudden expansion”, *Japanese Journal of Applied Physics*, vol. 47, no. 3 PART 1, pp. 1683–1689, 2008.

# 7

# Conclusion

## Thesis conclusion

This thesis embodies research into liquid dosing on the microscale. First, the literature was surveyed to gain a broad perspective on applications benefiting from increased volume dosing resolution, as well as to present methods and techniques that serve this purpose. Special attention was paid to single-cell research, where the controlled transport of substances through the cell membrane allows scientists to gain a better understanding of biological processes within the cell.

Direct penetration through the use of femtopipettes was distinguished as a versatile and promising technique due to its positional accuracy, selectivity and multifunctionality. Especially the hollow AFM cantilevers proved attractive due to the added benefit of force sensing capability.

Different dosing methods were compared based on the reported achieved volume dosing resolution. Although pressure actuation had a lower resolution compared to electrowetting and thermal actuation, it came out as the most straightforward and versatile technique. With the methods, the smallest volume that could be controllably dispensed or aspirated with a pressure actuated femtopipette was found to be 100 fL. This lead to the following research question:

> **"How can a pressure-actuated femtopipette reach a volume dosing resolution beyond 100 fL?"**

To answer this question, two new concepts were proposed that were both good candidates for increasing the volume dosing resolution: 1) the addition of a flexible membrane barrier to the femtopipette and 2) the addition of 'phaseguides' to the femtopipette. The theory and feasibility of each concept was first analysed before fabricating the prototypes to test their functioning. Moreover, in the case of the phaseguides concept, a new piece of theory was developed and experimentally tested that further improved the understanding of the functioning of this concept.

For both concepts, a multi-scale 3D printing methodology —first developed by Kramer et al. [1] and then improved by Van Altena et al. [2] —was used to fabricate prototypes. In this research, this methodology was further optimized. The main advancement was made by adding a laser drilling step that reduced the aperture size in the fluid interface from ~200 µm to ~70 µm. Consequently, the 2PP printing time of dome-structures was cut back significantly from ~60 minutes to ~5 minutes.

The concept with the embedded flexible membrane was able to control the liquid meniscus to some extent, showing a displaced volume in the range of one picolitre. The membrane was first characterized and behaved predictably with respect to the analytical deformation model. However, when embedded within a 2PP printed femtopipette, the deflected liquid volume was not in agreement with the volume displacement expected from the deformation of the membrane, in the order of 100 fL. This lead to the impression that the membranes were porous. This porosity was difficult to classify and challenges were encountered in the reproducibility of these femtopipettes, likely originating from the development process and the inherent difficulties of developing closed 2PP printed channels.

On the other hand, the phaseguide concept proved very successful in controllably dosing discrete amounts of liquid. Discrete liquid dosing steps of 10 pL, 200 fL and 60 fL have been demonstrated, thereby beating the state of the art of pressure actuated volume dosing. The dosing was repeatable and robust: even for the highest volume dosing resolutions, the syringe acting as a pressure source

could be operated by hand. Furthermore, the amount of liquid that is dosed can be customized by the designer. All together, the addition of phaseguides to the femtopipette makes for a very promising and versatile advancement of the state of the art in pressure driven femtopipetting.

In this research, the implementation of phaseguides into a femtopipette has lead to unprecedented volume dosing resolutions. The implementation of a membrane could not achieve the same level of resolution nor control. The membrane concept may still be a viable option to dose liquid volumes with a high resolution, but more research and optimisation would be needed.

In conclusion, the research question and the sub-questions formulated in section 4.1 have been answered throughout this project. One concise answer could be formulated as follows:

> **"A pressure-actuated femtopipette can reach volume dosing resolutions beyond 100 fL by implementing axisymmetrical phaseguides"**

**Key contributions**

Overall, this work has not only demonstrated new concepts, but has also contributed to the existing notion of functional, 2PP printed microfluidic cantilevers. The most important contributions are listed below:

- **Laser drilling of fluid interface apertures introduced**
  The introduction of an additional process step where the apertures in the fluid interfaces were drilled by a laser have reduced the aperture size from ∼200 µm down to ∼70 µm. The time needed to 2PP print domes structures was thereby significantly reduced from ∼60 minutes to ∼5 minutes.
- **Reduced development time**
  The introduction of a purge-channel together with the application of Novec™ developer solution lead to better development of small microfluidic channels. Where previous methods required up to 48 hours of submersion in developing solution [2], now the development seldom took longer than 45 minutes.
- **Tested the concept of microfluidic cantilevers with embedded membranes**
  Both mechanical deformation and liquid behaviour of the membrane concept were tested and compared to analytical models.
- **Introduced concept of axisymmetrical phaseguides**
  A novel concept was proposed inspired by existing literature on the phenomenon of capillary pinning. The concept was developed, fabricated and tested.
- **Achieved unprecedented volume dosing resolution with pressure actuation**
  The fabricated prototypes of the phaseguide concept were able to improve upon the state of the art in pressure driven femtopipetting. Liquid volumes of 10 pL, 200 fL and 60 fL were successfully dispensed into another liquid.
- **Extension to theoretical model proposed and tested**
  An extension to the existing theory on geometry dependent capillary pinning was proposed, specifically for the scenario when liquid is compelled past geometrical barriers by an opposing gas pressure. An experiment was devised that yielded results supporting the proposed theory.
- **Introduced a novel way to determine the static contact angle at the microscale**
  A novel device was introduced that employed a microfluidic channel with subsequent geometrical expansions. Observing the spontaneous liquid entry due to capillarity revealed the maximum expansion angle that could be passed. This behaviour could directly be related to the static contact angle.

# Recommendations

This research reports a proof of concept for techniques that allow increased volume dosing resolution with pressure actuated femtopipettes. I hope this project opened the door to new applications in the fields of micro-engineering, micro-chemistry and micro-biology. To anyone that wants to pursue this line of research I have a few recommendations that could potentially improve the methods presented in this work.

- **Demonstrate AFM functionality**
  As a first step in advancing on the body of work presented here, one could use the phaseguide concepts and apply AFM functionality to the cantilevers. The cantilevers in this project were already designed with this purpose in mind, so this step should not be too difficult. The challenge lays in designing a cantilever tip that can be used as an AFM tip, but also embeds the liquid dosing functionality of the axisymmetrical phaseguides.

- **Optimize laser drilling procedure**
  The presented procedure for laser drilling the apertures into the fluid interfaces could be optimised to create even smaller holes. Not much time was spent to optimise the parameters of the Optec micromachining protocol once it seemed to produce holes of consistent size. A more thorough approach should be taken to find the parameters optimal for drilling the smallest hole possible, while only drilling through the top surface and not all the way through.

  A major opportunity comes with the new Lasea femtosecond laser that has been installed in our lab. It is likely that this machine allows for much greater precision [3] and possibly user-friendliness.

- **Improve the fluid interface layout in the sample cup**
  One bottleneck that poses a limit on the further automation of the presented workflow, is the difficulty experienced when the objective of the Nanoscribe unintentionally loses contact with the resin droplet. This scenario often occurred when the objective was finished with one cantilever and then moved to the next printing location. Due to the gaps between the fluid interfaces, the resin tends to be drawn away from the objective. This has as a consequence that the objective had to be manually focussed again for each printing location. The layout of the fluid interfaces within the sample cup could be optimised and the sample cup could be adjusted such that the gap between printing locations is less pronounced.

- **Automate the aperture finding procedure**
  Once the previous issue is addressed, one could try to further automate the process of determining the exact coordinates of each fluid interface aperture in the sample cup. The global coordinates of each aperture are known by design, but due to handling and manual alignment of the sample cup within the nanoscribe holder, a small variation exists for each aperture location. Therefore, before printing, the exact coordinates of each aperture need to be found manually.

  An interesting solution to this might be to use a custom script that uses image recognition in combination with control over the motion stage to determine the coordinates for each aperture. Recently, Nanoscribe has released new features in their software that allow a link to external scripts called ‘Servermode’ and ‘CommandLineSlicer’ [4].

- **Advance production of fluid interfaces**
  One could experiment with the methodology used for the production of the fluid interfaces. Using the Lasea femtosecond laser mentioned before, a new range of possibilities may open up. For example, one may choose to use fused silica as a 2PP printing substrate, through laser drilling apertures into the fused silica and then bonding the other side to a DLP printed fluid-connector. This may improve the automation of interface-finding of the Nanoscribe without having to sputtercoat the DLP printed samples. The smooth surface of fused silica may facilitate a leak-free connection to the femtopipette.

  Other ways of machining the fluid interface can also be researched. One such promising method is the use of Selective Laser Etching (SLE). Here, three-dimensional shapes (such as microchannels) can be machined into transparent materials such as fused silica or PMMA using a femtosecond laser [3], [5].

- **Surface functionalization**
  The cured and developed IP-Dip resin used for 2PP printing proved hydrophilic with a water contact angle of $\sim 65°$. When working with cellular content, it might in fact be better to use a femtopipette that is hydrophobic, in order to prevent biological matter to adhere to the surface of the device [6]. In principle, the concept of phaseguides should also work for hydrophobic channels [7]. Therefore, it might be worth pursuing methods that can make the surface of the femtopipette hydrophobic. This might be done through experimenting with different types of photoresist, but it is likely more straightforward to use a surface functionalization strategy [8].

- **Sharper nozzle tip**
  Due to the aforementioned hydrophilicity of the IP-Dip liquid had the tendency to also adhere to the outside of the femtopipette. Thus, when exiting a droplet after aspiration, some liquid would bead up on the outside. This liquid then added to the dosed amount when the femtopipette would perform a dispensing action. This side effect could likely be mitigated by making the tip of the nozzle sharper, so that the liquid has less area to attach itself to.

  Furthermore, a sharper tip might help in detaching the dispensed amount from the nozzle, and likely also benefits imaging of the dispensed droplet.

- **Detaching the dispensed liquid amount**
  In the demonstration of the dosing capability with the phaseguided femtopipette, water droplets were dispensed into oil. However, due to the properties described in the previous points, the water droplet stayed attached to the nozzle. Efforts were made in trying to separate the droplet from the nozzle by vibrating the femtopipette, but the adherent properties proved too strong. One idea to separate the formed droplet is to assert force to the droplet by moving the nozzle past a predefined edge on the substrate surface. Such an edge could be present in for example microwell-arrays.

  Another way might be to alternately aspirate small amounts of water and oil. Then, if a water droplet is dispensed into an oil droplet, the water amount may be ‘pushed out’ by the oil amount directly following the water.

- **Improve volume dosing measurement**
  The applied method to measure the resulting volumes of water amounts dispensed within the oil proved to be rather inaccurate. Each dispensing step was measured manually by drawing a circle around the resulting droplet. This was not the most reliable measurement method since the edges of the resulting droplet were not very clearly defined. This may be improved by for example adding colour to the water amount—like food colouring or fluorescent dye. In the latter case, the intensity of the fluorescent dye could be measured and compared to the intensity of a known volume (like the inside of the femtopipette) to determine the volume of the dispensed amount [9].

  Another way to improve upon defining the edges of the dispensed amount could be to convert the image to greyscale and let an image processing script run that recognizes the change in contrast.

- **Vary constriction diameter of stepped phaseguides**
  The constriction diameter is the main determinant of the burst pressure. Therefore, to increase robustness of the volume dosing control using axisymmetrical phaseguides, it may be interesting to incrementally increase or decrease the constriction diameter of each consecutive phaseguide step. This may allow working with a pressure controller and controllably increasing the pressure for each step. The main disadvantage would be that the dosing control in this way likely only works in one direction.

- **Experiment with time dependency**
  In this research, only phaseguides with the same constriction diameter were used. Still, it was observed that the meniscus pinned on consecutive steps. This might be because of a time dependency in the system. The proposed model is valid for static situations, but it may be necessary to extend it to include properties such as viscosity, that influence the dynamic behaviour of the liquid. Perhaps the application of Washburn’s law could lead to a model that includes viscous properties and time dependency [10].

A further understanding of the dynamic behaviour may enable to use pressure pulses of a certain magnitude and length to burst through one phaseguide at the time. The benefit of this is that it should work in both aspirating and dispensing direction. A more repeatable control over each single phaseguide could potentially increase the versatility of the phaseguided femtopipette.

- **Apply numerical model**
  In the beginning of the project, I looked into the possibilities of modelling capillary properties numerically. To my first judgement, the options that were available to perform such a numerical analysis were quite limited. COMSOL multiphysics does offer microfluidic packages, but for capillarity I felt that it seemed more to mimic the phenomenon than to really predict it. To get useful results, it would likely take a long time to tweak the parameters. Another software called Surface Evolver also exists, that applies a minimal energy method to approximate liquid interfaces. This software seemed not very user-friendly, and had limited freedom in the design of microfluidic structures.

  In hindsight, having a very clear use-case, it might be worth spending time to build and tweak a numerical model. Especially considering the phaseguides, it may yield additional insights in their behaviour and would serve as an extra comparison to the proposed burst pressure model.

- **Further testing membrane concept**
  The tests with cantilevers with embedded membranes soon lead to the impression that some form of porosity might be present in the membranes. This was not in line with the initial expected functioning of the concept, and thus it was decided to focus more on the emerging new concept with phaseguides. In retrospect, it might be interesting to investigate whether the porosity can be further characterized and used as a potential feature. For example, porosity of the membrane should allow filling the entire nozzle-chamber up to the membrane. Then, dispensing the entire liquid portion is likely not possible in a controlled fashion, however, it may still be possible to actuate and deflect the membrane. This would in principle still force out a small amount of liquid from the nozzle, potentially with the desired control that was initially expected from this concept.

# 8

# Reflection

While I was orienting on different possible thesis subjects, I had a few requirements for myself that I thought would combine into a suited project for me. I wanted the focus to be on the design and conceptualisation of new ideas; I wanted to translate these designs into reality by prototyping and tinkering something physically; preferably I wanted to employ additive manufacturing in the fabrication process; and potentially I wanted to do up some experience with cleanrooms and high-tech equipment.

Looking back at my journey now, I am contented to conclude that this project has ticked all the boxes—and more.

This project allowed me to take a deep dive into fields that I was not familiar with before I started. I appreciated the bridge to cell-biology as an element that enriched the mechanical challenges involved in this project. I enjoyed spending time in the initial phase to get familiar with the new concepts I encountered. Perhaps my literature reviewing phase took a bit longer than usual, but I didn't mind as I realized that all the knowledge I gained here was directly useful for the next phases.

As an additional opportunity I was offered to be a mentor to a Bachelor End Project (BEP) group, who had an assignment similar to my project. I joined their meetings every week, and it was nice to hear their fresh ideas and brainstorm with them.

I spent time to think about possible production methods and experiments, and used this when making a planning for the whole project. From my previous experience with such plannings, I did not expect it to be very accurate due to unexpectancies encountered in the lab. However, to my surprise, the initial planning almost kept up throughout the entire production and experimental phase.

The production and testing phase was the most fun of all. Bringing plenty different designs to life gave great satisfaction—especially when they worked according to my intentions. I was impressed by the level of freedom and responsibility that was entrusted to me being able to work with specialty tools and sensitive instruments. In all, I moved between 7 labs, having access to more than 15 high-tech pieces of equipment.

From the start, my main focus had been the membrane concept. The phaseguide concept was something of a novel idea that arised during the end of my literature phase. I was already far in the process of preparing and testing membranes, when I decided to print a cantilever with phaseguides, just out of curiosity. This worked so well that I decided to spent more and more time on this interesting concept. In the end, I did not manage to get the membrane concept to live up to its expectations. However, with the phaseguides, I soon was able to print femtopipettes that could control liquid doses beyond the "world record" of 100 fL.

I am very proud that this invention lead to the development of a patent and perhaps also a scientific publication. I could not have dared to hope for such a positive outcome of my thesis project. I have learned an incredible amount, and I look back on my journey through the graduation project satisfied with the body of work I was able to produce.

# Appendices

# A

# Design

## A.1. Fluid interface

The fluid interface is a crucial part of the femtopipetting system, as it enables a fluidic connection to the femtopipette. The fluid interface is 3D printed using a DLP desktop printer (Micro Plus HiRes, EnvisionTEC GmbH). This allows for ultimate design freedom and ease of manufacturing. The fluid interface encompasses three basic functions and subfunctions thereof:

1. Allowing a connection to a pressure source
   (a) The conncection should be reversible (not permanent)
   (b) The connection should be leak-free
   (c) The connection should be able to withstand pressures within the working range
2. Supplying a suitable substrate for 2PP printing
   (a) The substrate should adhere well to the 2PP print
   (b) The substrate should be compatible with the chemicals used in the 2PP process
   (c) The fluid interface should accomodate for easy chemical development of the 2PP printed parts
   (d) (ideally) The substrate should allow for automatic interface finding of the Nanoscribe
3. Allowing the femtopipette system to be handled
   (a) The fluid interface should allow for handling with tweezers
   (b) The fluid interface should accommodate a fit to the intended test setup
   (c) The fluid interface should fit into the appropriate sampleholder of the Nanoscribe

The first function was met by using a plug-type connector together with flexible tubing (Microflex Transfer Tubing, Tygon® ND-100-80 Microbore, ID 1.02mm, OD 1.78mm). By testing different dimensions of the plug (mainly the diameter), eventually a fit was found that was easily reversible without breaking the plug, was leak free and was able to withstand pressures $> 4.5$ bar (max of pressure test setup). The final plug outer diameter was 1.5 mm.

For the second functional requirement, it was found that the in-plane (XY) surfaces of the DLP printed part are best suited for the use as a 2PP substrate. On the vertical surfaces (Z), small ridges are present due to the layer stacking. These ridges proved to complicate the interface finding, and hindered a solid connection to the 2PP printed part. The in-plane surfaces were not perfectly flat due to small irregularities of the printbed, but were sufficiently flat for good interface finding and adhesion. As a resin, the material 3DM Tough Clear (ADMAT SASU) was used. Other resins have been tested but were discarded.

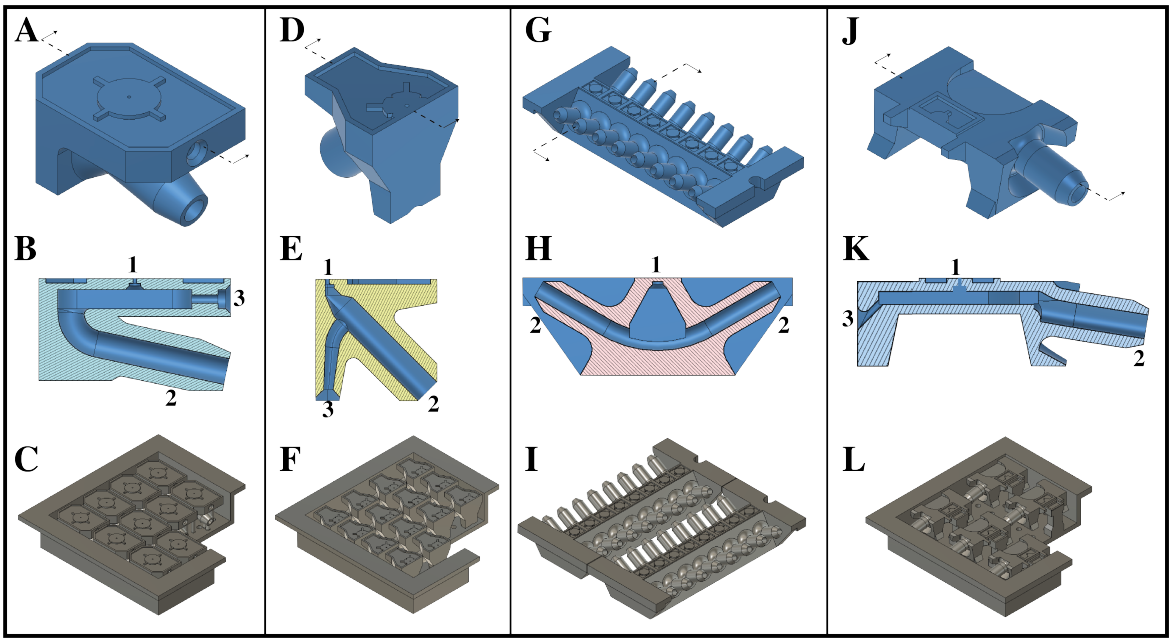


Figure A.1: *CAD models of the four generations of the fluid interface. The sectional views of each generation are displayed below, revealing the 2PP printing site (1), the plug-type connector (2) and the purge channel (3). Finally, each configuration for the Nanoscribe sampleholder is also shown.*

Lastly, the fluid interface was designed with the final test setup in mind. Through the course of the project, four different versions of the fluid interface were designed and used that each served a unique application purpose. These four generations of the fluid interface are shown in figure A.1.

Each generation of the fluid interface was designed to fulfil all the functions stated above. All generations share the same concept of the horizontal 2PP substrate (fig. A.1(1)); the plug type connector (fig. A.1(2)) and a purge channel to accommodtae better chemical development (fig. A.1(3))(In the third generation, (fig. A.1G-I), the purge channel consists of a second plug type connector channel). Some additional details shall be highlighted briefly for each generation:

**A-C**: The first generation was intended for the printing, handling and testing of horizontal membranes. These fluid interfaces could be incorporated separately into the white-light measurement setup. Ten fluid interfaces could be fitted into one sample cup (fig. A.1C).

**D-F**: The second generation was designed specifically for vertical membrane orientations, but could also be used with horizontal membranes. This design is symmetrical about an axis through the plug-type connector, allowing the fluid interface to be positioned in two convenient orientations. The footprint was reduced such that one sample cup could hold 14 fluid interfaces. (fig. A.1F)

**G-I**: For the quick iteration of 2PP printed cantilevers, a new fluid interface concept was designed where eight separate 2PP print sites are combined into one part. The purge channel is replaced with a second plug-type connector to easily alternate between a plugged configuration and an open configuration. The combination of multiple print sites allowed for quick assessment of each 2PP printed cantilever, where the pressure tubes could be easily exchanged between separate print sites. Two fluid interfaces with eight 2PP print sites each could be fitted adjacently into the Nanoscribe holder. Moreover, all the print sites could be covered with one single IP-Dip resin ‘droplet’. The objective remained in contact with this resin droplet during the entire operation, and the chance of the objective moving out of the resin was thus eliminated. This enabled the printing of all the devices in one go, without the need for manual adjustments.

**J-L**: The final fluid interface was designed for testing functional femtopipettes. The shape of the interface is such that it can be fitted to the probe holder of the JPK bio-AFM system. The two protrusions next to the print site are to protect the suspended cantilever in case the fluid interface tips over to its side. Five fluid interfaces fitted in one sample cup. The sample cup has special ‘resin-towers’ adjacent to the print sites, to keep the Nanoscribe objective inside the resin while printing the suspended cantilevers.

## A.2. Membranes

To be able to characterize various membranes, mainly three different membrane versions were designed and made. For the measurement of the deflection of the membrane, both a horizontal and a vertical orientation were printed (2PP print direction indicated by red triangles in figure A.2). The CAD models of both orientations were made parametrically, such that dimensions of the membrane and dome could be easily modified. The use of the symmetrical fluid interface (see previous section) was convenient to be able to orient both horizontal and vertical membranes right for the whitelight measurement (indicated by purple arrows in figure A.2).

At a later stage, also domes with intentionally porous membranes were designed. The pore-size and distribution could be changed parametrically. The idea was that the porous membrane could act as a capillary barrier, thus also containing a liquid volume of a known amount in the nozzle. In fact it is here that the idea of phaseguides originated. The porous membranes could be characterized by performing a so called 'bubble-point test'. The bubble-point being an equivalent to the burst pressure, encompassing information about the pore-size and the wettability properties.

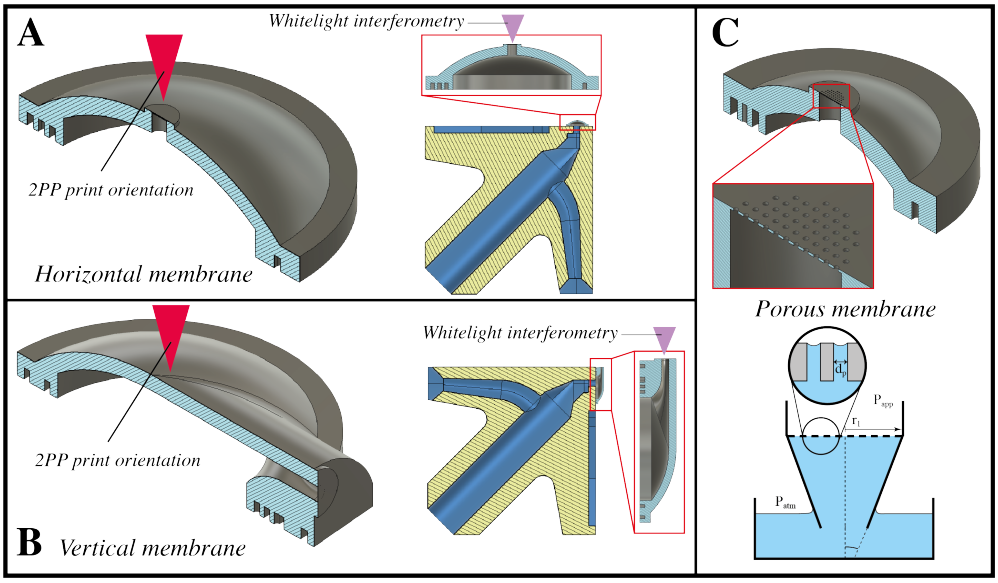


Figure A.2: *Three membrane variants. A: Horizontally 2PP printed membrane (red arrow indicates 2PP orientation). The position on the fluid interface for whitelight measurement is also shown (purple arrow). B: Vertically 2PP printed membrane, also with shown orientation for whitelight measurement. C: Porous membrane. Pore-size and distribution could be changed parametrically.*

## A.3. Femtopipette

The design of the domes (see previous section) only needed to be slightly adjusted to accommodate for the suspended cantilevers. The channel lead through the dome towards the side, where it came to a 45°slanted edge (see figure A.3A1). The cantilever (fig. A.3A2) could be printed attached to this slanted edge. The cantilever then extends horizontally and embodies a cylindrical channel (D=20 µm). At the end of the cantilever another 45°slanted edge is made, where the nozzle (A.3A3)) is attached. Some important dimensions are given in figure A.3B. Using this modular way of design, different parts could be iterated independently. Especially the nozzle design was iterated often. The four main nozzle designs are highlighted in figure A.3C-F.

To test the analytical model that was proposed to describe the behaviour of geometrical changes in phaseguides, a special cantilever was designed that incorporates incrementally changing channel geometries (see figure A.4). The cantilever was designed to gain information about both the aspiration direction and the dispensing direction (indicated in fig. A.4). Several consecutive channel expansions were designed, each with a slightly different expansion angle $\beta$, varying $\beta$ in both the aspiration and dispensing direction.

The varying expansion angle $\beta$ in the aspiration direction was used as a measure for the contact angle $\theta$ between the liquid and the cantilever walls. By submerging the system in liquid without ap-

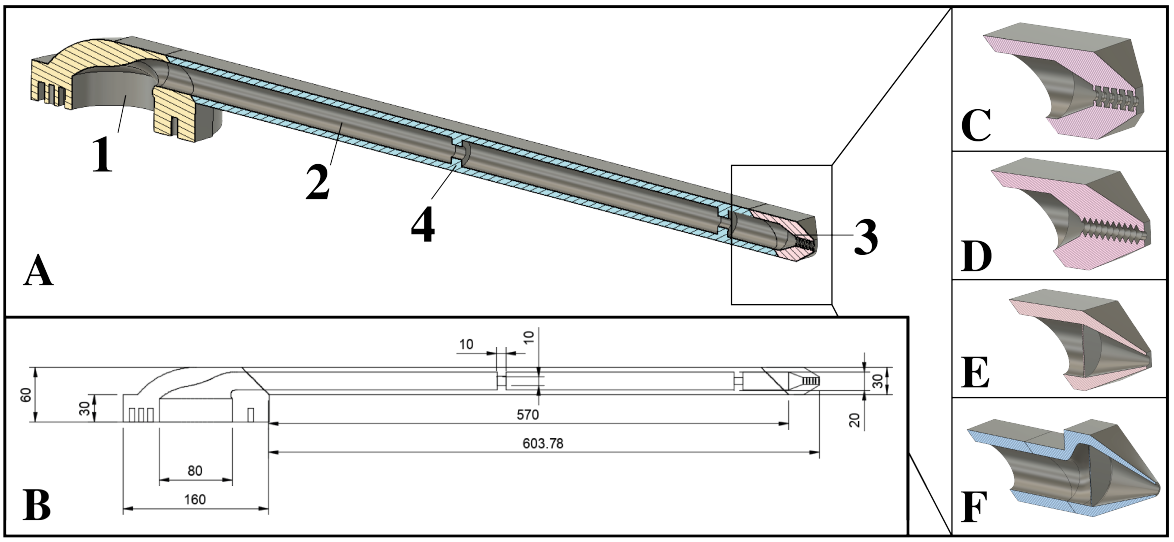


Figure A.3: *Femtopipette design. A CAD model of the entire femtopipette is shown in A, comprising the dome (1), the cantilever (2) and the nozzle (3). Some important dimensions are given in B (unit =* µm*). Different nozzle designs are highlighted in the insets. C: Rectangular phaseguide design. D: Triangular phaseguide design. E: Nozzle with* 20 µm *vertical membrane. F: Nozzle with* 30 µm *vertical nozzle.*

plying pressure, the liquid would enter the femtopipette until an equilibrium was met. The point were the liquid would stop advancing was a direct indication of the contact angle according to $\theta = 90° - \beta$. This method does not take into account the surface roughness inside the channels. Hypothetically, small ridges caused by the 2PP printed voxel-lines could alter the behaviour of the capillary flow.

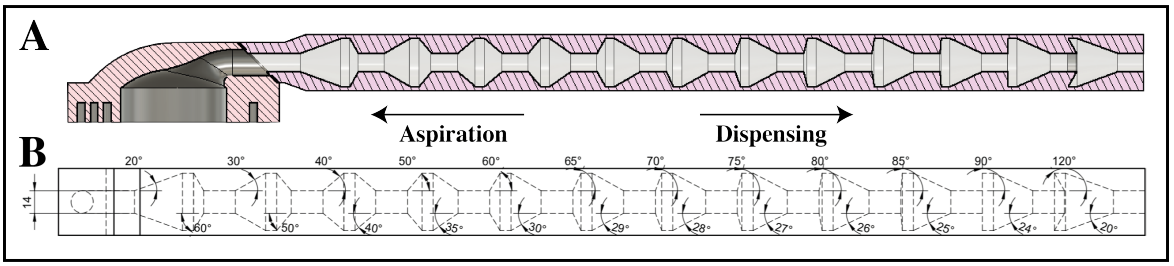


Figure A.4: *Special cantilever that was designed to test the proposed theory on burst pressures. A: cross-sectional view of the cantilever attached to the dome. Aspiration and dispensing directions are indicated with arrows. B: Drawing of the expansions revealing the increasing expansion angles $\beta$ in both aspiration and dispensing direction.*

## A.4. Miscellaneous

### Fluid interface clamps

To easily handle the fluid interfaces (sec. A.1), special customized tools were designed. These tools where also 3D printed with the DLP printer, and could perfectly accommodate for the shapes of the fluid interfaces. These tools were used for holding the interfaces in position for the white-light measurement or optical inspection, but they were also used for the manual operation of clogging each purge-channel. Two different clamps were made, one for the fluid interfaces of the horizontal membrane configuration (fig. A.5A), and one for the vertical membrane interfaces (fig. A.5B). These clamps were spring-loaded so they could securely hold the interfaces during the measurement. They were made such that the pressure tube could be easily connected to the interface when they were clamped. This ensured proper handling and prevented damage to the 2PP printed devices.

### Tube connectors

Different types of tubing were used throughout the project. Each tube comes with its own specific connector, but finding the right connectors and adapters to link everything together proved quite a challenge. This, together with the relatively high costs involved in ordering separate connector types,

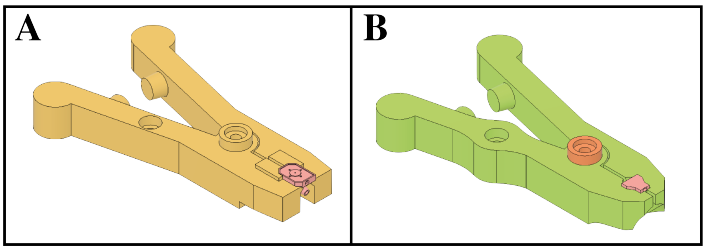


Figure A.5: *Custom fluid interface clamping tools. Two versions of clamps were made, each to fit perfectly to one type of fluid interface. The clamps were spring-loaded to maintain the fluid interface during the experiments.*

lead to the decision to manufacture some of my own specialty connectors. These connectors, shown in figure A.6, were also 3D printed with the EnvisionTEC desktop DLP printer.

Especially the conncector shown in fig. A.6A was very useful to connect a syringe to 4mm Festo pressure tubing. A connection that would otherwise need a plethora of different adapters. A Luer-Lock™ type connector was designed to fit securely and leak free to the syringe. The other end made use of a so-called 'barbed connector' that plugs leak free and securely into the 4mm pressure tube.

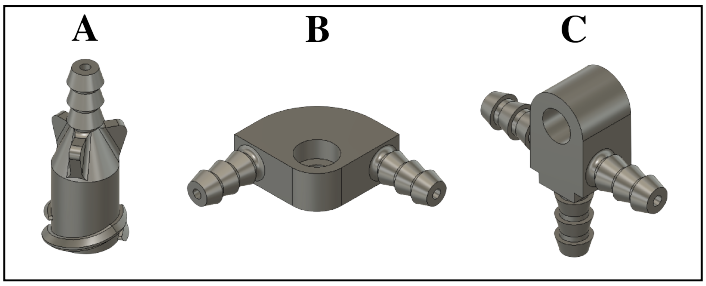


Figure A.6: *Custom DLP printed tube connectors used in this project. A: Barbed adapter to connect 4mm Festo pressure tubing to a syringe (Luer-lock). B: Tight corner connection for reduced real-estate on the test-rig (see following section). C: Barbed T-junction connection.*

## Test-rig

A special test-rig module was designed to keep the test setup portable, and keep all the components securely together. The test-rig accommodated the pressure sensor together with its adaptors and routed the required pressure tubing neatly from the source to the fluid interface. The fluid interface clamping tool was held in place by magnets and could be easily exchanged. The whole test-rig could be placed on the stage of the whitelight interferometer. Changing and testing different fluid interfaces this way was easy, and it was simple to re-align each interface.

## Sorting trays

Early on in the project I realized that the iteration of designs lead to a huge number of samples. The way that other researchers stored their samples was by putting them in labelled petri dishes. Due to the slow but constant stream of new samples, the number of petri dishes soon piled up. It was then that I decided to invest some time in thinking of a proper bookkeeping system to better keep track of each iteration step.

I designed stackable, modular sample trays that each fitted ten sample cups, labelled 1-10. Multiple trays could be labelled and stacked. A stack of trays could be topped with a special cap to keep the dust out. Since the cut-out squares were designed to be the same size as the Nanoscribe sample-holder, also 25X25mm glass or silicon samples could be included.

An Excel-sheet was made to complement the physical bookkeeping system. In the Excel-sheet, each stack was subdivided in trays that were in turn subdivided into sample cups, that were finally subdivided into separate fluid interfaces. Important parameters were noted down for each separate fluid interface—from the manufacturing details till the measurement notes. This way, each single fluid interface was traceable from the start, and it allowed for a quick overview of different iteration steps.

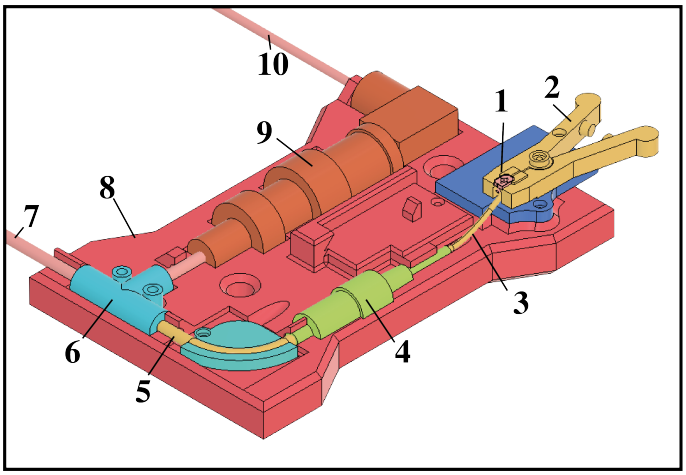


Figure A.7: *Test-rig used in the experiments with the white-light interferometer. A fluid interface (1) could be clamped into the custom clamping tool (2) and connected to Tygon® tubing (3). Pressure coming from the pressure source (7) in 4mm Festo tube (5) was splitted in a press-fit (6) and distributed to both the pressure sensor (9) and the tube adaptor (4). The sensor data came through a cable (10) to a data acquisition unit (NI-DAQ). Everything was held together by an FDM 3D printed test-rig (8).*

## Aperture alignment

When the fluid interfaces were loaded into the Nanoscribe in their respective sample cups, the precise coordinates of the apertures needed to be determined. First, the Nanoscribe stage was moved to the approximate coordinate, known by design. However, the real aperture position was never exactly at this known position due to the manual placement of the sample cup into the Nanoscribe holder, and possible minor deformations of the sample cup during handling.

The 63x objective was used for 2PP printing, and therefore also the camera-feed is magnified by this amount. This made finding the apertures sometimes quite difficult, as it can be hard to recognize the features of the fluid interface when you are zoomed in that much.

Moreover, the cameraview is not exactly centred with the writing field of the laser. The relative centre position of the writing field is different for each objective. As a quick and dirty method, it is possible to briefly turn on the 2PP laser manually (while being at the right interface height), such that a bright spot of autofluorescence can be observed indicating the centre of the writing field. To save this centre-location, I made another special tool that could be clamped to the corner of the screen. This tool then holds a cross-hair in front of the screen, where the centre of the writing field can then be aligned by dragging the cameraview window. Then, the laser can be turned off again, but the centre-position will be known to align with the fluid interface apertures.

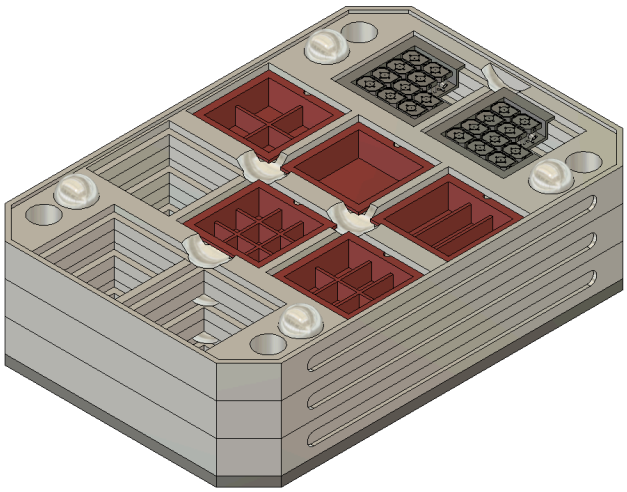

Figure A.8: *Bookkeeping system with sample trays. Each tray has room for 10 sample cups or other 25X25mm samples. The trays could be stacked easily. A top and bottom cover were also present. An accompanying Excel sheet was maintained to store details on the process and experimental steps of each sample.*

Figure A.9: *Screen corner clamp, used as a quick and dirty way to align the apertures of the fluid interface to the 2PP writing field. The cross-hair could be positioned on the camerafeed window at the location of the centre of the writing field. The spring-loaded clamp could easily be attached and removed.*

# B

# Production

## B.1. Workflow

In this section, the general steps of the production process will be treated chronologically. More details about protocols and parameters can be found in the subsequent sections.

1. **DLP slicing**
   The first step in the production process is the DLP printing of the fluid interfaces. An .STL file of the assembly with the fluid interfaces aligned in the sample cup is loaded into the proprietary DLP slicing software (Perfactory Slicer, EnvisionTec GmbH). The support structure is automatically generated, connecting the fluid interfaces to the sample cup and the sample cup to the buildplate.

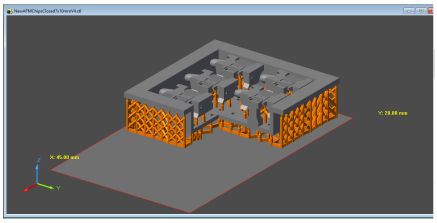

Perfactory slicer with generated support structure.

2. **DLP printing**
   Then, the sliced file is printed on a desktop DLP printer (EnvisionTec Micro PLus HiRes, EnvisionTec GmbH). A layerheight of 35 µm is chosen. The transparent photoresist 3DM Tough Clear (Admat Sasu) is used. Two sample cups can be fitted on the buildplate. Printing takes ~ 100 minutes.


EnvisionTec Micro Plus HiRes.

3. **DLP cleaning**
   When the print is finished, it is removed from the printbed with a sharp scraper. Then it is submersed in IPA and ultrasonically cleaned for five minutes. The uncured resin dissolves into the IPA. Another cleaning round with fresh IPA is often necessary to remove the last bits of uncured resin. (Note that the IPA from the second round can be recycled for use in another first round). After the second round, the sample is gently blow dried with compressed air. A final curing step is applied in a UV oven (Photopol Dentalfarm) for 6 minutes.


Ultrasonic cleaner and UV curing oven.

4. **Aperture lasering**
   The next step is to 'drill' the apertures using the Optec Micromachining Laser system. The sample cups with fluid interfaces are secured onto a non-porous ceramic plate with double-sided tape. The ceramic plate is then placed onto the vacuum bed of the motion stage. A camerafeed can be used to align the horizontal and vertical axes of the sample cup. After alignment, the vacuum is turned on and the sample is secured to the motion stage. The coordinates of the apertures can be targeted. A .DWG file is drawn consisting of circles of 10 µm at the found relative coordinates. The laser repeats each circle 15 times at a laser power of 15W at 50kHz and a writing speed of 15mm $s^{-1}$.

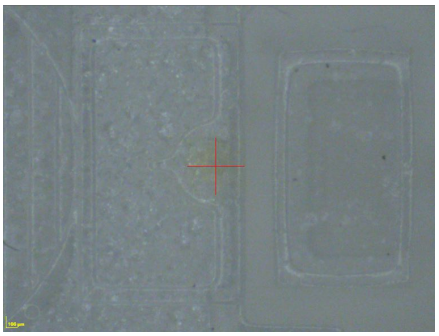
Camerafeed showing fluid interface and alignment cross at the aperture location.

5. **Gold sputtering**
   As a last step before 2PP printing, the fluid interfaces need to be sputtered with a thin layer of gold, to increase the reflectivity of the surface. This enhances the automated interface finding function of the Nanoscribe. A gold layer of ~ 3 nm can be created on the top surface by sputtering the sample for 5 seconds at 10 mA and 20mm working distance (Jeol JFC1300 sputter coater).

Jeol JFC1300 sputter coater with gold sputter target.

6. **Securing sample cup in Nanoscribe holder**
   The sample cups are designed to fit the sample holder of the nanoscribe. They can be inserted in the holder such that the top surfaces are levelled with the surface of the holder. Then, they can be secured with two pieces of tape (with the edges folded for easier removal). Since the sample cup is asymmetric, it is easy to position the cup in the same orientation each time. This further simplified the coordinate finding of the apertures.

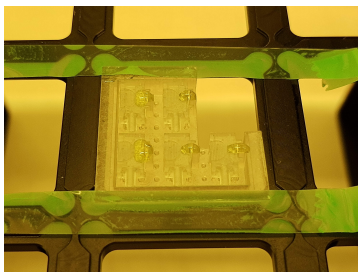
Nanoscribe holder with sample cup inserted an taped.

7. **Applying IP-Dip to fluid interfaces**
   When the sample cup is secured, the 2PP printing resin can be applied to the print sites on the fluid interfaces. Since the 63x objective is chosen, IP-Dip resin is used. This resin comes in syringe-like cartridges, allowing accurate dosing of the resin to the print sites. Ideally, only the print sites would be supplied with resin, but sometimes the resin also spreads out to other areas.

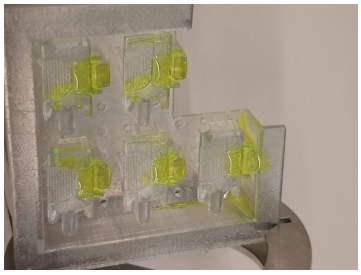
A droplet of IP-Dip applied (yellow) to each fluid interface.

8. **Finding the apertures**
When the sample is loaded into the Nanoscribe, the motion stage is first brought to the approximate coordinate of the first aperture. The objective can then be raised until contact with the resin is observed through the camerafeed. A careful manual first approach step is performed until the surface of the fluid interface can be observed. An automatic interface finding step can then be initiated to accurately determine the level of the surface. The joystick can be operated manually to find the location of the aperture. When the aperture is found, it is aligned to the screen-corner tool (see appendix A.4) and the coordinates are recorded.


Me, looking for interfaces.

9. **2PP printing**
Three separate .STL files for 1) the dome, 2) the cantilever and 3) the nozzle are first imported into DeScribe. Upon importing, the wizard is moved through, selecting the appropriate slicing options for each part. Different .GWL files are generated, which can be combined by importing them into one script. The found coordinates can also be programmed. The print can be started and monitored live through the process camerafeed.

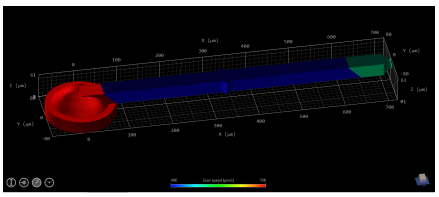
Femtopipette with dome, cantilever and nozzle merged in DeScribe.

10. **Developing the 2PP print**
When the print is finished, the objective can be lowered and the sample holder can be removed from the Nanoscribe. The sample cup can then be taken out of the holder by removing the tape. Then, first, the sample is submerged into PGMEA for (at least) 25 minutes. It may be necessary to refresh the PGMEA half-way. Secondly, the sample is submerged into IPA for 5 minutes. Third, after gentle blowdrying, the sample is placed for one minute in a shallow layer of Novec solvent (capped, to suppress evaporation). After a final blowdrying, the sample can be inspected under an optical microscope, to see if the channels in the cantilever are cleared. If not, an additional round of developing can be applied.

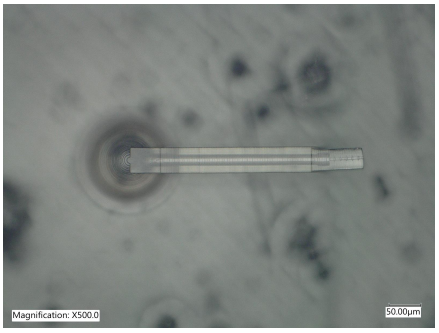

Optical microscope image to check printed cantilever.

11. **Harvesting fluid interfaces**
When the 2PP printed elements look good under the optical microscope, the final production step is to ‘harvest’ the fluid interfaces. Very gently, the individual interfaces can be broken loose from their sacrificial support material with tweezers. Great care must be taken not to destroy the 2PP printed parts: a steady hand is vital. Then, the purge channel of each fluid interface needs to be ‘plugged’. This is done by dipping a sharp piece of plastic into the 3DM Tough Clear resin, and gently applying it to the location of the purge channel. Capillary action will cause the channel to fill. Each fluid interface is then secured on a piece of double-sided tape inside a petri dish. Finally, the fluid interfaces go into the UV oven to cure the resin.

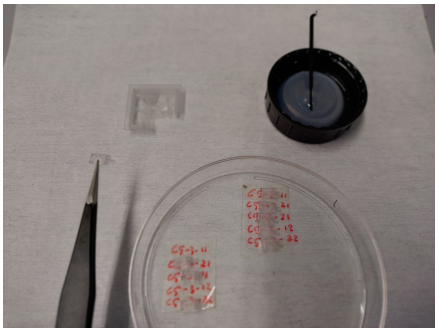
Harvesting with tweezers, applying resin and securing of fluid interfaces.

## B.2. DLP process

In the CAD software of choice, the fluid interfaces can be assembled with known coordinates relative to the sample cup (Autodesk Fusion 360 was used in this project). The CAD assembly can then be exported as one single .STL file. This makes sure that the relative positions are maintained throughout further processing steps. The .STL file is then imported into the proprietary DLP slicer (Perfactory Slicer, EnvisionTec). The model should be placed a certain height above the print bed to allow for support generation—2 mm was used. Then, the supports can be generated automatically using the 'small' supports presetting. Minor tweaks to the supports-settings may be necessary (mainly: maximum support height and maximum self-supporting distance). After the support generation, some support points can be added or removed manually. It requires some experience to tell which areas may need additional support. Lastly, it is wise to make sure that no unwanted supports are generated inside the channels of the fluid interfaces. This can be checked by applying a section view of the model after support generation.

The printer profile for HTM140V2 material with a layerheight of 35 µm is used in this project. Through trial and error, it was established that 3DM tough clear can be printed in high resolution using this profile, since the exposure time was similar to HTM140V2.

Another material, E-Glass2.0, was also ordered because it was expected that this material might demonstrate an equally high resolution due to the compliance to the Envisiontec system. Two new print profiles were installed, coming with the new material. However, the resolution turned out to be lower than hoped for, though the surface quality was arguably better than 3DM tough clear. At this stage, the main goal was still to decrease the size of the DLP printed apertures. It was briefly investigated whether the new print profiles could be used together with the present resins and vice versa, but this lead to no results. 2PP printing on top of this material was tested, which again revealed the need for gold sputtering. Adhesion of the 2PP printed parts to the E-Glass2.0 interface seemed equally solid. Perhaps with the latest production process—employing the laser drilling strategy —E-Glass2.0 may still prove itself as a feasible material.

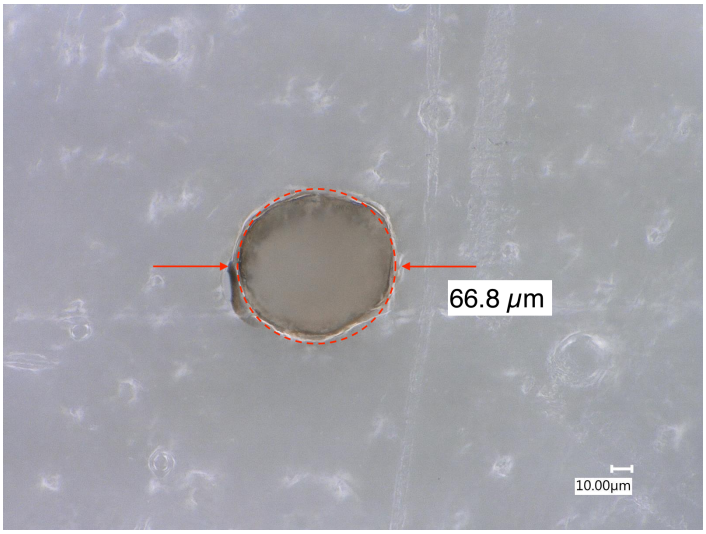


Figure B.1: *Typical example of a lasered aperture. The edges are clear-cut and slightly brown-ish, possibly indicating ablation of the material.*

## B.3. Laser process

Using a laser to drill apertures in the fluid interfaces was first suggested by Gideon Emmanueel, a lab technician in the PME labs. Initial tests with different laser parameters in the OpTec micromachining laser system showed promising results in terms of aperture size. The focal spot of the laser is said to be roughly 20 µm and circles were drawn of 10 µm. By varying mainly the laser writing speed, and the number of repetitions, a setting was chosen that yielded apertures with consistent diameters (~ 50 µm tot 70 µm) that did not penetrate all the way through the bottom of the fluid interfaces. It might be possible to optimize the writing parameters further, such that even smaller apertures (nearing the

20 µm focal spot size) could be achieved.

Since the cured DLP resins are crosslinked, they are thermosetting. Therefore, it is likely that the laser completely ablates the areas of intersection. This may in fact be beneficial, as no melted or visibly affected zone presents itself. Indeed, the apertures were neatly circular, greatly improving upon the previously 3D printed apertures. Sometimes, small cracks around the perimeter of the aperture could be visible. It is expected that these occur due to the rather severe heat gradient upon lasering, likely causing heat stress. A typical aperture resulting from laser drilling is shown in figure B.1.

A promising next step could be to employ the new Lasea femtosecond laser system. Likely this machine is able to drill much smaller apertures with better control over the power and heat that is delivered to the material.

## B.4. 2PP process

### Preparing the print

As was seen in the workflow in the previous section, after sputtering the fluid interfaces they are ready for 2PP printing. They are inserted into the Nanoscribe holder, always in the same orientation for ease of use. Then, IP-Dip resin is applied to the print sites. In the case of the fluid interfaces designed for the AFM, this presented another challenge: printing the suspended cantilevers protruding over the edge of the interface. The resin droplet is sandwiched between the fluid interface and the Nanoscribe objective, but when the objective moves beyond the edge of the fluid interface, contact with the resin droplet is often lost. This results in printing 'in the air', so that nothing is printed and the print is failed. This was resolved by Van Altena by adding a small 'resin tower' next to each fluid interface, attached to the sample cup (see figureB.2) [2]. The IP-Dip resin droplet would then be placed such that it covered both the fluid interface and the resin tower, keeping the objective inside the same droplet during the entire print.

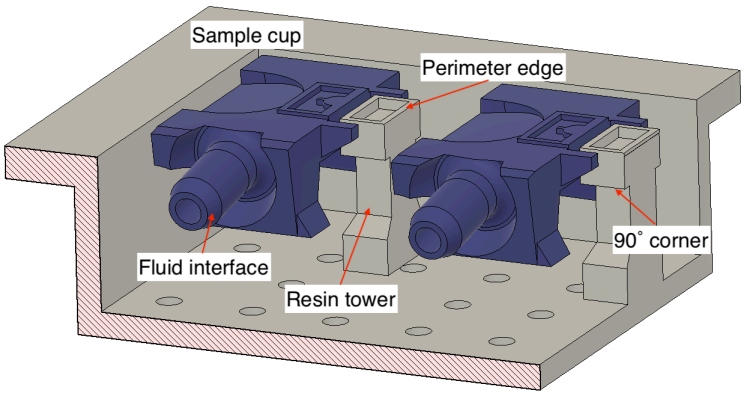


Figure B.2: *Section view of the sample cup showing two fluid interfaces and the adjacent resin towers. The resin towers are shaped to retain the resin-droplet and decrease the chance that the Nanoscribe objective moves out of the resin.*

However, this solution solved one problem but introduced a new one. Due to the small space between the resin tower and the fluid interface, the resin droplet would often be drawn inwards due to the capillary force originating from the close spacing between the two faces. This was mitigated a bit by changing the geometry of the resin towers a bit: introducing a small edge around the top perimeter to act as a capillary barrier and adding a 90°corner in the vertical wall of the tower facing the fluid interface (fig. B.2). Although this improved the resin containment a little bit, still it was often experienced that the objective would move out of the resin during printing, resulting in failed prints. In another attempt to mitigate this problem, some quick tests were performed with making the the fluid interfaces more repellent (hydrophobic and oleophobic)(some elaboration on these methods in appendix C). This did cause the resin droplets to bead up nicely, but still problems were encountered with the objective moving out of the resin.

In the end, the method with the least failures was to supply the fluid interfaces with a surplus amount of resin. This is not an elegant solution, and therefore there is some room for improvement

here. A possible way to make this step better could be to design the sample cup in a way that the gap between the fluid interface and the cup is minimized, while also keeping in mind the trajectory of the objective. In the ideal case, this would lead to a setup where the objective remains in the same droplet during the entire operation —just like the fluid interface with multiple parallel print sites, see section A.1(G-I). This eliminates movements between droplets which risk the chance that the contact with the next droplet fails.

## Slicing

When an .STL file is imported into DeScribe, a wizard pops up allowing to set a specific 'slicing recipe' for that particular part. In this recipe, geometry specific data can be set-up like the part orientation, slicing/hatching distance and block stitching. After the wizard is completed, a .GWL script is generated that contains all the geometric information and allows to program process parameters like scanning speed, laser power, coordinates, interface finding and everything else. The relevant parameters are listed in table B.1. This way, separate .STL files were imported for the dome, the cantilever and the nozzle, thus allowing the recipe to be adjusted for each. Then, inside the DeScribe script, the separate files could be linked together, as shown in figure B.3.

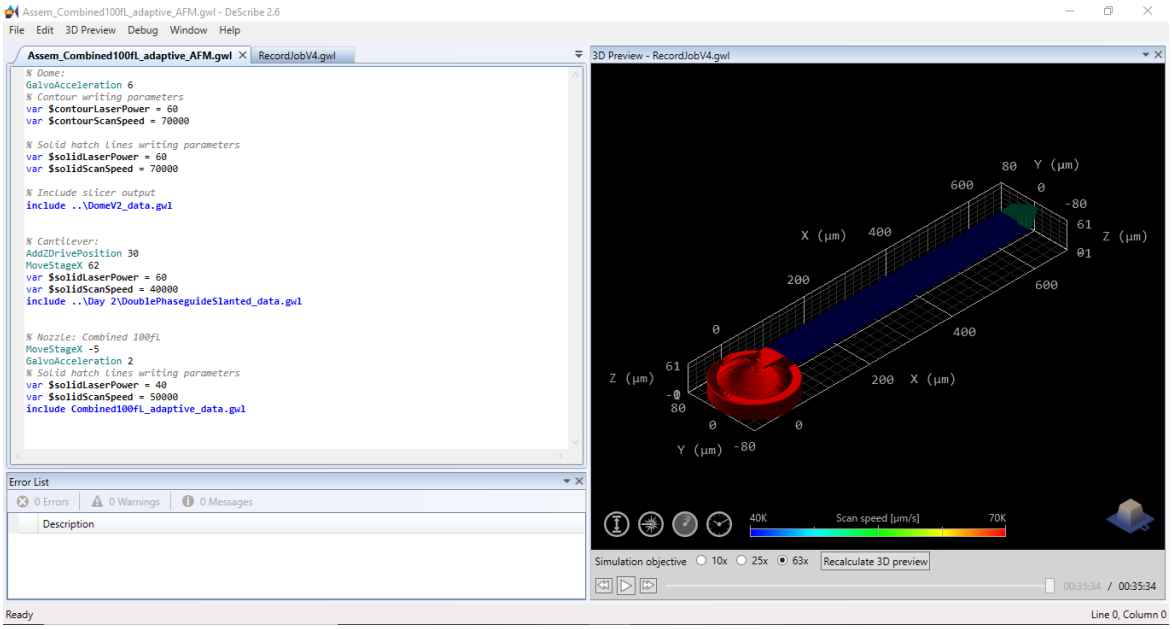


Figure B.3: *DeScribe screenshot of 'assembly-script', where the different parts are linked together, and the individual laser writing parameters are set.*

First, the dome would be printed, using relatively 'rough' settings to minimize print time. The interface finding command is normally issued at the beginning of the part printing. For the dome, the interface could usually be found right at the location of the aperture, since the interface finding occurs slightly off-centre in the writing field and the aperture was small enough. If the interface was not found automatically, a command could be issued to move to a spot away from the aperture (usually +200 µm in X and Y), find the interface there, and move back to the aperture (−200 µm in X and Y).

Then, the .GWL script of the cantilever and nozzle should be edited such that all 'find interface' commands are removed because these parts should be suspended above the surface. The stage would have to be moved to the starting point of the cantilever before continuing to print—usually +60 µm in X and +30 µm in Z, relative to the starting point of the dome. The amount of movement can be iterated in the DeScribe editor until they line up nicely with an appropriate amount of overlap.

The cantilever and the nozzle are printed suspended above the surface. The strategy there is to split these parts into blocks that are overlapping at a 45°angle, see figure B.4. This not only helps in securing that the overhanging parts are printed well, but also allows to print parts that are bigger than the writing field (200 µm in diameter). The motion stage moves for each separate block. It is obvious that the order of the blocks then becomes relevant, and it is wise to check in DeScribe if the blocks are indeed printed from left to right, dome to nozzle. I found that unselecting the 'Avoid flying

| | Dome | Cantilever | Nozzle | PG-test |
|---|---|---|---|---|
| Laser power | 60% | 50% | 40% | 50% |
| Scanning speed [mm/s] | 70 | 40 | 50 | 40 |
| Slicing distance [µm] | 0.35 | 0.2 | Adaptive (0.05-0.3) | 0.2 |
| Hatching distance [µm] | 0.25 | 0.2 | 0.15 | 0.2 |
| Contour count | 3 | 0 | 0 | 3/0 |
| Galvo acceleration [$V/ms^2$] | 6 | 6 | 2 | 6 |
| Find interface at [µm] | 5-10 | - | - | - |
| Block splitting size (X) [µm] | - | 8 | 4 | 6 |

Table B.1: *Relevant process parameters. The phaseguide expansion angle test cantilever is noted as 'PG-test'.*

blocks' checkbox in the slicing wizard prevents unwanted changes in the printing order.

In the beginning of the project, the methodology with the laser-drilled aperture was not yet applied. The apertures were 3D printed and were therefore considerably larger (effective diameter ~200 µm). This meant that the domes could not cover the entire aperture within one writing field (200 µm for the 63x objective). Therefore, the domes needed to be stitched as well. The block shape, position and sizes used in the stitching could be chosen, and special care was taken that no block-stitching line would be present on the membrane surface. The block-stitching lines can be visible on the print as small egdes, and their presence may have influenced the behaviour of the membranes.

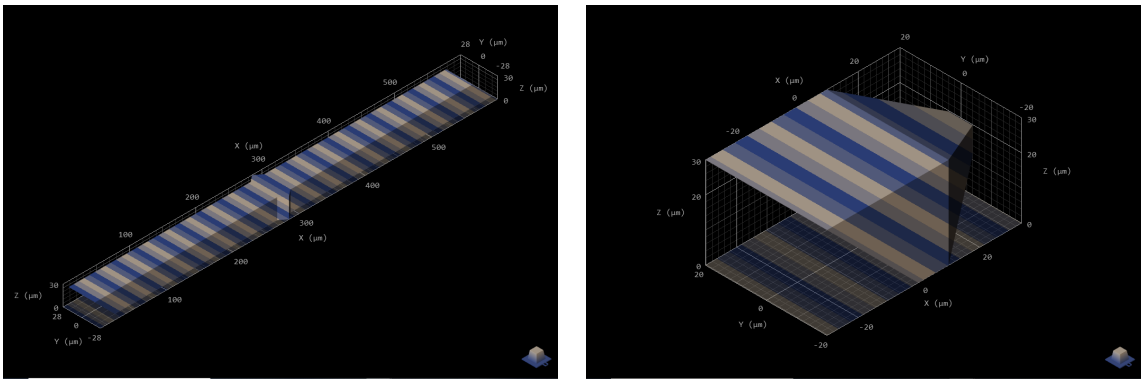

(a) *Cantilever blocksplitting, showing blockwidths (X) of* 8 µm. (b) *Nozzle blocksplitting, showing blockwidths (X) of* 4 µm.

Figure B.4: *DeScribe screenshots of .STL importing wizard, showing the blocksplitting at a 45° angle. The thickness of the blocks can be set.*

## Developing

After 2PP printing, the samples were developed using mainly the standard developing protocol advised by Nanoscribe [11]. During the project, some experiments were performed with increasing the development time, raising the temperature of the developer on a hot plate, stirring the developer with a magnetic stirrer, and putting the developer in an ultrasonic cleaner. Usually, longer development times helped with the removal of uncured resin material, but increasing the temperature and stirring sometimes led to the detachment of the 2PP printed parts.

In the end, the best way to develop the channels in the cantilevers was to use Novec™ as a last development step. Novec™ is very volatile so it is best to cover the beaker to suppress unwanted evaporation. Only a very small amount of Novec™ is necessary.

## Additional tests

For determining specific parameters of the 2PP printing process, several additional tests were performed. A standard testing procedure in 2PP printing is the so-called 'dose test', where a grid is printed with varying laser parameters. The combination of scanning speed and laser power determines the total amount of power received by the parts. When the dose is too low or too high, either no polymerization occurs or bubbles get formed. Finding the optimal dose is also dependent on the

type of part that is printed.

To investigate certain aspects of the designs, test parts were printed that focussed on critical features. In figure B.5, three such test parts are displayed, together with the SEM images to analyse them. First, several orientations and thicknesses of membranes were investigated with the part shown in figure B.5A. In this stage, both the 25x and 63x Nanoscribe objectives were considered. SEM images of the horizontal membrane configuration printed with the 25x objective (fig. B.5G) quickly revealed that the minimum membrane thickness was limited to the voxel height of $\sim 3\,\mu m$, which makes sense because the theoretical voxel height is 3313 nm [12]. The minimum membrane thickness printed with the 63x objective was significantly less, also resulting in thicknesses in line with the expected voxel size of 830 nm (fig. B.5H).

Vertical membranes were also investigated in a setting that more resembled the actual part design (fig. B.5B). This part comprised a vertical, circular membrane and two half membranes in both horizontal and vertical dissected orientation. These prints gave some insight in the structural rigidity of the membranes at different writing doses (fig. B.5E), and allowed for measuring the thickness of the vertical membranes (B.5I). Again, the thickness was in line with the theoretical lateral voxel dimensions of 340 nm.

The SEM images of the dose tests on vertically printed membranes revealed that the membranes were sagging in some cases, showed holes in other cases and were totally missing in yet other cases. This underlines the difficulty in finding the right optimum in the printing parameters for vertically printed thin membranes.

Lastly, the printable sizes of pores were also investigated with a part comprising varying pore sizes in horizontal, vertical and diagonal orientation (B.5C). In the SEM image (B.5F), the smallest designed pores (<150 nm) showed visible alterations in the part surface, but only pores >600 nm seemed open. However, the SEM images were not decisive in determining if pores were truly open.

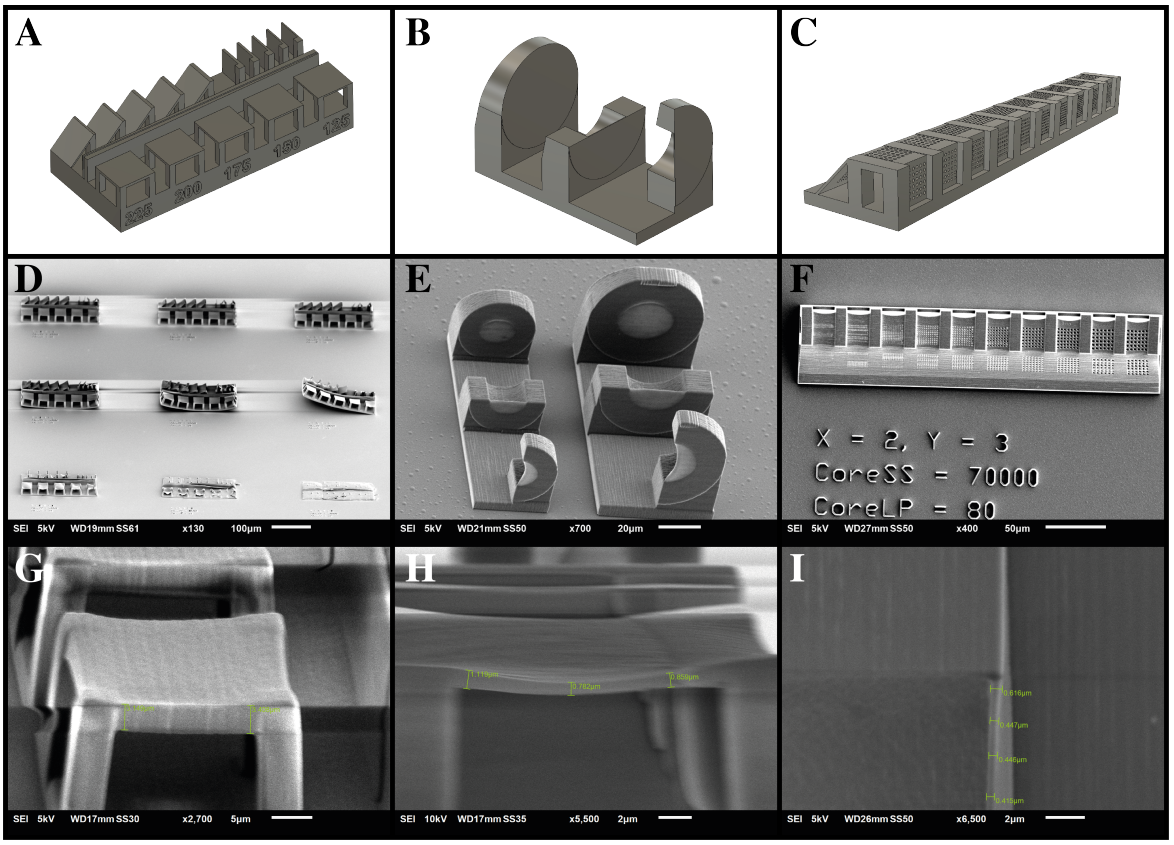


Figure B.5: *2PP printed test parts. A: Part for investigating the membrane orientations with varying thicknesses. B: Part for investigating thickness and rigidity of vertical membranes. C: Part for investigating printability of pores in different sizes and orientations. D: Dose-test of membrane test part, varying scanning speed and laser power. Clearly the dose in the bottom-right was too low. E: Inspection of vertical membrane test part. F: Inspection of dose test of pore size part. G: Horizontal membrane printed with 25x objective, revealing minimal thickness of* $\sim 3\,\mu m$. *H: Horizontal membrane printed with 63x objective, yielding membrane thickness of* $\sim 850$ *nm. I: Measurement of vertical membrane showing thickness of* $\sim 400$ *nm.*

# C

# Characterization

## C.1. Pressure application and measurement

Accurate pressure measurement was necessary in multiple experiments. First, the pressure that was applied to deform a 2PP printed membrane was measured and compared with its deflection. Then, later, the pressure was measured during the burst-pressure experiments, both with porous membranes and with the variable-geometry cantilever. The pressure sensor used in the experiments was the Gems 3500 sensor, valid from 0-4 bar with an accuracy of $\pm$ 10 mbar (Gems Sensors Inc.). Later, for the burst pressure measurements, an even more accurate sensor of the same type was used: a Gems 3500 sensor, valid from 0-2.5 bar with an accuracy of $\pm$ 6.25 mbar.

Both sensors were hooked up to a data acquisition system (NI-DAQ, National Instruments). This NI-DAQ needed to linked to a LabView program on a laptop (linked through USB) to read the data output. Both the sensors and the LabView program were kindly provided by Jos van Driel (measurement shop, IWS). An image of the entire setup used for the measurement of the deflecting membranes is shown in figure C.1.

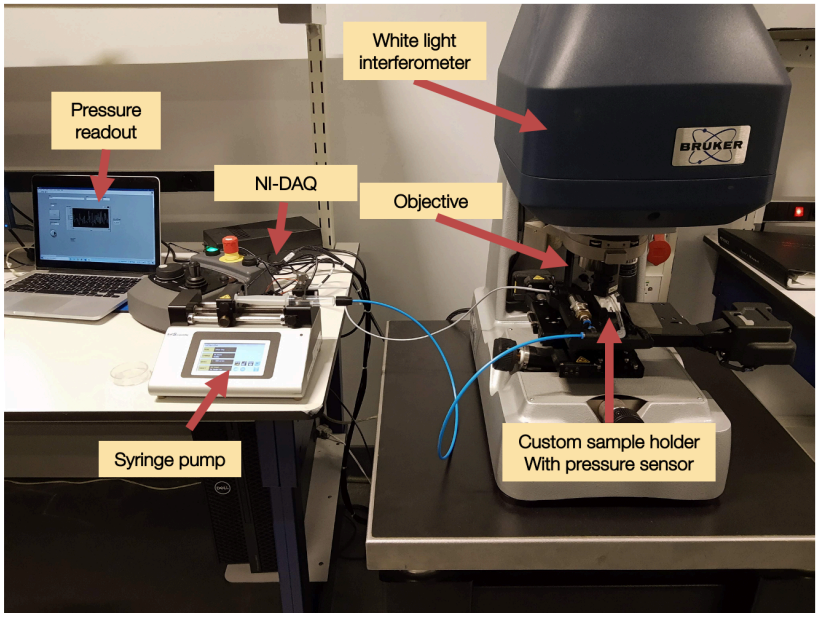


Figure C.1: *Overview of the entire setup used for measuring the pressure and deflection of the 2P printed membranes.*

During the experiments, pressure was supplied by a syringe (60mL, BD Plastipak) on a syringe pump (KDS legato 111, KD scientific). Pressure was lead through a 4mm Festo® pressure tube to a T-junction on the test-rig (see app. A.4). There, the pressure sensor was connected in series.

The pressure could be viewed live in the LabView program, or recorded for later analysis. Pressure was increased very slowly by selecting a low flow rate on the pressure pump.

Especially in the case of the variable-geometry cantilever used for determining the geometry-dependent burst pressure, there was quit some tubing distance (~0.5 m) between the cantilever pressure sensor. Since this tubing was very thin (inner diameter of 1.02 mm), initially it was a concern whether a delay in the pressure sensing would be present between the location of the pressure sensor and the sample. A quick and dirty way to quantify this was to record the pressure with a tube that was blocked on the location of the sample. Then, by quickly removing the blockage, a 'step response' in the pressure could be observed (see figure C.2). Although this is by no means an accurate measurement, it does give a feeling for the delay in the system. From figure C.2, it can already be observed that a longer Tygon tube does indeed increase the response-time. For a 1 m tube, the response-time was in the order of 250 ms, which is still reasonable considering the pressure was increased very slowly.

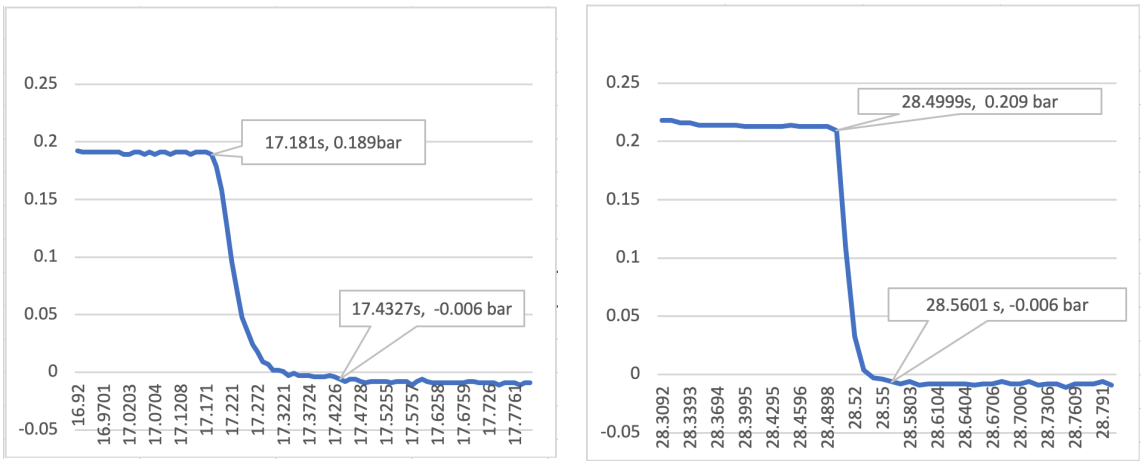


(a) (b)

Figure C.2: *Quick and dirty response time measurement of pressure measurement setup. The vertical axis show the measured pressure and the horizontal axis shows the elapsed time. Figure (a) shows the response-time of 0.25s for a Tygon tube of 1m. Figure (b) shows the response-time of 0.06s for a Tygon tube of 0.2m.*

## C.2. Volume dosing

The working of each new cantilever iteration was first tested on the combined fluid interface (see app. A.1G-I). This fluid interface was perfect for the quick assessment of a new design, because it could be handled easily, needed no plugging of the purge-channel. Furthermore, this fluid interface was very well suited to be submerged in a droplet of water, which was retained nicely by the geometrical rim-features along the edges of the top-surface. This enabled quick testing straight out of the development process, with no need to move between labs. Videos of cantilevers tested on this combined interface are available online [13], [14].

Two tubes would be connected to the interface of interest: one that was permanently blocked (acting as a plugged purge-channel) and the other connected to the pressure source (syringe). The water droplet would be gently applied by a small disposable pipette filled with DI-water. The whole interface would be placed under the optical microscope on a piece of double-sided tape to secure it and prevent sudden undesired movements originating from handling the connected pressure tubes. Gas pressure was thus supplied from the 'back' side of the cantilevers, while water could enter from the nozzle-side ('front'). This way, by actuating the syringe manually, water could be aspirated and dispensed, while observing whether the desired pinning behaviour would occur.

With this method, liquid was already 'dosed' in steps, but to really move towards a more realistic application, an experiment was devised with two different immiscible liquids. This experiment was performed on the JPK Bio-AFM, to benefit from the precise motion stage and the inverted optical microscope in-place. To fit cantilevers to this AFM, a special fluid interface was used (see app. A.1J-L).

Both a water-glycerol droplet (50/50 wt%) and an oil droplet (Mineral oil, Bio-reagent) were to be placed on a microscope slide. A glycerol mixture was used to suppress evaporation. This was necessary especially for the smallest amounts of aspirated liquid. Then, using the motion stage of

the AFM, the cantilever would be moved from droplet to droplet, aspirating from one, and dispensing into the other. The microscope slide that was used was very hydrophilic (glass) and the droplets would spread too much to be useable. Therefore, the microscope slide first needed to become hydrophobic/oleophobic (repellent).

This was achieved by coating the microscope slide with Sigmacote® (Sigma Aldrich). The microscope slide was first cleaned thoroughly with aceton and IPA respectively, before putting it in the plasma oven for 5 minutes. Then, it was placed on a tray in the desiccator, above a small petri-dish containing several drops of Sigmacote®. The desiccator vacuumed and left closed for 1 hour, according to the protocol prescribed by Cytosurge [15]. It should also be possible to apply Sigmacote® directly to the glass surface. After this treatment, the glass microscope slide was well repellent, and both water and oil droplets beaded up nicely (see figure C.3(a)), after which the slide could be placed in the AFM, above the objective of the inverted microscope.

The fluid interface with the cantilever to be tested was then first mounted on the JPK-probeholder by fastening the clip-screw. When secured, it was easy to plug the Tygon pressure tube to the fluid interface. Next, the probeholder would be positioned in the (fully retracted) AFM head and secured with rotating clips. Carefully, the AFM head could be lifted—making sure no cables or tubes would get caught—and positioned in the motion-locks. The AFM head was then lowered in steps. The focal distance of the optical microscope was used to check if the cantilever was nearing the surface of the microscope slide. At this point, usually a video recording would be started. The live videofeed from the optical microscope could be shown in the proprietary Zen-Blue software (Zeiss) (see figure C.3(b)).

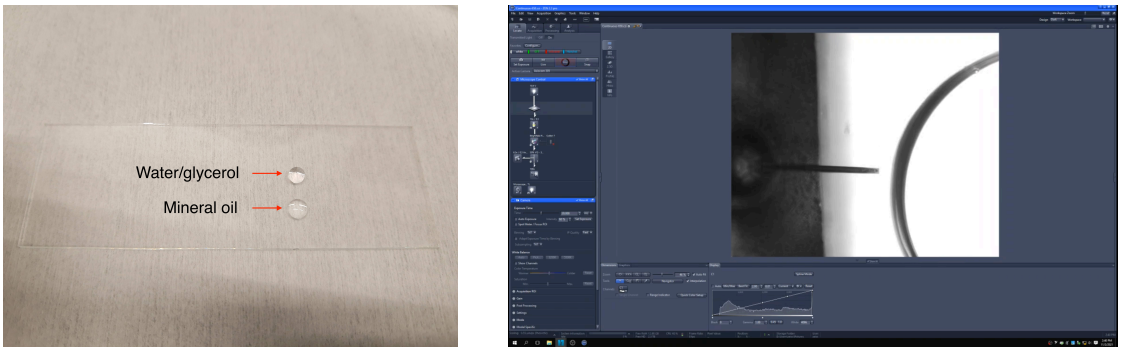


(a) (b)

Figure C.3: *Liquid dosing experiment. (a): Glass microscope slide made repellent with Sigmacote®. The water/glycerol droplet and the mineral oil droplet both beaded up nicely. (b): Screenshot of the Zeiss Zenn Blue software, where a live videofeed could be shown from the inverted optical microscope.*

Once in proximity, the droplets could be positioned with the XY motion stage such that the cantilever (pointing to the right) would enter the droplet from the left. Entry of the droplet was clearly visible due to the change in the surface of the droplet. If no entry was observed, the AFM head was still too high and needed to be lowered in small until entry was observed. Refocussing was needed inside the droplet due to the difference in refractive index. Generally, the best images were obtained when the cantilever was closest to the surface of the microscope slide, but fringes were inevitable.

Then, a small amount of liquid would be aspirated—controlled manually with visible feedback. Sometimes, liquid would burst past the last phaseguide incidentally, but another 'back-up' phaseguide was present in the channel that prevented liquid from entering beyond the cantilever. From this back-up phaseguide, it was easy to apply a bit of overpressure and get the liquid-air meniscus back to the last phaseguide step.

Next, the cantilever could be moved out of the droplet. Due to the hydrophilicity of the cantilever material, usually a small amount of liquid would adhere to the outer surface and bead up near the nozzle. This additional amount would later add-up to the dispensed amount as a small volume offset.

The cantilever could then be moved to the other droplet, which was also penetrated. Dispensing small amounts of liquid into the other droplet was also done manually, but it required a steady hand and close optical control through the oculars of the microscope (the videofeed was too slow to be usable for good control). Video's of the process are available online [16], [17].

In some uneventful cases, the fluid interface itself would make undesired contact with the droplets

on the microscope slide. They would then instantly attract the entire droplet, and the measurement would be ruined. Rinsing with IPA was required to get rid of oil/water remnants.

## C.3. Deflection measurement

Deflection measurements were performed on the whitelight interferometer (ContourGT-X, Bruker), using the test-rig treated in appendix A.4 and the setup shown in figure C.1. The fluid interface with the 2PP printed element could be positioned with the membrane surface facing upwards, held within their custom spring-loaded clamps. This way, pressure could be supplied without the risk that the sample would move —which would compromise the whitelight measurement.

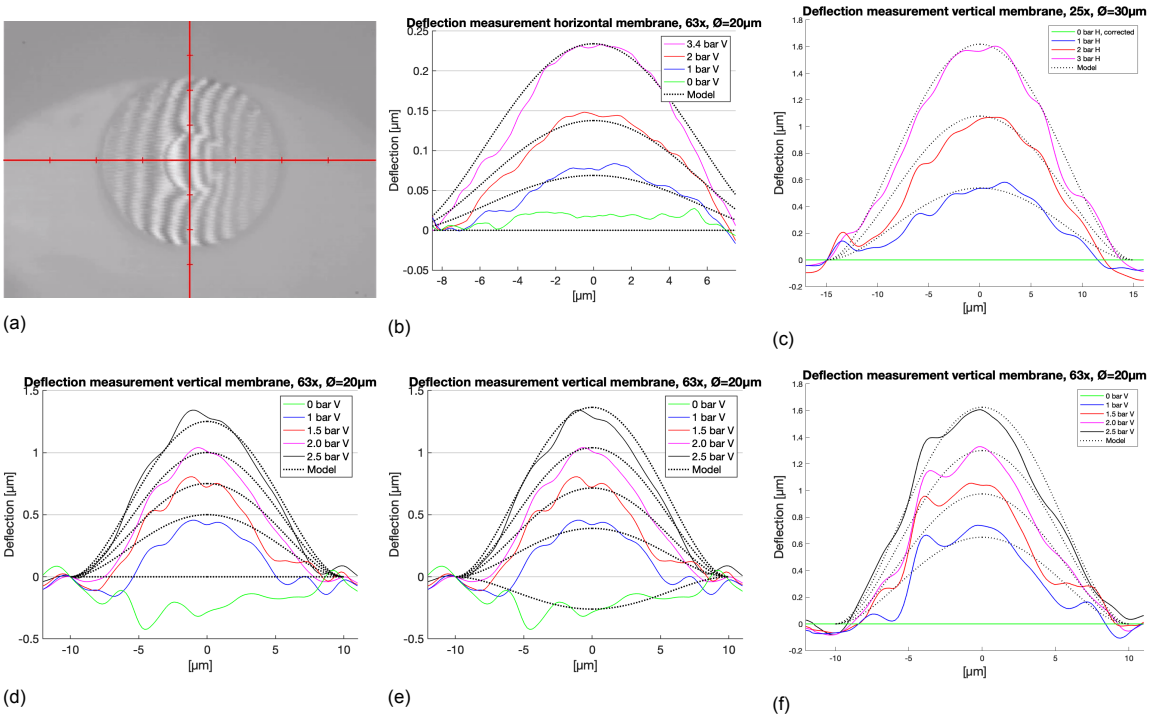


Figure C.4: *Deflection measurements. All plots show measured deflection for different static pressures, compared the analytical model. (a): Cameraview of the membrane, showing fringe lines indicating the right focus depth. (b): Horizontally printed membrane (63x). (c): Vertically printed membrane, printed with the 25x objective (IP-S resin). (d): Vertically printed membrane (63x), modelled membrane thickness 480 nm. (e): Same as (d), but with offset applied to model, resulting in membrane thickness of 480 nm. (f): Same as (d) and (e), but with zero-line subtracted from data, resulting in membrane thickness of 440 nm.*

After positioning the sample, first the location of interest would be found by using the lowest magnifying objective. The approximate Z-height can be found by moving the sample up or down and looking for fringe-lines appearing on the camera view. Then, a higher objective could be used to zoom in on the area of interest. Usually, green light (narrowband) yielded the best results. Sputtering the membranes with a thin layer of gold further improved the amount of data that was collected.

The neutral position of the membrane ($\Delta P = 0$) was always recorded first. Then, pressure was increased ($\Delta P > 0$) and held constant during the next measurement (usually takes up to 10s). Sometimes, a small decay in the pressure could be observed, indicating a tiny leakage somewhere in the system. This could be compensated by applying a very low flowrate on the syringepump during the measurement, that equalized the outflow. The maximum pressure that could be achieved with the used syringepump-syringe combination was approximately 3 bar —the stepper motors would stall for higher pressures —but this could be increased somewhat by 'helping' the syringepump manually. No bursting of the membrane or detaching of the 2PP printed elements was ever observed, so the maximum tolerable pressure is at least ~4.5 bar.

After the measurement, the data would be saved as a .OPD file, containing all the topological information. This file could then be opened and post-processed with the Gwyddion open source software (V2.6). Here, the data could be levelled and filtered before extracting a horizontal and vertical profile across the centre of the membrane.

These profiles were then exported as .TXT files, and added to the columns of an Excel file. This Excel file then contained all the measurements of one particular sample. The next step would be to import these columns into Matlab, where the last steps in the post-processing would take place. Here the acquired data could be plotted in comparison to the analytical model. Some resulting plots are shown in figure C.4.

During the project, some tests were also performed with membranes printed with the 25x objective in IP-S resin. The axial voxel size for the 25x is relatively large (3313 nm [12]). Therefore, printing membranes in the horizontal orientation resulted in membranes that were too thick and stiff to be useful (see figure B.5G). However, making use of the vertical membrane orientation, the lateral voxel size (595 nm [12]) was exploited. This resulted in feasible membranes where the deflection was measurable, see figure C.4(c).

Sometimes the measurements of the membrane in its neutral position ($\Delta P = 0$) revealed that the membrane was not perfectly flat, as is clearly visible in figure C.4(d). In that case, when comparing to the analytical model, a discrepancy is visible between the modelled zero-line and the data (best fit: thickness $t = 480$ nm). To adjust for this discrepancy, initially it was tried to apply a negative pressure offset to the model to better fit the neutral data curve (figure C.4(e)). Indeed, the model then better fitted the data this resulted in a membrane thickness of $t = 440$ nm. Yet another improvement was to simply subtract the values from the neutral-data-curve from all the other curves, the resulting curves thus representing the absolute deflection from the neutral state (see figure C.4(f)). Here, again a thickness $t = 440$ nm was found that best fitted the model.

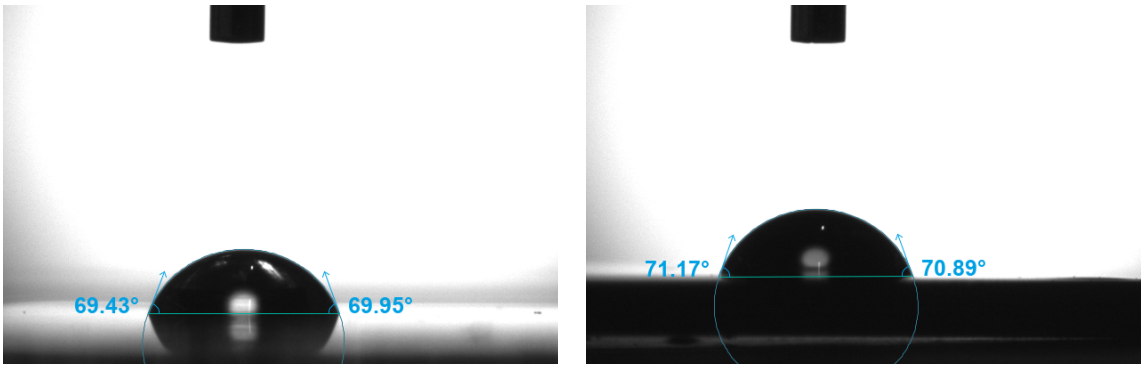


(a) (b)

Figure C.5: *Examples of macro-scale contact angle measurement with an optical tensiometer. (a): Cured IP-Dip resin. (b): Cured IP-S resin*

## C.4. Contact angle measurement

A very important unknown variable during this project was the *contact angle*. The contact angle is an observable property at a liquid-gas-solid contact point, forming an equilibrium between their respective surface energies. In this project, we were interested in the contact angle between liquid (usually water) and the 2PP printed material (cured IP-Dip). Only two mentions of the IP-Dip-water contact angle were found in literature: 72° [18] and 80.5° [19], thus both marginally hydrophilic.

Since no consensus about the exact contact angle of IP-dip was found, it was decided to perform a macro-scale contact angle measurement as an additional reference. To do this, IP-Dip and IP-S resins were spin-coated on coverslips with the Laurell spincoater. (4000rpm for 30s), after the coverslips were cleaned and treated in the plasma-oven for 5 minutes. Then, the curing of the bulk resins turned out not as simple as expected. Heat treatment on a hot plate (as mentioned in the nanoguide [11]), caused the resin to be very fluid before resulting in uneven spreading and cracks in the resin surface. The UV oven (Photopol, Dentalfarm) was also not able to fully cure the resins, even after multiple runs of 20 minutes (max runtime). As a last resort, a powerful UV spot source (Bluepoint 4 Ecocure, Honle UV technology) was used, which finally resulted in smooth cured surfaces.

These cured resin samples were then developed in PGMEA and IPA using the standard developing protocol [11] to make sure no uncured resin was present on the surfaces and to resemble the intended chemical treatment of the 2PP printed elements. The samples were then taken to an optical tensiometer (Theta Lite, Biolin Scientific, present in the material-science lab). There, small ~3

µL droplets of MilliQ DI-water were deposited on the resin surface, and the contact angle could be aut omatically measured by a camera from the side. This resulted in measured macro-scale contact angles of $62.3° \pm 4.8°$ (N=18) for IP-Dip and $68.9° \pm 1.3°$ (N=21) for IP-S.

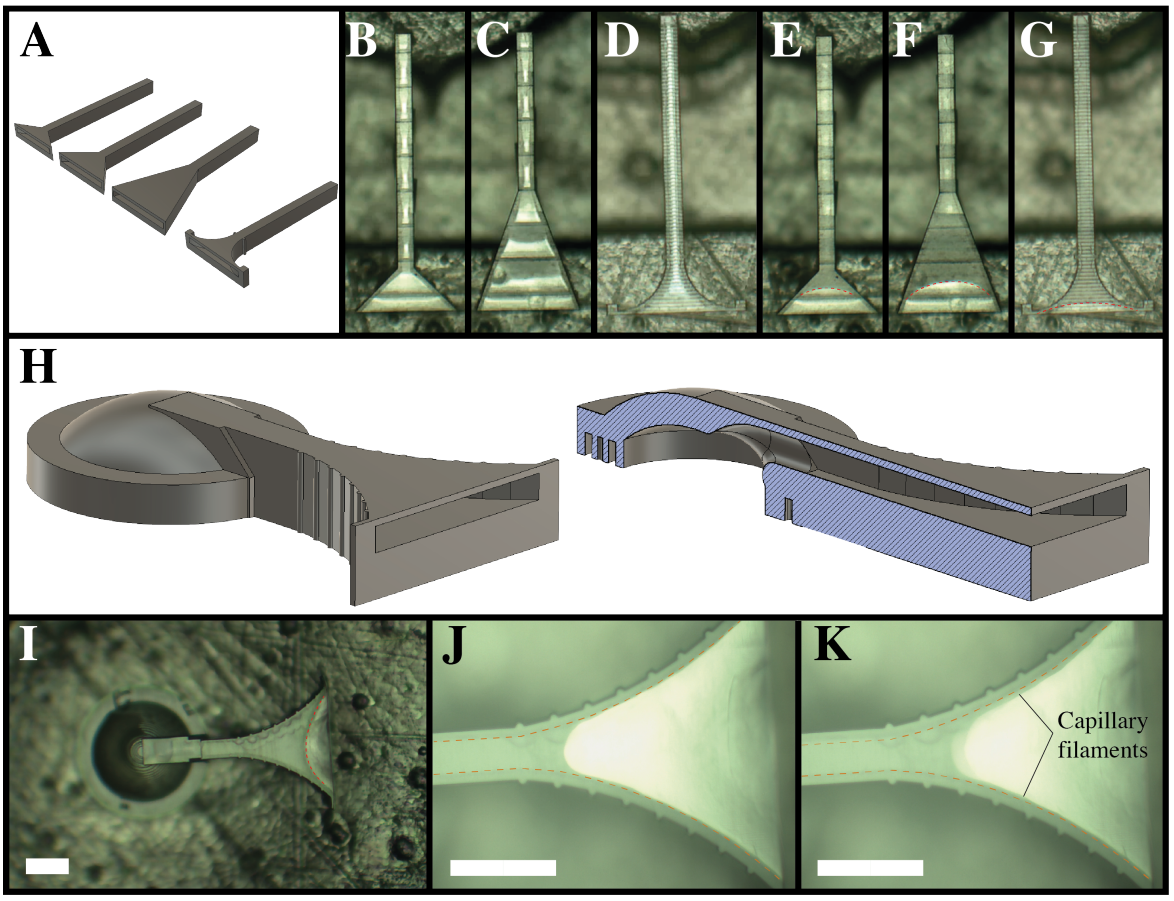


Figure C.6: *Initial attempts to determine the contact angle on the micro-scale. A-G: Square, open-ended channels with geometrical expansions. A: CAD models with expansions: 60°, 45°, 20°and rounded. B-D: Empty channels. E-F: filled channels with meniscus indicated by subtle dotted line. H: CAD model of dome with rounded, rectangular opening. Cross-section is also shown. I: Complete filling of dome with rounded opening from the back-side. J-K: Close-up frames of filling video, showing capillary filaments in the corners of the rounded channel. (Scalebar* 60 µm*)*

However, the macro-scale contact angle may not be representative for the contact angle with 2PP printed elements on the micro-scale because the macro-scale measurements represent a 'bulk-average'. In literature, not a lot was found on the measurement of contact angles on the micro-scale, therefore, new methods had to be invented.

As a first attempt to study the contact angle $\theta$ on the micro-scale, different types of rectangular channels with geometrical expansions were printed (see figure C.6A-G, and supplementary video online [20]). These channels were open on both sides, and a droplet of DI-water could be pipetted near the top opening. The idea was that capillarity would than cause the water to enter the channels, where it would stop at a certain angle of the geometrical expansion, based on the theory presented in section 6.2. The critical angle $\beta_c$ beyond which the water should not be able to pass is given there as $\beta_c = 90° - \theta$. Sudden, linear expanding channels could thus serve as a discrete way to find out at which angles the liquid could pass, where it was expected that the rounded openings could give a more precise 'analogue' indication of the contact angle. With these channels, it was quite difficult to get the water droplet on the right location to fill the channels from the right side. Therefore, the device shown in figure C.6H was made, that could be connected to the aperture in the fluid interface, such that water could be supplied *through* the fluid interface—directly supplying it to the right location.

To our surprise, all the devices that were printed filled completely, even the ones with expansion angles way beyond the expected critical angle $\beta_c$ (as can be seen in figures C.6E-G&I). Upon further inspection of the recorded video-frames taken during the filling of the channels (C.6J-K), it was ob-

served that a thin layer of liquid at the edges proceeds the meniscus before it fills completely. It turns out that such behaviour is known in literature as ‘capillary filaments’ of ‘Concus-Finn filaments’ [21], where the corners of the rectangular channel also allow for capillary wetting behaviour—rendering the square channels unsuitable for this experiment.

This lead to a new design with circular channels and axisymmetrical expansions, as already treated in section 6.4 and shown in figure 6.5. Not only was this new design used for the measurement of the geometry-dependent burst pressure, but it could also be used to determine the static contact angle. This methodology has been treated in section 6.4 and section A.

However, this method does have its limitations in terms of measurement resolution. First, the used cantilever with subsequent expansions only measures in discrete steps, determined by the consecutive expansion angles $\beta$. Creating more steps with smaller increments could serve as a way to get a more precise measurement. However, it is likely that the limiting factor is not accuracy of the Nanoscribe in printing angled walls, but more the inherent character of the surface quality of the 2PP printed parts. Any 2PP printed part is composed of (overlapping) rows and layers of voxels (see figure C.7(d)). The final surface quality can be improved somewhat by optimising the slicing settings, but some amount of alterations is inevitable.

To get a feeling for the approximate surface roughness of the 2PP printed channels with geometrical expansions, these parts were printed half—with their internal channels exposed (fig. C.7(a-c)). The parts were printed with the same parameters used for printing the ‘real’ cantilevers, 45°overlapping slabs can be distinguished in figure C.7(c). Although no precise surface roughness measurement was performed, from the SEM images, it can be estimated that the surface roughness $Ra$ is in the order of $\sim$100-300 nm.

This surface roughness will likely have an effect on the liquid behaviour near an intended sharply printed corner. More experiments with varying printing parameters could give better insights in the variance of the contact angle.

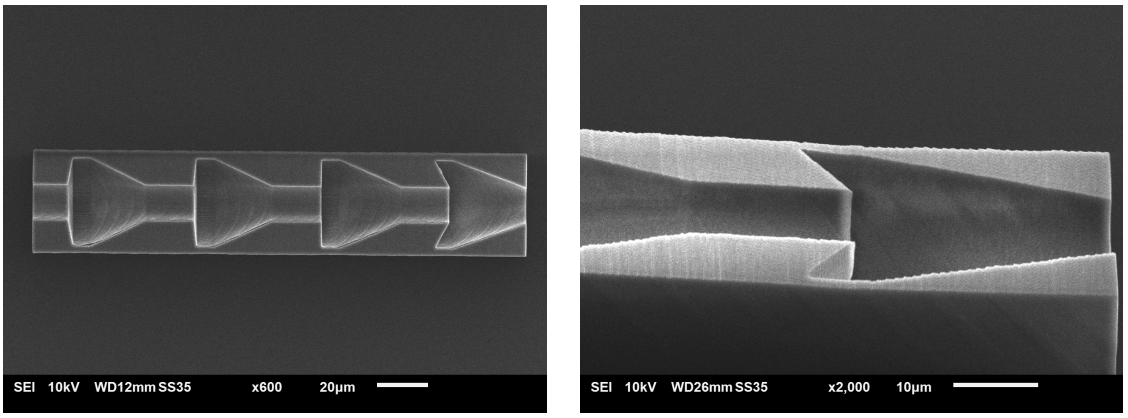


(a) (b)

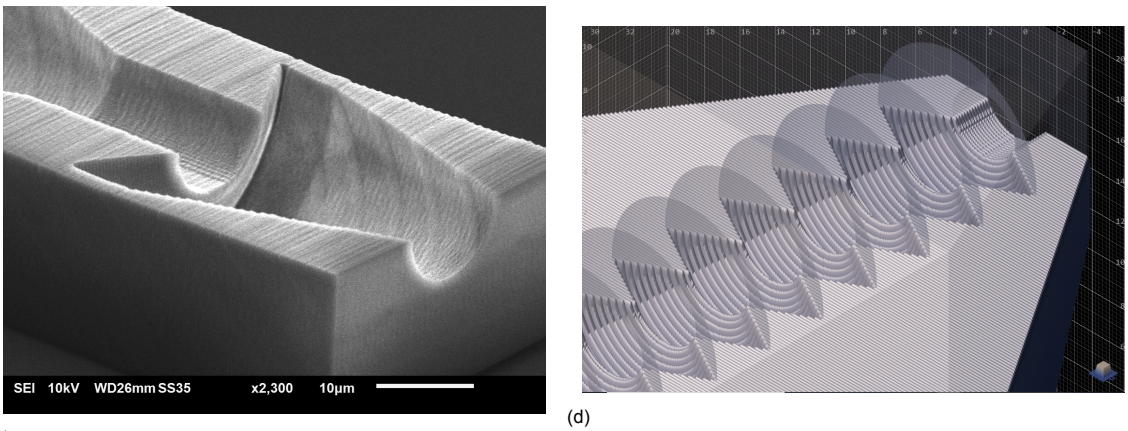


(c) (d)

Figure C.7: *Examples of the inevitable surface roughness of 2PP printed channels. The channels are printed half—to expose their inner channels to the SEM view. In figure (d), a screenshot of the DeScribe slicing software is shown, revealing the rendered lines of voxels.*

# Supplementary References


[1] R. C. L. N. Kramer, E. J. Verlinden, L. Angeloni, A. van den Heuvel, L. E. Fratila-Apachitei, S. M. van der Maarel, and M. K. Ghatkesar, "Multiscale 3D-printing of microfluidic AFM cantilevers", *Lab on a Chip*, vol. 20, no. 2, pp. 311–319, Jan. 2020.

[2] P. F. J. Altena van, "Multiscale 3D printed polymer probes for single cell experiments", Master's thesis, TU Delft, Delft, 2021.

[3] Y. Bellouard, A. Said, M. Dugan, and P. Bado, "Fabrication of high-aspect ratio, micro-fluidic channels and tunnels using femtosecond laser pulses and chemical etching", *Optics Express*, vol. 12, no. 10, p. 2120, 2004.

[4] Nanoscribe GmbH, *Nanoguide: Servermode and commandlineslicer*, https://support.nanoscribe.com/hc/en-gb/articles/360003617073-ServerMode-and-CommandLineSlicer, 2022.

[5] R. Calmo, A. Lovera, S. Stassi, A. Chiadò, D. Scaiola, F. Bosco, and C. Ricciardi, "Monolithic glass suspended microchannel resonators for enhanced mass sensing of liquids", *Sensors and Actuators, B: Chemical*, vol. 283, no. August 2018, pp. 298–303, 2019.

[6] O. Guillaume-Gentil, R. V. V. Grindberg, R. Kooger, L. Dorwling-Carter, V. Martinez, D. Ossola, M. Pilhofer, T. Zambelli, and J. A. A. Vorholt, "Tunable Single-Cell Extraction for Molecular Analyses", *Cell*, vol. 166, no. 2, pp. 506–516, 2016.

[7] J. M. Chen, C. Y. Chen, and C. H. Liu, "Pressure barrier in an axisymmetric capillary microchannel with sudden expansion", *Japanese Journal of Applied Physics*, vol. 47, no. 3 PART 1, pp. 1683–1689, 2008.

[8] J. Zhang, H. Ding, X. Liu, H. Gu, M. Wei, X. Li, S. Liu, S. Li, X. Du, and Z. Gu, "Facile Surface Functionalization Strategy for Two-Photon Lithography Microstructures", *Small*, vol. 2101048, pp. 1–9, 2021.

[9] O. Guillaume-Gentil, E. Potthoff, D. Ossola, P. Dörig, T. Zambelli, and J. A. Vorholt, "Force-controlled fluidic injection into single cell nuclei", *Small*, vol. 9, no. 11, pp. 1904–1907, 2013.

[10] E. W. Washburn, "The dynamics of capillary flow", *Physical review*, vol. 17, no. 3, p. 273, 1921.

[11] Nanoscribe GmbH, *Nanoguide: Sample development*, https://support.nanoscribe.com/hc/en-gb/articles/360001344673-Sample-Development, 2022.

[12] ——, *Nanoguide: 25x objective*, https://support.nanoscribe.com/hc/en-gb/articles/360002482713-25x-Objective, 2022.

[13] M. Blankespoor, *First tests with 2pp printed microfluidic cantilevers*, https://vimeo.com/692217088, 2022.

[14] ——, *Cantilevers with embedded membranes*, https://vimeo.com/692217196, 2022.

[15] Paul Monnier, *Fluidfm probe coating with sigmacote*, https://www.cytosurge.com/forum/help-1/question/fluidfm-probe-coating-with-sigmacote-99, 2018.

[16] M. Blankespoor, *Experiment demonstrating dosing capability of 2pp printed cantilevers with axisymmetrical phaseguides*, https://vimeo.com/692216865, 2022.

[17] ——, *Discrete femtolitre liquid dosing using axisymmetrical phaseguides*, https://vimeo.com/692222490, 2022.

[18] A. D. Lantada, S. Hengsbach, and K. Bade, "Lotus-on-chip: Computer-aided design and 3D direct laser writing of bioinspired surfaces for controlling the wettability of materials and devices", *Bioinspiration and Biomimetics*, vol. 12, no. 6, 2017.

[19] M. F. Berwind, A. Hashibon, A. Fromm, M. Gurr, F. Burmeister, and C. Eberl, “Rapidly prototyping biocompatible surfaces with designed wetting properties via photolithography and plasma polymerization”, *Microfluidics and Nanofluidics*, vol. 21, no. 9, pp. 1–7, 2017.

[20] M. Blankespoor, *First contact angle measurements*, `https://vimeo.com/692217324`, 2022.

[21] D. Gosselin, J. Berthier, G. Delapierre, D. Chaussy, and N. Belgacem, “Capillary Flows : Dynamics & Geometry Effects”, 2015.